A Comparative Study on PID Controller Tuning of Load Frequency Control in Three-Area Power System Using Soft Computing Technique

Yosef Worku Bedada

A Thesis Submitted to

The Department of Electrical Power and Control Engineering

School of Electrical Engineering and Computing

Presented in Partial Fulfillment of the Requirement for the Master of Science Degree in Electrical Power and Control Engineering (Control)

Office of Graduate Studies

Adama Science and Technology University

September 2021

Adama, Ethiopia

A Comparative Study on PID Controller Tuning of Load Frequency Control in Three-Area Power System Using Soft Computing Techniques

Yosef Worku Bedada

Advisor: Dr. Shubhashish Bhakta

A Thesis Submitted to

The Department of Electrical Power and Control Engineering

School of Electrical Engineering and Computing

Presented in Partial Fulfillment of the Requirement for the Master of Science Degree in Electrical Power and Control Engineering (Control)

Office of Graduate Studies

Adama Science and Technology University

September 2021

Adama, Ethiopia

DECLARATION

I hereby declare that this master thesis entitled "A Comparative Study on PID Controller Tuning of Load Frequency Control in Three Areas Power System Using Soft Computing Techniques" is my original work. That is, it has not been submitted for the award of any academic degree, diploma, or certificate in any other university. All sources of materials that are used in this thesis have been duly acknowledged through citation.

Name of the Student	Signature	Date

RECOMMENDATION

I, the advisor of this thesis, hereby certify that I have read the revised version of the thesis entitled "A Comparative Study on PID Controller Tuning of Load Frequency Control on Three-Area Power System Using Soft Computing Techniques" prepared under my guidance by Yosef Worku Bedada submitted in partial fulfillment of the requirements for the degree of Mater's of Science in Control Engineering. Therefore, I recommend the submission of a revised version of the thesis to the department following the applicable procedures.

Major Advisor	Signature	Date
Co-advisor	Signature	Date

APPROVAL SHEET

I, the advisor of the thesis entitled "A Comparative Study on PID Controller Tuning of Load Frequency Control in Three Areas Power System Using Soft Computing Techniques" and developed by **Yosef Worku Bedada, ID NO: PGR/19174/12**, hereby certify that the recommendation and suggestions made by the board of examiners are appropriately incorporated into the final version of the thesis.

Major Advisor	Signature	Date
Co-advisor	Signature	Date

We, the undersigned, members of the Board of Examiners of the thesis by Yosef Worku Bedada have read and evaluated the thesis entitled "A Comparative Study on PID Controller Tuning of Load frequency Control in Three-Area Power System Using Soft Computing Techniques" and examined the candidate during the open defense. This is, therefore, to certify that the thesis is accepted for partial fulfillment of the requirement of the degree of Master of Science in Control Engineering.

Chairperson	Signature	Date
Internal Examiner	Signature	Date
External Examiner	Signature	Date

Finally, approval and acceptance of the thesis are contingent upon submission of its final copy to the Office of Postgraduate Studies (OPGS) through the Department Graduate Council (DGC) and School Graduate Committee (SGC).

Department Head	Signature	Date
School Dean	Signature	Date
Office of Postgraduate Studies Dean,	Signature	Date

ACKNOWLEDGEMENTS

I would like to convey my heartfelt gratitude to my adviser, **Dr. Shubhashish Bhakta**, for his exceptional guidance, inspiration, steadfast confidence, ongoing encouragement, and support throughout this attempt, without which I would not have been able to accomplish it successfully. I also want to express my gratitude to **Mr. Addisu Teshale** for his informative comments and ideas, which have helped me to improve my knowledge. Most importantly, I would like to thank my family and friends for their constant support and encouragement in every situation. I would not have made it this far without them. Lastly, I would like to acknowledge all of my colleagues in our research laboratory. Special thanks go to **Mr.Tewodros Asfaw** and **Mr.Ashebir Birhanu**. I'd also like to thank my teammates and the staff of Ethiopian Electric Power's Koka Hydropower Plant for their encouragement and friendship during this research work.

TABLE OF CONTENTS

LIST OF TABLES

LIST OF FIGURES AND ILLUSTRATIONS

LIST OF ACRONYMS

AC	Alternating Current
ACE	Area Control Error
AGC	Automatic Generation Control
AGCS	Automatic Generation Control Simulator
ANFIS	Adaptive Neuro-Fuzzy Inference System
ALFC	Automatic Load Frequency Control
ANN	Artificial Neural Network
AVR	Automatic Voltage Regulator
BFA	Bacteria Foraging Algorithm
BPA	Back Propagation Algorithm
ChOA	Chimp Optimization Algorithm
DE	Differential Evolution
GA	Genetic Algorithm
GA-SFL	Genetic Algorithm-Sugeno Fuzzy Logic
GRC	Generation Rate Constraint
HIL	Hardware in Loop
HNF	Hybrid Neuro-fuzzy
H-PSO	Hybrid Particle Swarm Optimization Algorithm
HP	High Pressure
HSA	Harmony Search Algorithm
IAE	Integral Absolute Error
ISE	Integral Squared Error
ITAE	Integral Time Absolute Error
ITSE	Integral Time Squared Error
IV	Intercept Valve
LCOA	Lozi Map Based Chaotic Optimization Algorithm
LQR	Linear Quadratic Regulator

MFO	Mothe-Flame Optimization Algorithm
MFO-SFL	Mothe-Flame Optimization Algorithm-Sugeno Fuzzy Logic
MPC	Model Predictive Control
MVO	Multi-Verse Optimization Algorithm
PI	Proportional-Integral
PID	Proportional-Integral-Derivative
PS	Pattern Search
PSO	Particle Swarm Optimization Algorithm
QOHS	Novel-Quasi Oppositional Harmony Search Algorithm
SA	Simulated Algorithm
SLP	Step Load Perturbation
STR	Self-Tuning Regulator
TLBO	Teaching Learning Based Algorithm
OLR	Optimal Linear Regulator
UPS	Uninterruptable Power Supply
3DOF	Three Degree of Freedom

ABSTRACT

A disparity between power demanded, and power generated by the system generators results in the frequency deviation of the power system. So, the aim of Automatic Load frequency control (ALFC) is to preserve the frequency to its nominal value, and its allowed range. Nowadays, power systems are interconnected and grouped by numerous control areas. Tie-lines connect each control area, allowing electricity to be transferred between them. Thus, the second objective of ALFC is to keep the tie-lines power flow close to its planned value. So, an exact, and realistic LFC model is very essential. Many types of control tactics have been implemented by researchers so far to realize the objectives of LFC. In this thesis, essentially, three-area interconnected systems consisting of reheat, and hydro turbine with generation rate constraint (GRC) are presented. The parameters of the PID controllers gains (K_p, K_i, K_d) values are optimized by applying four different metaheuristics optimization algorithms, namely the Chimp optimization algorithm(ChOA), Novel quasi-harmony search algorithm (QOHS), Mothe- flame optimization algorithm(MFO), and Multi-verse optimization algorithm(MVO). The peak overshoot, undershoot, settling time, and steady-state error is the time domain specification used for measuring the controller's performance, and the suggested system employs integral time absolute error(ITAE) as an objective function. From the MATLAB simulation result, when 1% step load perturbation is applied to area 1, the QOHS-PID tuning gave a better result in area -1, and area-2 while MFO-PID tuning gave a better result in area-3. But in reducing deviation in tie-line power error MFO-PID tuning gives better results in all areas. When 10%, 5%, and 1% SLP is applied to area 1, area 2, and area 3 simultaneously, ChOA based PID controller gave a better result in area 1, and area 3, while MFO-PID tuning gave a better result in area-2. Again in reducing deviation in tie-line power error ChOA-PID tuning gives better results in all areas. From an execution time efficiency point of view, ChOA shows superior performance. Robustness was also checked by varying system parameters 1% step load change in area 1 and found that the system is achieving a steady-state position within the permissible time frame. It is concluded that a single control design technique cannot satisfy all of the requirements, including robustness to system uncertainties, simple/systematic design, and nonlinearity handling.

Keywords*:* AGC, ALFC, Area control error, Interconnected power system, PID controller tuning, , and Three-area control.

CHAPTER ONE

INTRODUCTION

1.1 Background

The electricity demand is increasing day by day for a variety of reasons. The generation should also rise in response to the demand. Ethiopia's entire installed generation capacity is currently around 4300 MW, with a peak load of 2164 MW [1]. Because of the country's rapid economic expansion, the total load has been steadily increasing, and the country's power infrastructure has been expanded in response [2]. However, meeting the demand is difficult for the country.

The mismatch in power generated and demanded causes in system frequency (f) and tie-line powers (Ptie) fluctuation. This makes the power systems unstable. Thus, scheduled frequency and tie-line powers must be kept within acceptable limits. Power system controllers are needed to be designed to regulate power flows between the tie lines, and frequency in the interconnected areas through Automatic Generation Control (AGC) [3]. AGC maintains frequency and ties line power within a predetermined range by making area control error (ACE) zero [4]. The difference between an area's actual and scheduled interchange is known as the area control error as long as the system frequency is equal to its stated value (ACE). If the ACE is negative, the area is under-generating and requires greater overall generation; meanwhile, if the ACE is positive, the area is over-producing and requires production reduction.

AGC consists of a feedback control loop to adjust the frequency in limits. AGC has two parts namely Load Frequency Control (LFC), and automatic voltage regulator (AVR) [3]. LFC provides zero steady-state errors along with optimization of transient behavior. Variations in real power influence primarily the system frequency, whereas reactive power is less delicate to changes in frequency and is primarily subordinate to changes in voltage greatness. Hence, real, and reactive powers are controlled separately.

With the increasing non-linearity and the complications of the power systems, the manufacturing sector has been strictly affected by the operating point variations which have increased the concern about power quality [4]. The power system network consists of many interconnected areas, and any type of fault, interruption, or disturbances adversely affects the power quality [3]. Thus, the LFC has picked up in significance with the development of interconnected power systems and has made the operation of interconnected systems conceivable [5].

On the other hand, an interconnected system is a single large electric circuit. It has traditionally been separated into operation zones (control areas). Typically, each operational region corresponded to a single power generation part of the grid. Tie-lines are lines that connect separate operating zones. The term interchange is the net movement of power out of a certain location. In a contemporary power system network, which consists of several utilities networked together, power is shared between places via tie-lines that connect them. The main advantage of interconnected power systems is, increase power supply dependability, peak load exchange, diversity factor, plant reserve capacity reduction, reduced capital and operating costs in the system, efficient operation, and utilization of aging plants. Over the last few decades, many studies [6] on the topic of AGC-linked power systems have been published. According to a survey of the literature [3], [7] the majority of previous work in the area of automatic generation control focused on interconnected thermal systems, with AGC of linked hydro-thermal systems merging thermal and hydro systems receiving significantly less attention.

Steam/ Water input to turbine/generators must be continuously controlled to match the demand in active power, otherwise, the machine speed will change with resulting in a change in frequency which may be extremely unwanted [8]. Similarly, generator excitation must be constantly adjusted to balance reactive power demand with reactive generation; otherwise, voltages at various system buses may exceed the prescribed limit [9]. But a change in frequency is directly linked to a variation in the speed of the user's plant, which affects the process of production. So, frequency control is more important than voltage control [10].

For voltage constant, there is a certain voltage stabilizer like uninterruptable power supply(UPS), but frequency stabilizer is rarely used [4]. For satisfactory operation of a power system in parallel, motors operate on the system bus at anticipated speed. However, the system's synchronous clocks provide the correct time, and the entertainment devices work properly. The permissible deviation in the frequency power systems in most of the countries are ±0.5Hz, and in a few countries ±2.5Hz like in India [10] while the permissible voltage range is about ±5% [4], [10]

Manual regulation is not possible in today's large-scale, interlinked power systems. As a result, each generator is installed with ALFC and AVR equipment [11]. The controllers, on the other hand, are programmed for a certain operation condition and handle minor fluctuations in load demand without frequency as well as voltage beyond the given limit [12]. Figure 1.1. below shows a block diagram of ALFC of single area power system including primary and secondary control loops.

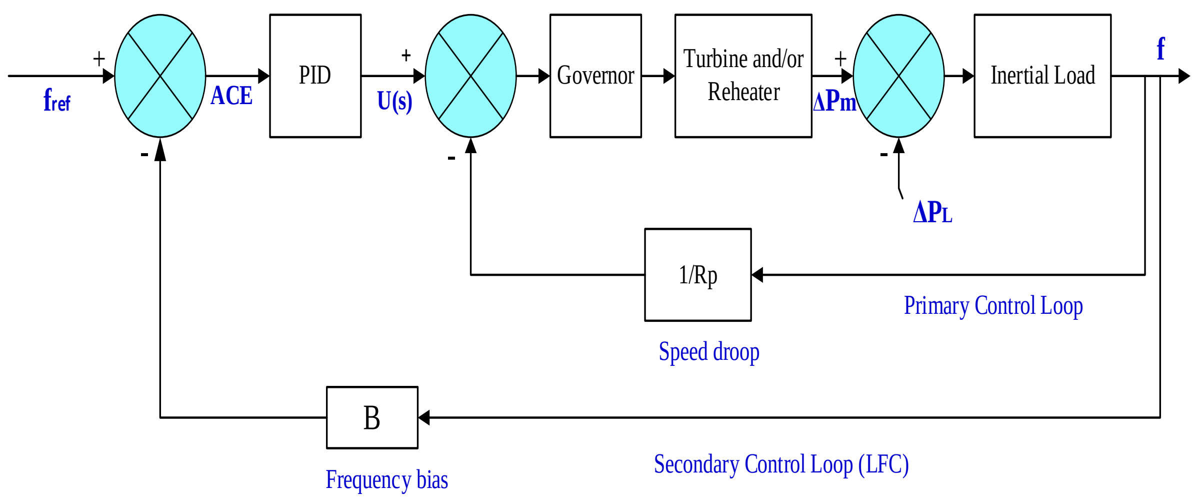

Figure 1. 1 Schematic block diagram of ALFC for single area power system [12].

Thus, to improve these problems now a day many researchers [11], [12], [13] et al., working on the area. Thus, this thesis is a continuation of research works on LFC of three areas (thermal: area-1, thermal: area-2, and hydro: area-3) interconnected power systems is considered in the study. The study focuses on tuning PID parameters (*Kp, Ki, Kd*) to get optimum value in reducing area control error to get the stable frequency and tie-line power. Metaheuristics optimization algorithms i.e., Chimp optimization algorithm (ChOA), Novel Quasi-oppositional harmony search optimization algorithm (QOHS), Moth flame optimization algorithm (MFO), and Multi-Verse optimization algorithm (MVO) were used in getting the optimized value of PID parameters.

1.2 Statement of the Problem

Many interconnected utilities comprise a grid in a power system, and power is transferred through the tie-lines. As the system frequency drops, the primary speed control will be provided by the speed governor for each generator, allowing the system power generation to match the load demand. This basic control step, however, is insufficient to restore the frequency. By modifying the generator output, a secondary control operation is necessary to eliminate any frequency deviation and maintain the flow of tie-line power. LFC is the name for this secondary control action. The AGC includes both primary and secondary controls. The primary, and secondary controls transient responses are measured in seconds, and minutes, respectively [14]. The area that is subjected to a load change in an interconnected network will acquire energy from the other locations via tie-lines. As a result, the affected area should be able to regain balance before the load change without requiring external intervention. Else, power swings in one location caused by transitory disturbances can cause power swings in neighboring areas through tie-lines. As a result, each area requires a controller that not only restores the original frequency but also corrects any mistakes in the tie-line power flow [15]. To assure continuous power supply, control engineers have turned to artificial intelligence approaches in recent decades [16]. However, in most LFC research, physical constraints (governor dead-band [17], generation rate [18], and communication link delay [19]) have been overlooked. But maintaining the frequency variation in their permissible range, and tie-lines power in their nominal values are a major research gap. This thesis work is a part of a research activity that focuses on obtaining an optimal gain value of PID Controller using QOHS, ChOA, MFO, and MVO for interconnected power system, considering physical constraint within an area in response to change in system frequency and tie-line power loading.

1.3 Objectives of Study

1.3.1 General Objective

This thesis work aims to examine an optimal gain value of PID controller using QOHS, ChOA, MFO, and MVO algorithm for a three-area interconnected power system within an area in response to changes in system frequency, and tie-line power.

1.3.2 Specific Objectives

The specific objectives of this thesis work include:

(i) To study the dynamic model of ALFC for a thermal power plant and hydropower plant.

(ii) To develop a Simulink model of a three-area interconnected power system comprised of two thermal plants, and one hydropower plant in areas 1 to area 3 respectively.

(iii) To study the changes that appear in the frequency and tie-lines power of the three-area power system in case of load change.

(iv) To obtain optimized gain parameters of PID controller via QOHS-PID, MFO-PID, MVO-PID, and ChOA-PID of the three-area power system.

(v) Finally, the performance of QOHS-PID, MFO-PID, MVO-PID, and ChOA-PID based designed controller is compared using MATLAB simulation.

1.4 Scope of the Study

The scope of this thesis is to study a PID tuning for a three-area ALFC for a hydro-thermal interconnected power system. The performance of QOHS-PID, MFO-PID, MVO-PID, and ChOA-PID based controllers is compared using MATLAB simulation. Integral time absolute error (ITAE) is used as a performance index to know the error magnitude. By altering system parameters in $\pm 50\%$ and by varying operating load conditions from their nominal values the robustness of the controllers is investigated. The impact of generation rate constraints (GRC) and variation in step load perturbations (SLPs) is also investigated.

1.5 Limitation of the Study

The thesis is restricted to the simulation of the system using MATLAB/Simulink by simulating the component of three-area power systems, and a single generator is considered in a given area; how the three-areas are interacting, what makes difference the interconnected, and isolated power system, and how frequency and tie-line power is changing by simulation only. This is because the implementation of a real system is difficult to procure the components. Along with it takes the additional time and cost incurred in making the actual prototype implementation in hardware in the loop (HIL). Considered disturbances are deterministic, and LFC considered in this thesis work is continuous time. The power systems considered do not consider other renewable energy(Solar) and battery effects. It does not consider non-linearity like governor dead band, boiler model, and communication link delay. The thesis work is also limited to considering generation rate constraint non-linearity.

1.6 The Motivation of the Study

As the population increase, the demand for electricity consumption also increases. With an increase in demand, there are many types of loads. Thus, the loads demand always fluctuates, this causes a disparity between load demand and power generation. As a result of this mismatch, frequency control has become a critical issue.

The frequency and bus voltages of the systems are affected by changes in load. As a load variation is not in our hands, it's impossible to control load variation, and it can't be predicted ahead of time; so that remedial action can be performed. The error function is derived employing frequency deviation and tie-line power of the control areas to achieve significant performance, and this error is known as the Area Control Error (ACE). The main goal of this research is to reduce the area control error and optimize the performance index using a controller whose gain values are obtained using a ChOA, QOHS algorithm, MFO algorithm, and MVO algorithms.

1.7 Significance of the Study

In all electrical power generation systems, there is a need to preserve the operating frequency at the desired, and nominal value. The change in frequency is due to the change in the load level of the system. This frequency variation can be controlled and regulated using an ALFC. Therefore modeling and designing an appropriate LFC is significant. As a result, the primary purpose of this thesis is to explore and propose the appropriate intelligent controller techniques for AGC of mixed thermal-hydropower systems. The thesis can be used as a reference for future studies that can be done on ALFC problems. In addition, anyone who is going to implement an intelligent ALFC in different power systems can also use it as a reference. The thesis work can also be used as a basis for further improvement on the ALFC system.

1.8 Organization of the Thesis

This thesis organizes into four chapters.

Chapter 1: Includes introduction of the research work, statement of the problems, objectives, significance, scope, and limitation of the research. Chapter 2: Includes a literature review on the Automatic load frequency control, the controller used, and different areas, and on a different type of power plant. Chapter 3: Describes the methodology followed in this research thesis. Chapter 4: Shows the proposed results and discussions. Chapter 5: Includes the conclusions and recommendations of the thesis.

CHAPTER TWO

LITERATURE REVIEW

2.1 Automatic Generation Control

To preserve voltage and frequency in a rated value, AGC is installed on each generator. The primary responsibility of an AGC is to ensure that an electric power system runs smoothly and efficiently [20]. AGC aims to enable each generator to control its generation independently to achieve zero steady-state value of area control error and economic loadings of its generators against random variations in the load demand which occur continuously in a power system [21]. As a result, to ensure an acceptable power supply, an AGC system must be complemented with current and sophisticated control approaches. So, for the last several years, AGC is becoming an important issue in power system control, and operation [20]. The turbine speed reduces when the load on the power system increases before the governor readjusts the steam/water input to the new load [22]. The error signal gets smaller as the variation in the value of speed decreases, and the orientations of the governor fly-balls get closer to the point required to preserve a constant speed.

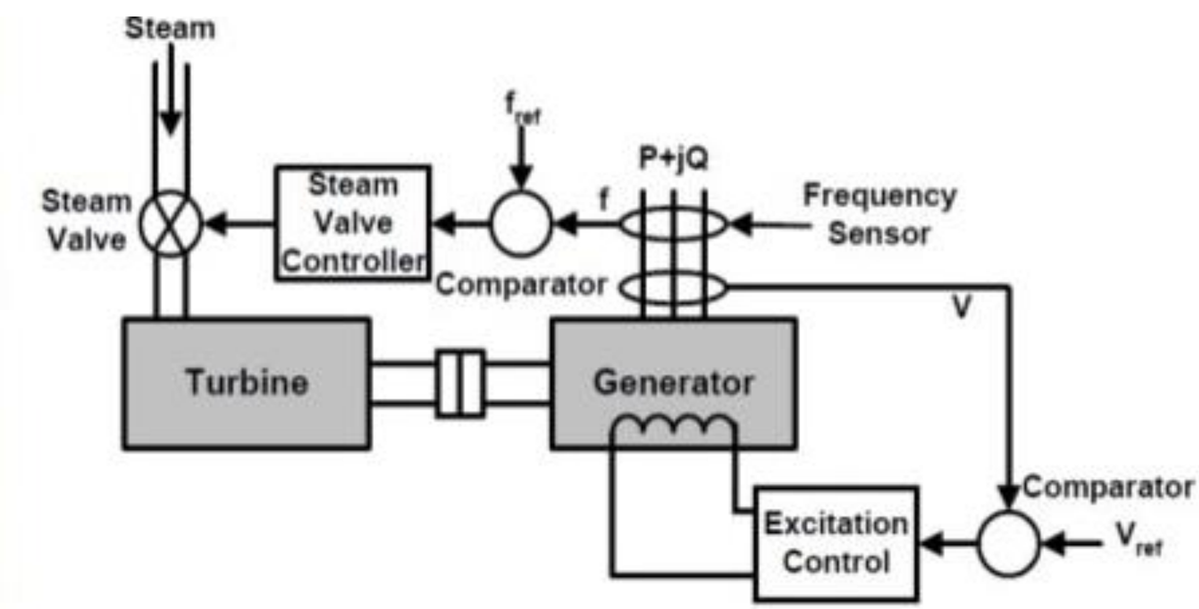

Figure 2. 1 Synchronous Generators LFC, and AVR schematic diagram [11].

The schematic diagram comprises two control mechanisms. The first is frequency control, and the second is voltage control. For the first case, the frequency sensor senses the frequency and provides to frequency comparator. Then the comparator compares the actual frequency with rated frequency (f_{ref}) and generates an error signal. This signal is then provided to steam valve control (thermal) or governor (hydro). Then the steam valve/governor regulates the opening, and closing of the steam valve/wicket gate. Then the regulated gate is provided to the turbine which is coupled to a generator. For the second case, voltage sensors sense the voltage and provide it to the comparator. Thus, the comparator compares the actual value of voltage with the reference voltage (V_{ref}) and generates the error signals. The signal is provided to excitation control, and accordingly, the excitation control is coupled with the generator. Hence, the frequency, and voltage sensor sense the frequency, and voltage output respectively. Controllers, on the other hand, are designed for a certain set of operating parameters, and they handle small fluctuations in load demand without frequency, as well as voltage beyond the permitted limits [23]. Active(*P*), and reactive (*Q*) powers can be stated as a function of voltage(*V*), and machine angle(σ). This can express by:

$$P = f(V, \delta) \text{ and } \frac{dP}{dt} = V\frac{\partial \delta}{\partial t} + \delta\frac{\partial V}{\partial t} \tag{2.1}$$

$$Q = f(V, \delta) \text{ and } \frac{dQ}{dt} = V\frac{\partial \delta}{\partial t} + \delta\frac{\partial V}{\partial t} \tag{2.2}$$

where *P*-active power, *Q*-reactive power, *V*-voltage, δ -internal machine angle

However, from the above two-equation, the change in active power demand (ΔP_d) is reliant on internal machine angle, and independent on machine voltages, while bus voltage rest on machine excitation, and it's independent on machine angle. So the equation becomes is shown in (2.3) and (2.4).

$$\frac{dP}{dt} = V\frac{\partial \delta}{\partial t} \tag{2.3}$$

$$\frac{dQ}{dt} = \delta\frac{\partial V}{\partial t} \tag{2.4}$$

So, change in active power demand causes in angle δ, and thus causes the variation in speed of a machine. Power systems frequency can be controlled using dual control loops, namely primary, and secondary loops. The primary control loop prevents instant variations in the frequency before triggering the frequency protection switches. It is provided through the governor droops that typically give rise to the steady-state error. Secondary control is an ALFC that is implemented to control the system frequency to its scheduled value in the power system network [10]. That is:

(i) Primary Control: This sort of control is used on a local level to preserve the system generation and demand balance. The frequency deviation in the area is detected by the speed of turbine governors, which adjusts the generator output in response to the frequency deviation. If a large disturbance occurs, the primary control allows the network to be stabilized by balancing generated and utilized power at a frequency different from the set-point quantity. The integrator is in charge of this control operation.

(ii) Secondary Control: This kind of control is applied to employ an automatic centralized process in the control building block. It has two functions:

(a) It maintains the anticipated value of the interchange power linking the control block and its neighboring blocks.

(b) It restores the frequency's setpoint value in the event of a significant frequency drop.

2.3. Automatic Load Frequency Control

For minor changes, LFC, and excitation voltage control are non-interactive, and can be modeled, and studied separately. However, excitation voltage control is quick (small-time constant), whereas power frequency control is slow (large-time constant)[10]. So, in focusing on frequency control, the regulator which is insensitive to fast random change must be designed; If not, the system will hunt, causing extra wear and tear on spinning machines and control equipment. Today many researchers [8], [11], [12], [21], [22] are attempting to discover the optimal frequency control solution, since the synchronization of all generators in a given control area, as well as the proper matching of load demand, and generation in a power system highly relies on frequency [23]. Voltage is a function of reactive power, whereas frequency is a function of active power. As a result, the power system employs two control loops [24]. These are the active power-frequency(P-f) control loop, and reactive power-voltage (Q-V) control loop. Because of mechanical inertia constant in addition to the preceding difficulty, active power-frequency (P-f) control requires more attention than reactive power-voltage (Q-V) control. Two significant factors are the reliability, and quality of the power system [24]. LFC is critical for maintaining power system reliability, and quality [25]. The schematic diagram for ALFC is given in Figure 2.2.

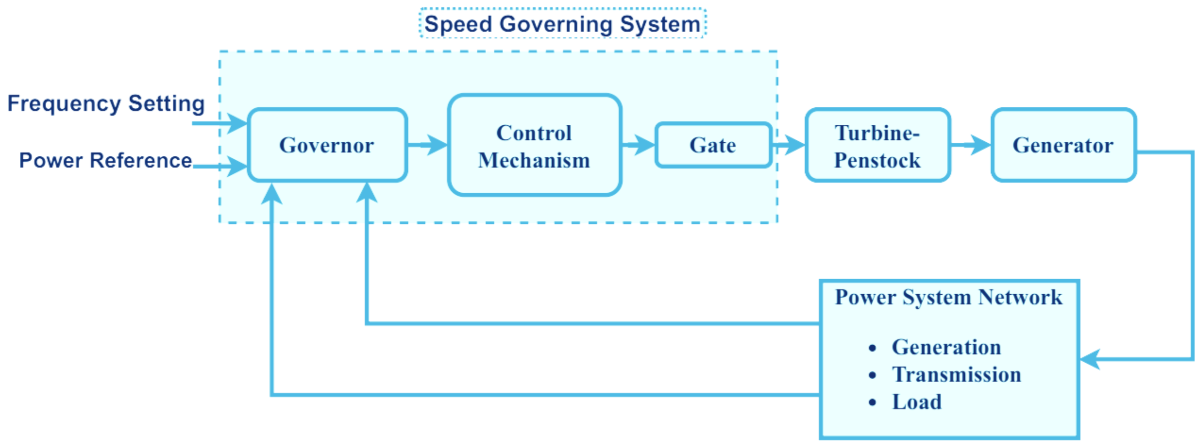

Figure 2. 2 Schematic block diagram for ALFC technique [10].

2.3.1 Automatic Load Frequency Control of Single Area Power System

The ALFC intends to keep the system's real power balance to control frequency deviation. Maintaining a constant frequency, regulating tie-line flows, and distributing load among participating generating units are all major responsibilities of the ALFC [4].

The tie-line deviation (ΔP_{tie}) is a control (input) signal that is measured from the tie-line flows, whereas the frequency deviation (Δf) is obtained by measuring the angle deviation. The error signals ΔP_{tie}, and Δf are amplified, combined, and transformed to a genuine power signal, which is then used to control the valve position. The turbine (primary mover) alters its output power based on the position of a valve to achieve true power balance [10]. Figure 2.3 depicts the entire control schematic.

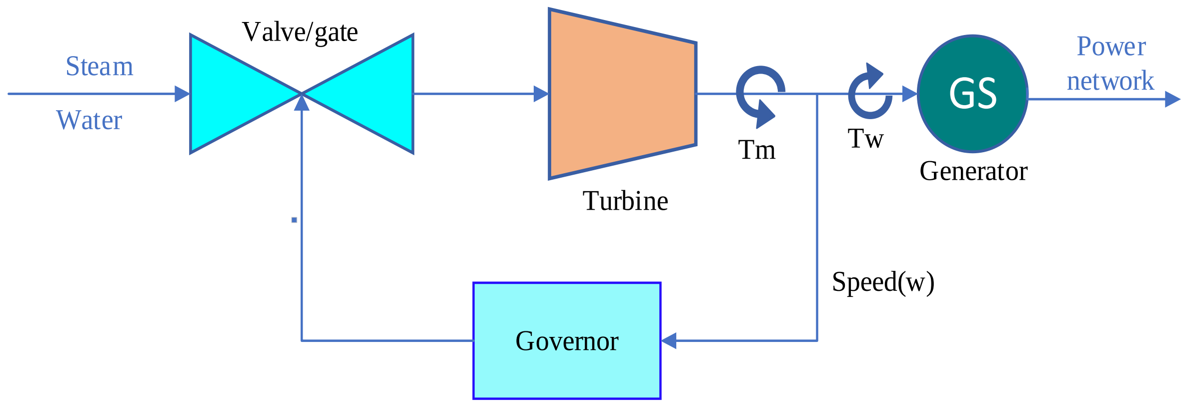

Figure 2. 3 The Schematic representation of single area ALFC system [4].

2.3.2 Turbine Speed Governing System

In reaction to load variations, the governing system controls the turbine governor speed, and hence the frequency and active power. The turbine governor controls the amount of water/steam that enters a turbine, which then rotates the generator to generate power [26]. The speed control mechanism includes relays, servomotors, pressure or power amplifying devices, levers, and linkages between the speed governor and governor-controlled gates. Normally, the speed governor operates the governor-controlled gates/valves, which regulate the water/steam input to the turbine via the speed control mechanism. The second high-power main gate servomotor's distributor or relay valve is controlled by the first low-power pilot servomotor. A mechanical governor or an electronic regulator controls the pilot valve on the pilot servomotor. The output of the speed-sensing devices is the deviation from the reference speed [10], [27].

The permanent speed droop(R_P) determines the amount of change in output a unit produces in response to a change in unit speed. The wicket gate location or the unit output power can both be used to create a permanent speed droop. The permanent speed droop can support stabilize unit speed control in isolated operations by giving intermediate feedback that restricts the overtravel of the turbine control servomotors while adjusting the unit speed. The levels of involvement the unit provides when responding to fluctuations in system frequency when connected to an interconnected power system are determined by the permanent speed droop [23].

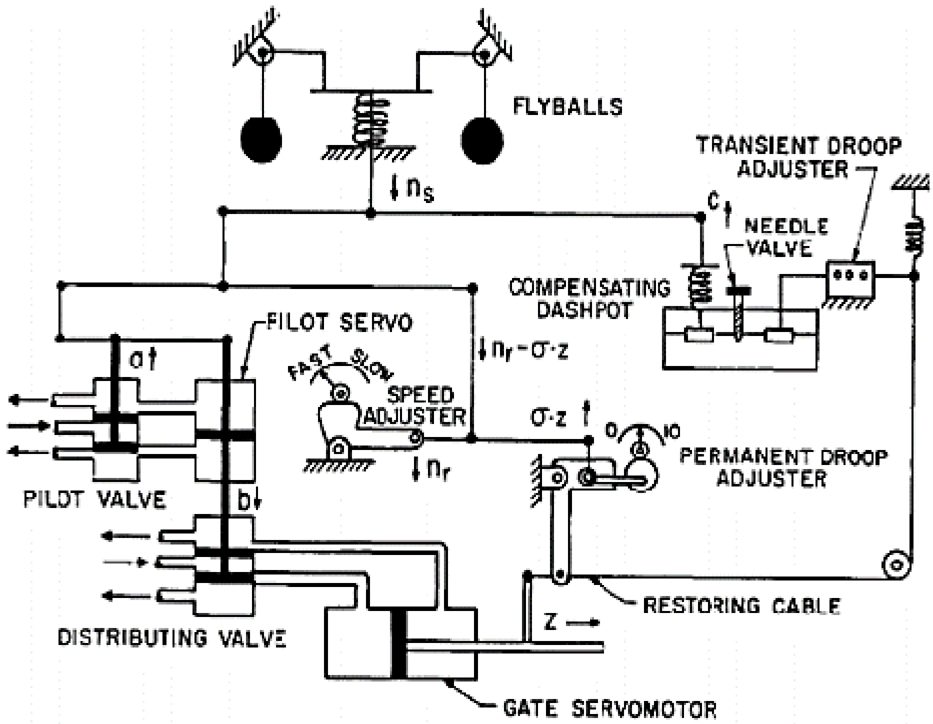

Figure 2. 4 Mechanical-Hydraulic Speed Governing System [10].

During a transient condition overshoot of the turbine, the control servomotor is limited by the temporary droop **(**R_T). A filtered derivative of wicket gate position can be added to the governor error summing point, or a dashpot can be connected from the wicket gate position to the governor error summing point to create the temporary droop [28].

2.3.3 Load Frequency Control with Generation Rate Constraints

In the previously mentioned frequency control problem, the influence of limitations on the rate of change of power generation is not taken into account. Power generation in power systems with steam plants can only vary at a certain maximum rate [18]. The majority of a reheat unit has a very small generation rate which has 3%/min. while some reheat units have a generation rate that ranges from 5%/min to 7%/min. If the effects GRCs are not considered, the power system goes to large momentary disturbance, which may result in excessive wear, and tear of the controller [29]. Numerous approaches have been presented to study the effect of GRCs on the design of AGC. The system dynamic model becomes non-linear when GRC is considered. Hence, for the optimization of the controller setting, linear control methods cannot be functional. To consider a GRC in a power system limiters are added to governors of all areas to be considered [10], [29], [30]. The limiters set a maximum rate at which the valve can open or close. Because the rate at which generation can change in the area is limited by the constraints established, GRCs result in higher ACE deviations. As a result, compared to the case where the generation rate is not regulated, the period for which electricity must be imported increases significantly.

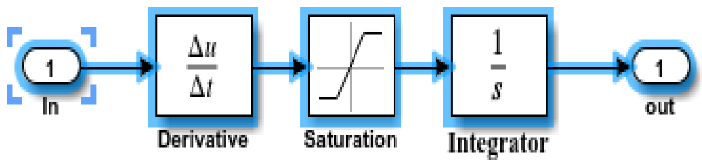

Figure 2. 5 Schematic diagram GRCs [30].

2.3.4 Interconnected Power System

The LFC of interlinked power systems is substantially more critical than the isolated power system [31]. While recognizing the overall view of an interconnected power system needs knowledge of isolated power system theory and expertise. In an interconnected system, since every power systems are connected to their surrounding areas, the LFC problem has become a major challenge. Before connecting a power system, each area must agree on the adoption, regulation, and control tactics, as well as equipment, that will be useful in both normal and abnormal circumstances. Except for the scheduled share of other members' loads, which must be carried by their control areas under normal operating conditions, the loads shall attempt to be carried by their control areas under no circumstances [32].

Previous electric power systems frequently functioned as separate units. Nowadays power system interconnection was realized due to greatness in the advantage of power system inter-connection over the islanded. Some of the advantages of interconnected power systems are the use of old plants, increase power supply reliability, peak load exchange, rise diversity factor, decrease plant reserve capacity, and decrease operating cost and capital. The detailed explanations are shown below:

(i) **Using of old plants:** There are some obsolete and insufficient generating stations in the power system network. These stations are capable of carrying short peaks of load. However, these power plants are insufficient to operate on an unceasing basis. If the system is integrated, these plants will be related to a transmission line, and it enhances in fulfilling the peak load demand [31]. As a result, these generating stations are combined with modern plants to attain this goal.

(ii) **Increase the reliability of power supply:** All loads in an interlinked power system have multiple sources of power supply. If one supply fails or is out of commission, the load is provided by another source. As a result, if the power station suffers a significant failure, the load is transferred to another healthy power station [32]. As a result, the load is always connected to an uninterrupted power source, increasing the system's reliability.

(iii) **Exchange of peak load:** The load curve of the power station shows a peak demand during peak load season. However, this peak demand may be greater than the generation capacity of the power system. In this situation an additional load must be shared by the power plants, else, an overload relay may function, and load shedding will be done to minimize the burden on a power station [31].

(iv) **Increase the diversity factor:** The load curve for all power generating plants in the interlinked power system is not similar. As a result, the system's maximum demand is lower as compared to the sum of individual maximum demands on separate power plants. In addition, the system's diversity has improved. As a result, plants' effective capacity is boosted [33].

(v) **Plant reserve capacity reduction:** Each power station has a backup generator in case of a power outage. All plants in the interconnected system are connected in parallel. As a result, the system's reserve capacity is reduced, and its efficiency is increased [31].

(vi) **Reduce capital, and operating cost:** Plant efficiency is raised, and power generation costs are decreased in an integrated system. The capital and operating costs are lowered in this system. As a result, the price per kW is also reduced [32].

Even though interconnected power system has lots of advantage, there exist some problems associated with satisfactory implementation interconnected power systems. These are frequency control problem, voltage control problem, communication problem, metering and instrumentation problem, and shortage of reserve capacity [31]. The details are expressed below:

(i) **Frequency Control:** The frequency and load demand are inversely related. When load demand rises, frequency declines, and vice versa. The frequency is quite low during the highest load demand. The frequency of the system must be kept between 49.5 and 50.5 Hz. If the system frequency falls out of this range, the frequency relay will activate, and disconnect the load.

(ii) **Voltage Control:** The voltage is a crucial characteristic in an interconnected system, and at any point in the power system it must remain constant. Due to the large inductive load demand, the system voltage may drop.

(iii) **Communication:** Due to Congestion of the available frequency spectrum, the communication facility is insufficient to allow improved operation in the interconnected power system.

(iv) **Metering and Instrumentation:** Meters and sensors are positioned at various stages of the power system network to measure quantities such as active power, reactive power, current, voltage, frequency, and so on. These meters and devices are very expensive.

(v) **Reserve Capacity Shortage:** All power generation station has a certain amount of reserve power used to achieve the peak load demand at a time of peak load. This is very important in meeting the problem of load variation, and forecasting error.

2.3.5 A three-Area Interconnected Power System

A three-area interconnected power system wherein the three areas are interconnected through a tie line is shown in Figure 2.6. The individual region has its control area, and a tie line allows power to move from one control area to another. Frequency variation is very low in a single control area [34]. That means a network is very strong. However, for interconnected power systems containing three areas, individual control areas are strong, while the three areas are interlinked by weak tie-lines. Thus, several control areas can be interconnected by tie-lines.

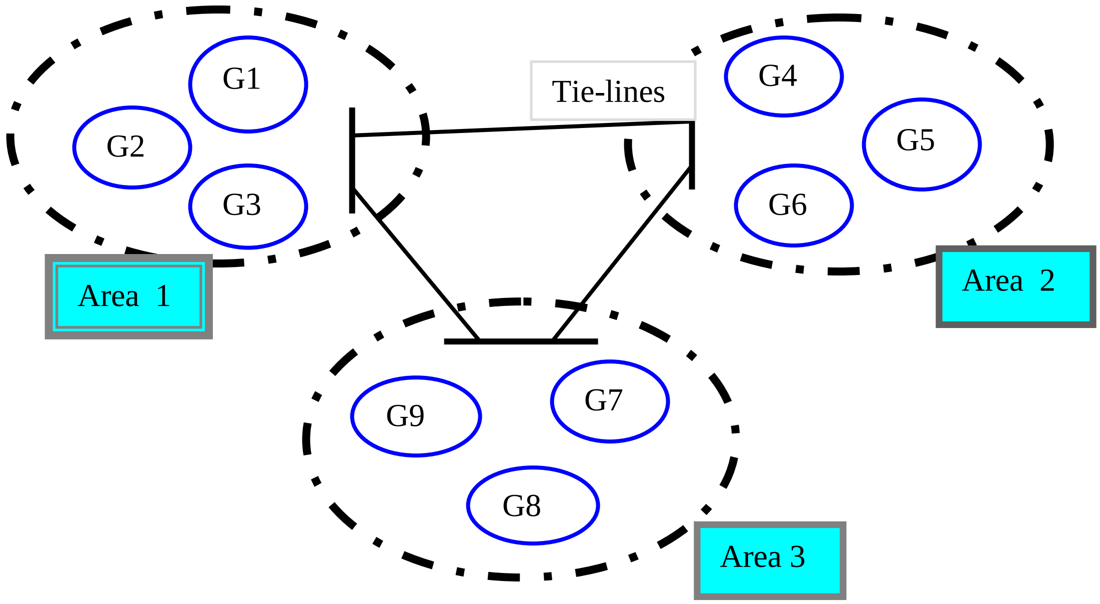

Figure 2. 6 Three interconnected power systems.

2.3.6 Area Control

Area control is defined as a system in which the common generation control or the LFC scheme can be used. A control area is usually used to describe a self-governing area. Electrical interconnection in each control area is quite high when compared to the ties in the middle of adjoining areas. All of the generators in a control region travel back and forth in a logical, and consistent manner, which is represented by a specific frequency [35].

The ALFC difficulty of a huge interconnected power system has been examined by separating it into several control areas, referred to as multi-area. In the common steady-state process, each control region of the power system must attempt to counteract the demand for power by allowing tie-line power to flow across the interconnected lines [36]. In general, the control zones have only limited access to information from the entire grid and are only able to operate their buses. They cannot, however, change the parameters on the unknown buses directly [35]. However, an area can identify the dominance of surrounding areas by sensing the flow of power in and out of its bounds, which is referred to as tie-line power[37]. The power equilibrium equations are computed at the limits of each area, taking into account the increased load caused by the exported electricity [36].

2.3.7 Frequency Variation

For a grid-connected power system, there are many loads, such as residential loads, agricultural loads, public service loads, lighting loads, etc. These loads are switched ON, and OFF without intimation. Hence, the loads demand always fluctuates. The fluctuation can be based on population growth, economic growth, behavioral (temporal) change, and weather (climate) changes [35]. But generating units are designed to produce a particular power output, and it is difficult to change generation very quickly as it is a mechanical system [38]. The frequency and voltage must both remain at standard values during operation for the electric power system to be of excellent quality [36]. For Ethiopia, the standard frequency setting is 50 Hz.

2.3.8 Major Draw Backs of Classical Controller

The majority of traditional controllers are based on frequency domain graphical design methodologies. These are the most basic and well-understood controller design approaches, and they're quite straightforward to put into practice in real-world systems, particularly for single loops. Below are some limitations on the classical controller [35]:

(i) They take a long time to act.

(ii) Since they are linear controllers, they do not consider system nonlinearities like governor dead band effects and generation rate constraints (GRCs).

(iii) They have a limited capacity of set-point tracking when there is a continuous variation of operating point which is caused by continuous load variation.

The integrator gain must be adjusted regularly when the operating point changes for a better outcome. It should also make sure that the gain value is well balanced between low overshoot in dynamic response, and quick transient recovery [39]. This is hard to do in practice since an integral controller is essentially a fixed controller that is optimal in one operating point but inefficient in another [40]. The control rule must be able to deal with the power system's dynamics. As a result, a controller based on Meta-heuristics would be appropriate for controlling the system. Control techniques based on metaheuristics provide high adaptability to changing situations and the capacity to make quick choices by analyzing imprecise data [41], [42]. Nature-based programming, model-based reasoning, and computational approaches are some of these strategies (like fuzzy sets, Particle swarm optimization, Grey wolf optimization, Artificial neural networks, Novel quasi oppositional harmony search algorithm, Chimp optimization algorithm, Moth flame optimization algorithm, Multi-verse optimization algorithm, and Genetic algorithms) [42].

2.4 Review of Related Work

The LFC crisis has been largely treated for more than three decades. The pioneering work of some control engineers, most notably Bode, and Nyquist has set the relations among the frequency response of the control system, and its closed-loop operation in the time domain. Recent advances in this area are the use of perceptions such as neural networks, fuzzy logic, genetic algorithms, etc., to address the problems related to the construction of the LFC of power systems with non-linear models, and /or insufficient understanding of the system required its proper modeling [42]. Adopting the dynamics of the power system, as well as the effects on the functionality of the normal system that is fully dynamic; the present chapter includes an important evaluation of the various methods of LFC control for their key capabilities.

The authors in [43] have proposed an online smart control technique to improve the transient response of three areas interconnected power system comprises area one- Non reheat thermal, area two-reheat thermal, and area three-hydropower plant. The authors compared the performance indexes (IAE, ISE, and ITSE) and time-domain specifications such as settling time, overshoot, undershoot, and maximum range of a Hybrid Particle Swarm Optimization Algorithm (H-PSO) (i.e., combination of Bacteria Foraging Algorithm (BFA), and PSO). From the simulation results, H-PSO is considered to be superior compared to BFA and PSO optimization techniques. The drawback of the paper is that it does not consider the effect of governor dead band non-linearity, generation rate constraint, and communication delay link. In the deregulated power system, the authors in [44] present a model predictive control(MPC) concept introduce in two areas, and four areas thermal power plant by considering the various load conditions to evaluate the comparative performance of the controllers along with conventional PID controller. The simulation results indicate that the MPC scheme has robustness against the load perturbation with a good transient response. However, the research does not consider the effect of governor dead band non-linearity, generation rate constraint, and communication delay link.

An adaptive neuro-Fuzzy inference (ANFIS) based LFC technique with 1% step load perturbation on the area one is employed in a three areas interconnected power system (thermal-thermal-hydro) is proposed in [7]. With regards to the proposed power system, the comparative performance of ANFIS, conventional PID, and Fuzzy based controllers are presented based on the simulation. The results validate that the ANFIS based controller is faster than the conventional controller, hence, improves a dynamic response. However, the paper does not consider the effect of GRC, and governor dead band non-linearity. The deviation in load frequency and tie-line power of an interconnected thermal power system (three-area AGC) is simulated in [45]. The performance, and dynamic responses of load frequency, and deviation tie-line power are compared using GA based controller, and fuzzy logic controller. The results specify that the GA-based controller shows better performance and satisfies the AGC performance requirements with a reasonable dynamic response.

In [46], the authors simulated a hybrid neuro-fuzzy (HNF) for interconnected four area power systems: area one and area two comprise of a reheat thermal power plant, while area three and area four contain the hydropower plant. The performance evaluation is done by comparing HNF with Fuzzy, Artificial neural network (ANN), ANFIS, and traditional PI control. The result shows that improved dynamic response and faster response are found in intelligent HNF controllers. It also shows that HNF based controller can handle non-linearity.

The interlinked power system comprises hydroelectric power, and wind power plants are presented to control the frequency and tie-line power system [47]. A PID controller is employed in a power system comprised of a wind system (considering governor dead band, generation rate constraint, and turbine dynamics), and the hydropower plant (comprised of generation rate constraint). The simulation result depicts that the presented controller provides system security. A three-area LFC of an interlinked power system based on a decentralized adaptive control is presented in [48]. The paper compares decentralized adaptive control with conventional PI controllers. The simulation results reveal that a decentralized adaptive control scheme is responsive to changes in power system parameters and bounded disturbances acting on it. In [49] proposes an Adaptive Load Frequency LFC based on the Self-Tuning Regulator (STR) for a multi-area Automatic Generator Control Simulator (AGCS). The paper compares the tracking performance STR, integral, and combination of integral with STR. To accommodate a control center with adaptive LFC features, both dynamic and static solutions of an integrated power system are examined. The STR controller has greater tracking properties than the integral or a combination of integral and STR controllers, according to the simulation results.

A multi-source power generation is proposed in [50] for the LFC of a realistic power system. In the single area power system, the dynamics of thermal with reheat turbine, hydro, and gas power plants are covered. To eliminate the practical access, costly, and difficult problem of access to all the state variables, an optimal output feedback controller that uses only the output state variables is proposed. Thermal and hydropower plants are both considering GRCs. The optimal output feedback controller's performance is compared to that of the complete state feedback controller. With negligible steady-state error, this controller achieves an acceptable balance between frequency overshoot and transient oscillations. The influence of the regulatory parameter (R) on the frequency deviation response is investigated using sensitivity analysis. The simulation result shows that the proposed controller is quite robust and optimum. It also depicts that LFC design founded on an optimal linear regulator (OLR) is simple, cheap, systematic in methodology, and computationally efficient.

In [51] uses an optimal control method based on a linear-quadratic Gaussian (LQG) controller with integral action to solve the problem of compensating frequency disturbance during load variation. A two-area LFC power system with interconnections is being considered. Uncertainties and disturbances for robust control purposes are considered. Existing AGC, PID, LQR, and fuzzy logic controllers are compared to investigate the dynamic response of the proposed controller. The simulation result depicts that LQG shows better performance. To get the parameters of the proposed fuzzy-PID controller, a teaching-learning-based optimization (TLBO) approach is utilized in a novel fuzzy-based PID controller for AGC of an interconnected thermal power system in [52]. The proposed controller is compared with LCOA, GA, PS, and SA-based controllers. The simulation result reveals that TLBO based novel fuzzy PID controller shows the superior dynamic response in terms of settling time, undershoot, and overshoot in frequency, and deviation in tie-line power. By changing all the system parameters the robustness of the system is also studied.

Using PSO-based PID controller tuning, and AGC for a two-area interconnected power system has been constructed. A PSO-based PID controller generates the two control signals, one of which is fed to each area for frequency response augmentation. The integral Square Error is used to calculate the performance index (ISE). The simulation and comparison results suggest that AGC of a two-area power system using a PSO-based PID controller aids in achieving the nominal frequency response with load variation is reported in [53]. An ALFC of a single area power system based on PSO is presented in [54]. The result of conventional PI and PSO optimized PID self-tuning controllers are compared and the proposed method showed that the presented controller can produce the greatest dynamic response for a step load perturbation.

The decentralized LFC problem for three areas power system that functions under a deregulation scheme is described in [55]. The research presents a GA-based PID controller for solving the decentralized LFC problem in a multi-area power system. The effect of the possible contracts is regarded as a collection of new input signals in each control region. In the presence of plant parameter variations and system nonlinearities, this technique has the benefit of being insensitive to substantial load changes and disturbances. This technique results in a versatile controller with a simple structure that is straightforward to construct and beneficial in real-world power systems. The simulation result reveals that the GA-based PID controller shows robust performance. The paper in [56] presents the ALFC of three areas interconnected thermal power plants utilizing GRC, and ANN independently. The author compares the dynamic performance evaluation of GRC and ANN controllers. The simulation result shows that the execution of the ANN controller is better for GRC by reducing overshoots. It also reveals that ANN-based controller provides the more exact, and quicker result.

The AGC of an interlinked hydroelectric power system based on a feed-forward neural network is presented in [57]. Two networks are utilized, one for system identification and the other for control, both of which are trained using a backpropagation algorithm (BPA). The input-output mapping of hydro systems was examined using ANNs, and the controller was built on a two-area hydroelectric power system model. Results of the simulation showed the ANN superiority over traditional linear PID controllers. The paper in [58] proposes moth-flame optimization (MFO) algorithm for the AGC of a three-area hydropower scheme. This work is to defeat the damped oscillations, subjected to load disturbance concerning area frequency deviation, and tie-line power. The paper compares the performance of Sugeno fuzzy logic (SFL) based on MFO (MFO-SFL) with GA-SFL. The outcomes are compared both online and offline in normal working situations. Variation of several significant physical parameters that deviate by 25% from their rated values is used to test the robustness of the proposed MFO-SFL controllers. In comparison to the GA-based technique, the simulation results suggest that the MFO-based PID controller provides greater dynamic control and robust performance.

An MFO algorithm based on a PID controller optimal gain parameters finding for AGC is applied to a single area with hydroelectric, thermal, and gas hybrid power generation units. The efficiency of MFO is compared with TLBO and the Differential Evolution (DE) optimization algorithm. The performances of the controllers are compared with ITAE value, Settling time, and overshoot. Robustness analysis was also done by varying the parameters of the single area with hydroelectric, thermal, and gas hybrid power plant by ±25%. The author in [59] indicates that MFO based controller shows better performance as compared to that of the TLBO and DE algorithm-based feedback controller. A hybrid Fuzzy Fractional Order Proportional Derivative-Fractional Order Proportional Integral (hFOFPDFOPI) controller based Multiverse Optimization algorithm (MVO) is suggested in [60]. Here, MVO is applied to get optimal gain parameters of the hFOFPD-FOPI controller by employing the ISE criterion. The proposed controller is compared with numerous control methodologies with different optimization techniques-based controllers. The results are shown below:

Table 1 Performance indices of different controllers for the AGC problem are compared in this table.

Technology : Controller name	ISE Values x10-5
QODSA: PI	102
GA: PI	90.3

BBBO: PID	22.3
hFA-PS: PID	19.1
hGGSA-PS: PID	18.8
ICA: FPI	4.88
ICA: FFOPI	1.77
ICA: FFOPI-FOPD	0.468
Proposed MVO: hFOFPD-FOPI	**0.0456**

When compared to the results of other control approaches, the superiority of the envisioned controller is ensured. Further robustness analyses were carried out in a real-time simulation environment, taking into account three aspects: i) the effect of altering system characteristics such as time constants and others, ii) the influence of different nominal load demands, and iii) the effect of physical restrictions.

According to [55] the ALFC performance of a three-degree-of-freedom MVO-based proportional–Integrative–derivative (3DOF–PID) controller for a four-area linked (all reheat thermal) power system model. In one of the regions, the system under investigation was equipped with an interline power flow controller. Important physical constraints like time delay, governor dead band, boiler dynamics, and generating rate constraint are all implemented in the aforementioned system. The MVO-based controller's performance is compared to that of the GA-based controller. The simulation results show that the MVO-based 3DOF-PID controller is superior in terms of settling time, peak deviation, and oscillation magnitude. The sensitivity of the MVO-based 3DOF-PID controller from nominal to under loading, as well as model parametric uncertainties, are also investigated. This simulation result shows that the MVO-based 3DOF-PID controller produces almost similar responses.

In [13] a QOHS based PID gain tuning is applied to a single area, and two area hydropower system model of AGC. Optimization performance proposed algorithms are compared with IMC control, and maximum peak resonance specification (MPR) control. In addition, the single-area test system's robustness is assessed by varying the hydro-time turbine's constant by up to ±50%. Comparative dynamic performance analysis of the two-area test system is also carried out by applying step load perturbation at unequal time intervals in both regions. The simulation results show that the proposed QOHS enhances overall system performance and may be used as a hydropower system limited optimization issue.

To summarize, a comprehensive literature survey about the load frequency control problem is presented in this chapter. Various control techniques, such as classical, adaptive, and intelligent are discussed. The Summary of techniques used, an area considered, the proposed optimization technique, the controller used with main advantages, and disadvantages are shown in the table below:

Table 2: Sampled summary of literature review

Area considered	Power plants considered	Proposed optimization techniques	Comparison made between	performance evaluation criterion	Advantage of proposed techniques	Source
3- areas	Area-1: Non-reheat thermal Area-2: Reheat thermal Area-3: Hydro	H-PSO	PSO, BFA, and H-PSO are compared	IAE, ISE ITSE Settling time Overshoot	Better in small scale system - It can handle uncertainty and nonlinearity -Their insensitivity to changing loads	[43]
2-areas, and 4-areas separately	All areas are deregulated thermal power plant	IMC	IMC, and Conventional PID	Settling time & Overshoot	Works well in a MIMO system, good constraint handling systematic & performance	[44]
3- areas	Area-1 &2: reheat thermal Area-3: hydro	ANFIS	ANFIS, fuzzy sets, and Conventional PID	Settling time & Overshoot	Better in handling s uncertainty and nonlinearity Perform better in small-scale systems. Insensitivity to varying loads, hence, delivers a robust LFC performance.	[7]
3-areas	All are reheated thermal	GA	GA, and fuzzy based controller	Settling time & Overshoot	Better	[45]
4- areas	Area-1&2: thermal reheat, Area-3&4: hydro	HNF	Fuzzy, ANN, ANFIS, HNF, PI, and PID	Settling time & Overshoot	Better, and handling non-linearity	[46]

CHAPTER-THREE

METHODOLOGY

3.1 Preamble

This section deals with data collection, and analysis, mathematical modeling of the three areas interconnected power system, and design based on Metaheuristics optimization algorithms (ChOA, QOHS, MFO, and MVO) based PID controller to get an optimum result of tuning parameters. In considering a three area hydro-thermal interconnected power system only a single generator for each generating station is considered for each control area. Each generation station is assumed to have equal in each parameter used in the calculation for identical power plants. Finally, the system is simulated on MATLAB software both in Simulink and script.

3.2 Methods

As shown in Figure 3.1, to accomplish the required thesis work, the following procedure has been followed. The closely related papers and kinds of literature are studied. Then the essential data used throughout this research work are collected and analyzed. The collected data is analyzed mathematically and graphically for developing system modeling. The modeling and simulation result of the system is equated with different Metaheuristics based control algorithms for speed, and tie-line power control. The block diagram in figure 3.1 summarizes the method followed throughout the research work.

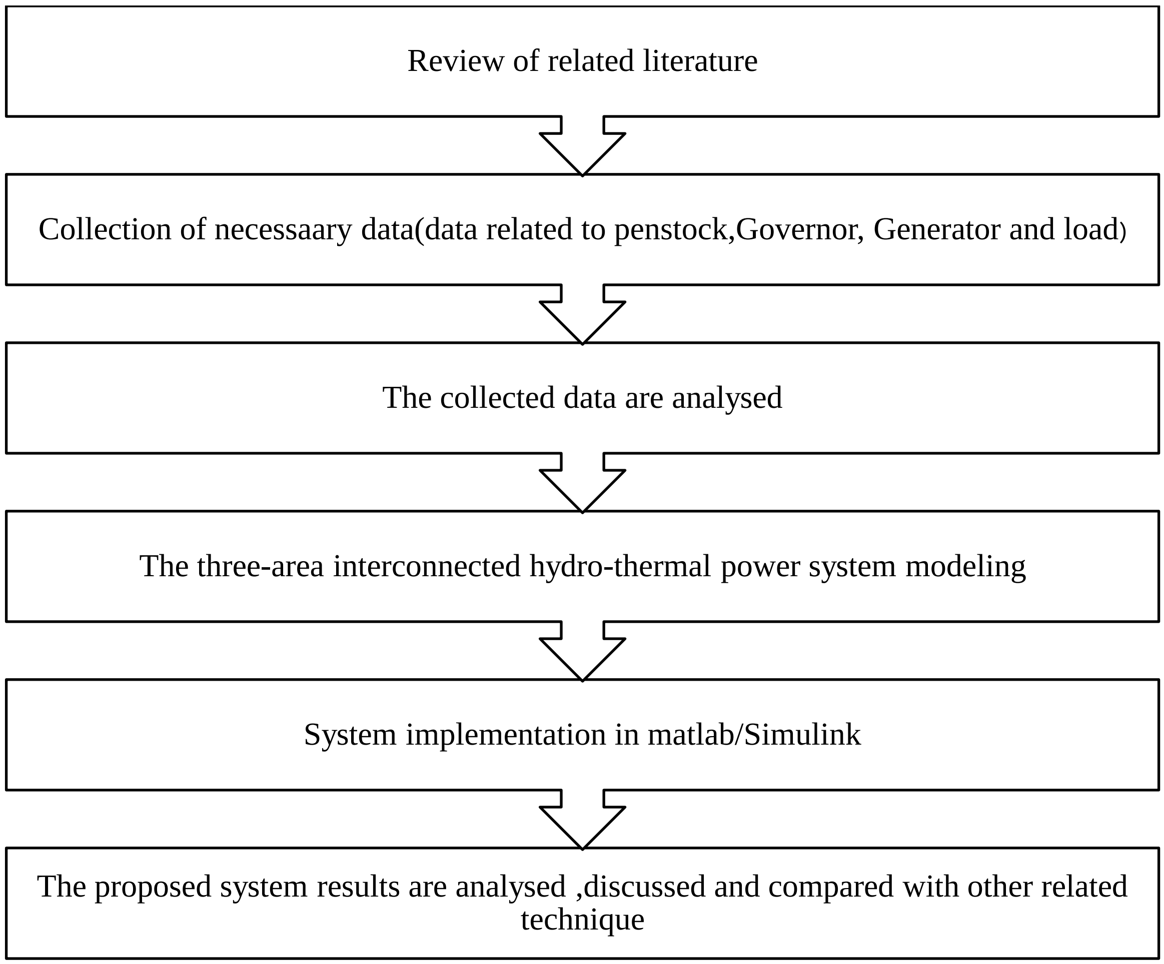

Figure 3. 1 Block diagram representing the research methodology.

3.3 Modeling of Automatic Load Frequency Control

The proposed system block diagram of the ALFC for the thermal-thermal-hydropower system is shown in Figure 3.2. The change in the reference speed and actual rotor speed is controlled by using a speed regulator. The governor is the equipment used to control the speed/frequency of a power system by checking the status of the wicket gate/valves.

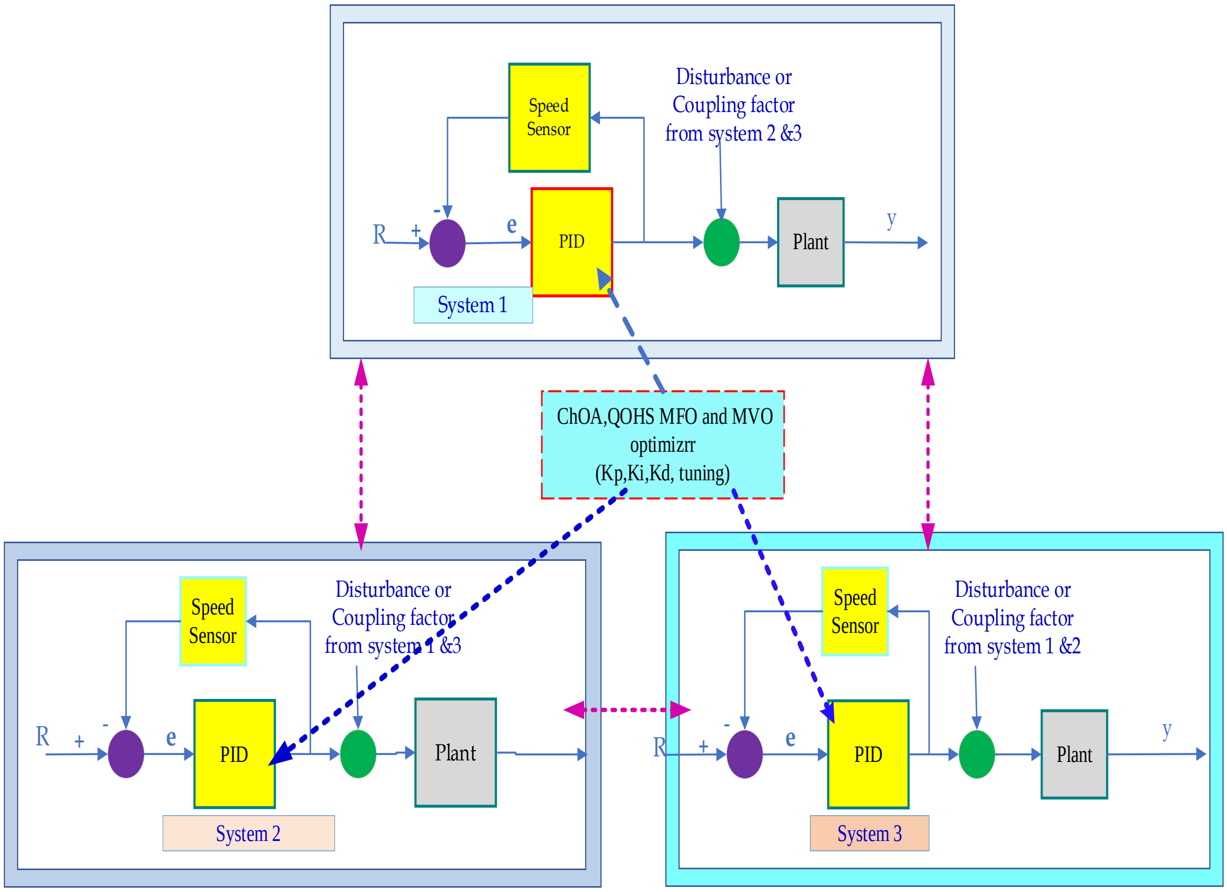

Figure 3. 2 PID tuning considered multivariable system.

3.4 Modeling of Hydro-Power Plant Components

3.4.1 Electro-Hydraulic Governing System

A governor is a device that regulates and measures the speed of a turbine. The primary functions of hydraulic governors are to start, maintain, and adjust unit speed for synchronization with the running units/grid, to maintain system frequency after synchronization by adjusting turbine output to load changes, to share load changes with the other units in a planned manner in response to the system frequency error, and to adjust unit output in response to the operator or other supervisory commands, and to accomplish normal shutdown or emergency over speed shut down for protection. There is two most common type of governors for power plants [4]. These are- mechanical governor and electro-hydraulic governors. In this study, the electro-hydraulic governor is considered. The operating principle of the electro-hydraulic governing system is very analogous to that of mechanical hydraulic governors. The main distinction is that speed detection, droop compensation, and processing tasks are all done electrically. The output drives the electrical-mechanical transducer, which controls a pilot valve and a pilot valve servomotor. The rotor speed of the turbine is measured electronically with high [9], [35]. The low-power functions are performed by a PID controller in this sort of governor. The controller can provide control action tailored to individual process requirements by changing the three parameters in the PID controller algorithm.

The responsiveness of the controller to an error, the degree to which the controller overshoots the setpoint, and the degree of system oscillation can all be used to describe its response. The proportional term results in a control action proportionate to the size of the error input, as well as an immediate response to the error level input. The proportionate term response has a substantial impact on the governed system's stability. The integral term generates a control action that grows in proportion to the magnitude of the error input. It also trims the error input to the governor controller to ascertain the governed system's steady-state accuracy. The derivative term generates a control action that is proportionate to the erroneous input rate of change. By permitting bigger proportional and integral gains while retaining a stable control system, the derivative term serves to increase the controlled system's stability limitations [29], [61].

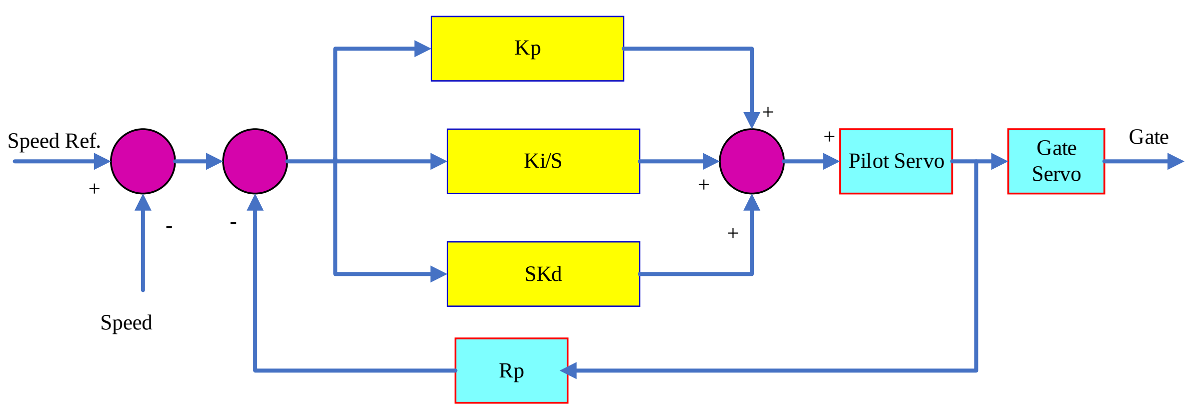

Figure 3. 3. Typical electro-hydraulic governor system [2].

where *Kp* represents the proportional gain constant and *Ki* represents the integral gain constant while *Kd* and *Rp* represent the derivative gain constant and permanent drop respectively.

In the equation, the PID governor's transfer function is expressed in terms of proportional, integral, and derivative gains (3.1).

$$\frac{y}{w_{ref} - w_s} = \frac{1}{R_p}\left[\frac{K_d s^2 + K_p s + K_i}{K_d s^2 + (K_p + {}^{1}\!/_{R_p})s + K_i}\right] \tag{3.1}$$

3.4.2 Hydro Turbine Model

The physical description of hydraulic turbines, as well as the equations characterizing the suitable mathematical models for their representation in power system dynamics, are presented in this section [36]. Variations in flow and output mechanical torque for turbine speed, gate opening, runner blade movement, and the differential in pressure between the turbine inlet and outlet characterize turbine dynamics.

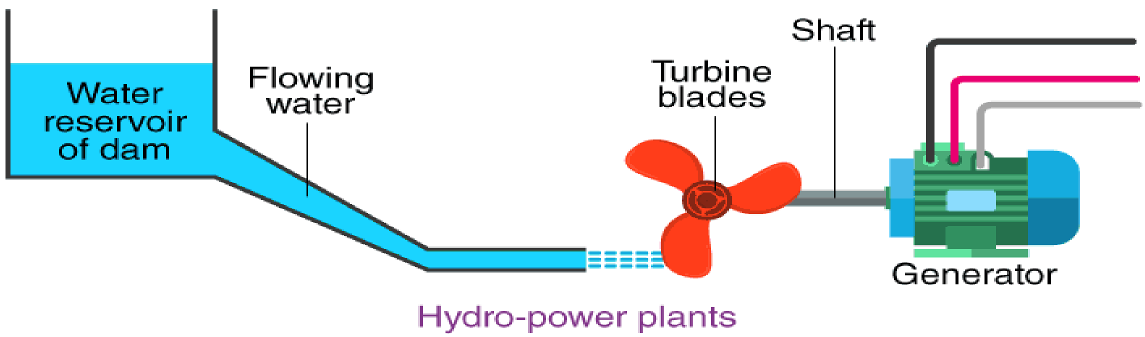

Figure 3. 4 Hydro-turbine block [36].

The water travels from the storage tank to the hydro turbine through the penstock. The tangent characteristic of a hydro turbine is determined by the dynamics of water flow in the penstock, and we shall determine the transfer function of the hydro turbine. When a minor disturbance to a steady-state situation is considered, the turbine can be represented by the linearized equations:

$$\begin{aligned} q &= a_{11}h + a_{12}w + a_{13}p \\ t &= a_{21}h + a_{22}w + a_{23}p \end{aligned} \tag{3.2}$$

where q- per unit deviation inflow, h - per unit change in the head, w - per unit change in speed, p- per unit variation in gate position, t - per unit variation in torque

The above two equation are an algebraic equation which relates the water flow following changes in height, and gate position similarly the change in torque produced following small change in head, speed, and gate position.

Using these equations and the dynamics of the water movement in the penstock, a transfer function model of the hydro-turbine can be obtained. The transfer function involving the mechanical power output of the hydro turbine to the gate position can be expressed as below:

$$\frac{P_{GV}}{P_m} = \frac{a_{23} - T_w(a_{13}a_{21} - a_{11}a_{23})s}{1 + a_{11}sT_w} \tag{3.3}$$

where P_{GV} gate position, P_M mechanical time constant, T_W water Time constant

The coefficient in the two algebraic equations can be interpreted as prior derivatives of deviation inflow (q) for the gate position, head, and speed. Similarly derivatives of torque (t) for the head, speed, and gate position as described below

$$\begin{aligned} a_{11} &= \frac{dq}{dh} \\ a_{12} &= \frac{dq}{dw} \\ a_{13} &= \frac{dq}{dp} \end{aligned} \quad \& \quad \left.\begin{aligned} a_{21} &= \frac{dt}{dh} \\ a_{22} &= \frac{dt}{dw} \\ a_{23} &= \frac{dt}{dp} \end{aligned}\right\} \tag{3.4}$$

For the design purpose an ideal turbine at nominal speed and head (lossless turbine) are considered with the following parameters:

$$a_{11} = 0.5,\ a_{12} = 0,\ a_{13} = 13,\ a_{21} = 1.5,\ a_{22} = -1,\ a_{23} = 1$$

If we make use of these values, and substituting them in equation (3.3) it can be reduced to an equation (3.5):

$$\frac{P_m}{P_{GV}} = \frac{1 - sT_w}{1 + 0.5sT_w} \tag{3.5}$$

From the above transfer function, the model of the hydro turbine has one zero on the right half of the s-plane. Such a system is known as a non-minimal phase system. If unit step input is applied to the turbine; the system gives the following expression:

$$\Delta P_m(t) = (1 - 3e^{\frac{-2t}{T_w}}) \tag{3.6}$$

Thus, $\Delta P_m(0)$ =-2, and $\Delta P_m(\infty)$=1

So, such special characteristics of hydro turbines need a special type of governor as shown below. Calculation of time constant of water; *Tw* is the time it takes for water in the penstock between the turbine inlet and the turbine to accelerate., and forebay.

$$T_w = \frac{LV}{H_T g} \tag{3.7}$$

where, *L*- Penstock length of in fed, *V*- Velocity of water in fed/sec, H_T - Head in fed, g- gravitational acceleration in fed/sec^2

3.4.3 Model of Synchronous Generator

The synchronous generator is the primary source of electric energy in an electrical power system. The electrical frequency is related to the mechanical rotation of the synchronous generator's rotor. This electrical frequency is determined by attaining active power balancing (electrical and mechanical torques), or a match between the generator's electrical power output and the system load. When a load changes, the generator's electrical torque changes instantly, resulting in an imbalance between the mechanical and electrical torques[10]. This is indicated as a net accelerating (decelerating) torque.

$$\mathrm{T}_a = \mathrm{T}_{\mathrm{me}} - \mathrm{T}_{\mathrm{el}} \tag{3.8}$$

where T_a -is a net accelerating torque (N.m), T_{me} - is a machine mechanical torque (N.m), T_{el} - is an electrical torque (N.m).

The mechanical and electrical torques on a generator are both positive. The unbalance in the applied torques accelerates the generator and prime mover's combined inertia. As a result, we have the equation of motion described as shown in Figure 3.9.

$$J \frac{dw_m}{dt} = T_a = T_m - T_e \tag{3.9}$$

where J – is the generator combined moment of inertia in the turbine ($Kg.m^2$), W_m- is the rotor angular velocity (mech. rad/sec), T-time (sec)

The inertia constant H can be defined as the ratio of kinetic energy (watt-seconds), and the VA base as shown in equation (3.10):

$$H = \frac{1}{2}\frac{J{w_{mo}}^2}{VA_{base}} \tag{3.10}$$

Then, J- Maybe written in terms of H as shown in equation (3.11):

$$J = \frac{2HVA_{base}}{{w_{mo}}^2} \tag{3.11}$$

Substituting equation (3.11) on equation (3.9)

$$2\frac{H}{{w_{mo}}^2}VA_{base}\frac{dw_m}{dt} = T_{me} - T_{el} \tag{3.12}$$

The per-unit form of equation (3.10)

$$T_{base} = \frac{VA_{base}}{w_m} \tag{3.13}$$

$$2H\frac{d\overline{w}_r}{dt} = \overline{T}_m - \overline{T}_e \tag{3.14}$$

$$\varpi_r = \frac{\omega_m}{\omega_{mo}} = \frac{\omega_r}{\omega_o} \tag{3.15}$$

where ω_r - rotor angular velocity [elec. Rad/s], and at rated speed, ω_o - rated angular velocity [elec. Rad/s]. Here the super bar notation signifies a per unit quantity. The mechanical starting time setting is described in equation (3.16)

$$M=2H(s) \tag{3.16}$$

The equation of motion may be written as:

$$M\frac{d\varpi_r}{dt} = \overline{T_m} - \overline{T_e} \tag{3.17}$$

It's worth noting that the terms inertia constant will be used interchangeably for M and H. It is better to express the relationship presented in equation (3.13) in terms of mechanical and electrical power rather than torque for AGC research. Equation (3.18) depicts the relationship between power P and torque T.

$$\mathrm{P} = \mathrm{T.W_r} \tag{3.18}$$

We can write as; because we are considering minor deviations (represented by the prefix Δ) from initial values (denoted by subscript), it can be described as in equation (3.19).

$$\left.\begin{aligned} P &= P_0 + \Delta P \\ T &= T_0 + \Delta T \\ \omega_r &= \omega_0 + \Delta\omega_r \end{aligned}\right\} \tag{3.19}$$

When equation (3.19) is substituted for equation (3.18), the result is shown in equation (3.20).

$$P_0 + \Delta P = (\omega_0 + \Delta\omega_r)(T_0 + \Delta T) \tag{3.20}$$

In equation (3.21), higher-order terms are ignored and only the link between perturbed values is considered.

$$\Delta P = \omega_0 \Delta T + T_0 \Delta\omega_r \tag{3.21}$$

Therefore;

$$\Delta P_m - \Delta P_e = \omega_0 (\Delta T_m - \Delta T_e) + (T_{m0} - T_{eo})\Delta\omega_r \tag{3.22}$$

Now that the electrical and mechanical torques are equal in the steady-state (T_{me}= T_{el}), and the speed expression in per unit =1, it may be written as shown in equation (3.23).

$$\Delta P_m - \Delta P = \Delta T_m - \Delta T \tag{3.23}$$

As a result, the motion equation may now be simplified as indicated in (3.24).

$$M \frac{d\omega_r}{dt} = P_m - P_e \tag{3.24}$$

Where M is measured in seconds and all other values are expressed per unit. Equation (3.24) can be represented in the Laplace domain to analyze power system dynamic performance, using the transfer function expressed in equation (3.25).

$$Ms\Delta\omega_r = \Delta T_m - \Delta T_e \tag{3.25}$$

Solving for the frequency change, it can be written as shown in equation (3.26)

$$\Delta\omega_r = \frac{1}{Ms}(\Delta T_m - \Delta T_e) \tag{3.26}$$

The change in electrical power is then written as an equation to account for the resistive (frequency-independent) and motor (frequency-dependent) loads (3.27).

$$\Delta P_e = \Delta P_L + D\Delta\omega_r \tag{3.27}$$

where ΔP_L - None frequency sensitive load change, $D\Delta\omega_r$ - Frequency sensitive load change, D -Load damping constant. The damping constant is represented as a one percent change in frequency caused by a one percent change in load. Equation (3.27) is substituted for equation (3.26), and the frequency change is calculated (3.28).

$$\Delta\omega_r = \frac{1}{Ms + D}(\Delta T_m - \Delta T_L) \tag{3.28}$$

The frequency deviation is used to characterize the dynamics of the synchronous generator. These are the results of a mismatch in MW generation and load demand. It also considers the power system's total inertia, as well as the load's frequency-dependent and independent components. For a power system with more than one generating unit, it can be described as equation (3.29).

$$\Delta\omega_r = \frac{1}{M_{eq}s + D}(\Delta T_{mi} - \Delta T_L) \tag{3.29}$$

Where: ΔT_{mi} - Change in mechanical power for generating unit i

$$M_{eq} = \Sigma M_i[s] \tag{3.30}$$

where $M_i -$ Inertia constant of generating unit i

This assumes that all generators respond to changes in system load in a consistent manner, allowing them to be replaced by an equivalent generator. Figure 3.5 depicts the synchronous generator's block diagram representation.

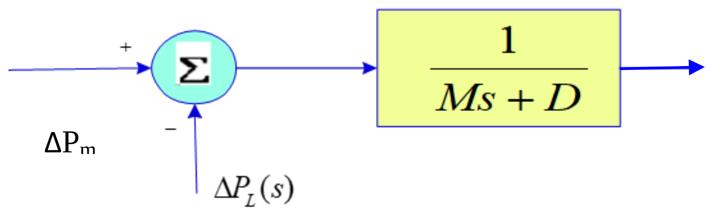

Figure 3. 5 Model of synchronous generator [4].

3.5 Thermal Power Plant Modeling

To develop a model for steam turbine, let's start with a transfer function model relating a steam entering, and leaving steam vessels.

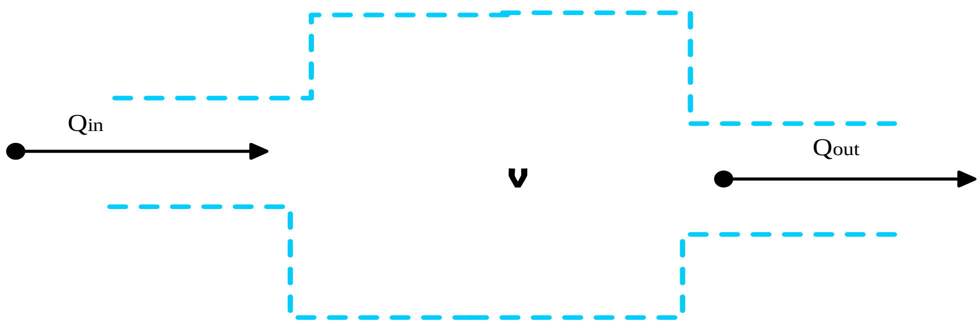

Figure 3. 6 Steam vessels equation [10].

The continuity equation for steam vessels is given by:

Steam mass in (Q_{in}) and mass out (Q_{out}) is given in equation (3.31)

$$Q_{in} = \rho A_1 V_1 \Delta t, and \; Q_{out} = \rho A_2 V_2 \Delta t \tag{3.31}$$

$$w = v * \rho \tag{3.32}$$

where w- the weight of steam in the vessel (kg), v- the volume of a vessel (m^3), ρ - Density of a steam (kg/m^3), Q- Steam mass flow rate (Kg/s), t- time in seconds

Assume that the flow rate out of a vessel is proportional to the vessel's pressure.

$$Q_{out} = \frac{Q_o}{P_o} P \tag{3.33}$$

where P- Pressure of steam in a vessel(Kpa), P_o- rate pressure, Q_o- rate flow out of a vessel

In a vessel with a constant temperature:

$$\frac{d\rho}{dt} = \frac{dP}{dt} \cdot \frac{d\rho}{dP} \tag{3.34}$$

where $\frac{d\rho}{dP}$ a change in steam density due to pressure.

Substitute the equation of continuity equation:

$$Q_{in} - Q_{out} = V \frac{\partial\rho}{\partial P}\frac{dP}{dt} = \frac{\partial\rho}{\partial P}\frac{P_o}{Q_o} \cdot \frac{dQ_{out}}{dt} \tag{3.35}$$

$$\mathrm{Q_{in}} - \mathrm{Q_{out}} = \mathrm{T_v}\frac{dQ_{out}}{dt} \tag{3.36}$$

Where $\mathrm{T_v} = \frac{P_o}{Q_o} V \frac{\partial\rho}{\partial P}$

The Laplace transform becomes equation (3.36) shown in (3.37)

$$\frac{Q_{out}}{Q_{in}} = \frac{1}{1 + \mathrm{T_v} s} \tag{3.37}$$

As a result, the Steam Vessel's transfer function is shown (3.37). where *Tv*- is the temporal constant for a steam vessel.

When steam enters the high pressure (HP) section through the control valve and the input piping, this study considers a tandem compound fossil fuel single reheat turbine, which is typically utilized. The steam chest is the enclosure for the control valve. The chest and the inlet pipe to the HP section store a significant amount of steam. Figure 3.7 depicts a tandem Compound Single Reheat Steam Turbine.

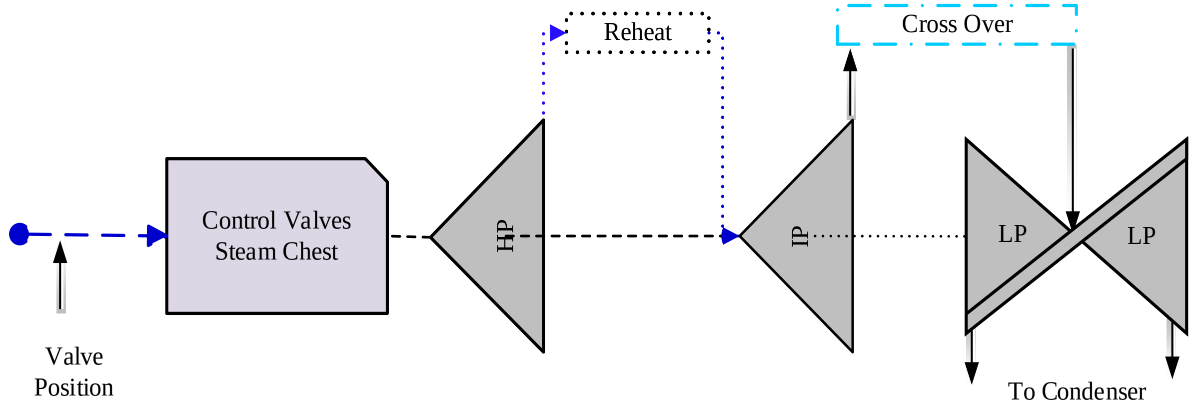

Figure 3. 7. Block diagram of tandem compound single reheats steam turbine [10].

Through the reheat intercept valve (IV) and the inlet piping, reheat steam enters the IP turbine section. The steam is routed through the crossover piping from the IP section exhaust to the LP intake. To develop a model for a steam turbine, let’s start with a transfer function model relating to steam entering and leaving a vessel.

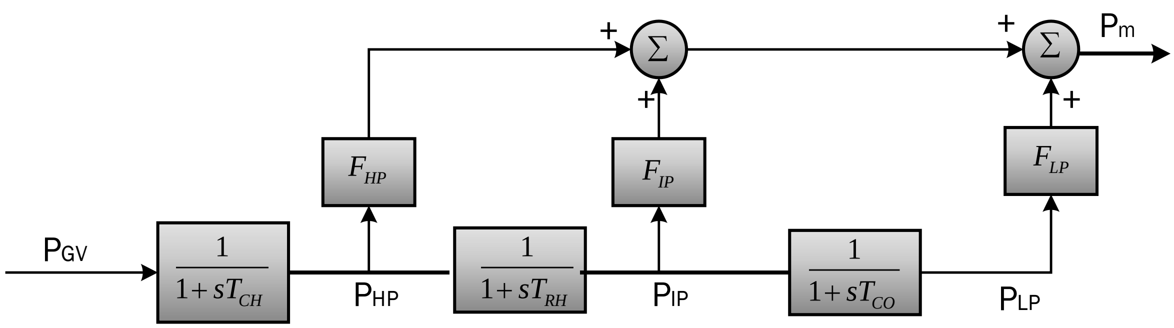

Figure 3. 8 Approximate linear models of steam turbine [10].

From the figure 3.8 block diagram, the transfer function on equation (3.38) can be developed.

$$\frac{dP_{HP}}{dt} = \frac{P_{GV} - P_{HP}}{T_{CH}} \tag{3.38}$$

$$\frac{dP_{IP}}{dt} = \frac{P_{HP} - P_{IP}}{T_{RH}} \tag{3.39}$$

$$\frac{dP_{LP}}{dt} = \frac{P_{LP} - P_{LP}}{T_{CO}} \tag{3.40}$$

$$P_m = P_{HP}F_{HP} + P_{IP}F_{IP} + P_{LP}F_{LP} \tag{3.41}$$

But, $F_{HP} + F_{IP} + F_{LP} = 1$

where P_{GV} - Output power from the control valve, T_{CH} - Time constant of steam chest, T_{RH} - Time constant of reheater, T_{CO} - Time constant of steam storage or Cross-over, F_{HP} - High-pressure turbine power fraction, F_{IP} - Intermediate pressure turbine power fraction, F_{LP} - Low-pressure turbine power fraction, P_m- Equivalent generator input mechanical power.

During normal operation, the control valves adjust the steam flow through the turbine for LFC. Due to the changing time of the steam chest and inlet pipes to the H_P section, the reaction of steam flow to a change in control valve opening exhibits a time constant T_{CH}. This time constant ranges from 0.2 to 0.3 seconds [10]. In the event of over speed, the intercept valve is often employed only for fast regulation of turbine mechanical output. Because it is the head of the reheater and controls steam flow to the IP and LP sections, which provide almost 70% of the total turbine power, it is particularly effective for this function. Only the building of pressure in the reheater volume can modify the steam flow in the IP and LP portions. The reheater holds a significant volume of steam, and the time constant T_{RH} is in the region of 5 to 10 seconds. The steam flow entering the LP portions is subjected to an extra-time constant T_{CO}, which is on the order of 0.5sec, due to the crossover pipes. The impacts of the incoming steam chest, reheater, and the nonlinear characteristics of the control and intercept valves are depicted in Figure 3.9, which depicts the block diagram of the tandem-compound reheat turbine.

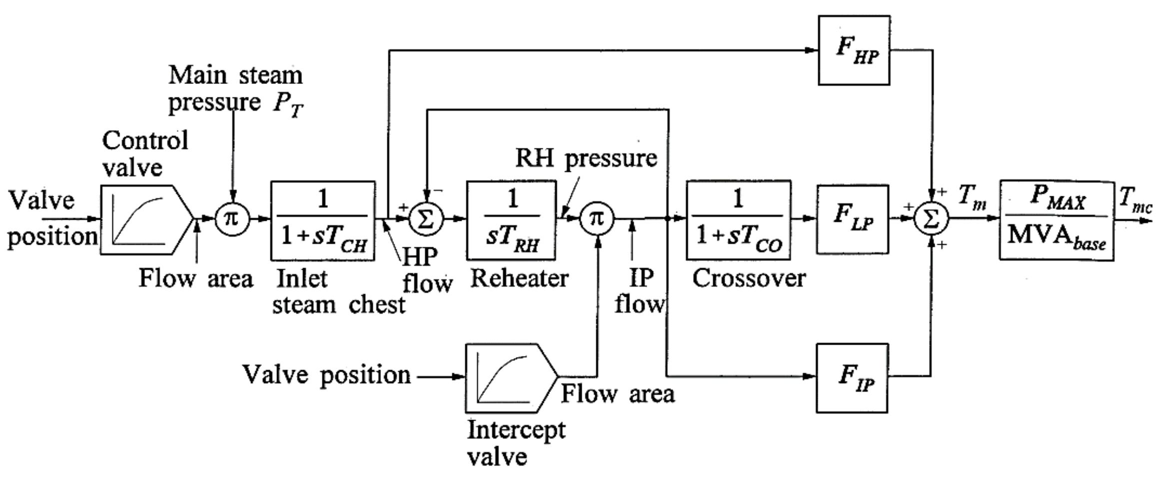

Figure 3. 9 A flow diagram of a single reheat tandem compound steam turbine model [4].

3.6 Modeling of the Tie-Lines

Through tie-lines, one or more transmission lines in an interconnected power grid can connect various places [31]. When two locations have different frequencies, there is a power exchange between the two places that are connected by tie lines. Tie-line trades in area *i* and area *j* (*Pij*), as well as the tie-line synchronization torque coefficient, account for the power (Tij). As a result, we can also state that the integral of the frequency divergence between the two locations is a power error owing to the tie-line.

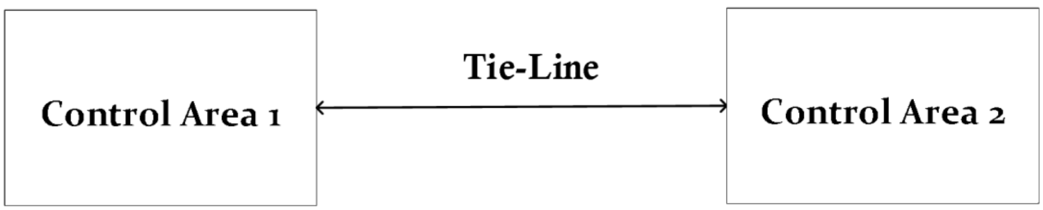

Figure 3. 10 Power transfer through tie line.

In Figure 3.10, there are two control regions, and power is to be transferred from one to the other. P12 denotes power transferred from area 1 to area 2 via tie lines, X12 denotes series reactance between areas 1 and 2, and |V1| and |V2| denote the magnitude of voltages in areas 1 and 2.

$$P_{12} = \frac{|V_1||V_2|}{X_{12}} \sin(\delta_1 - \delta_2) \tag{3.42}$$

$$P_{12} = \frac{|V_1||V_2|}{X_{12}} \cos(\delta_1 - \delta_2)(\Delta\delta_1 - \Delta\delta_2) \tag{3.42}$$

The order of the subscripts illustrates a positive power flow due to the tie lines in the direction of 1 to 2.For little deviation in the angles δ_1, and δ_2 changes by $\Delta\delta_1$ and $\Delta\delta_2$, the tie-line power changes as shown in equation (3.40).

$$\Delta P_{12} = \frac{|V_1||V_2|}{X_{12}} \cos(\delta_1 - \delta_2)(\Delta\delta_1 - \Delta\delta_2) \tag{3.43}$$

$$\Delta P_{12} = T_p(\Delta\delta_1 - \Delta\delta_2) \tag{3.44}$$

where, $T_p = \frac{|V_1||V_2|}{X_{12}} \cos(\delta_1 - \delta_2)$ - Torque produced

$$\Delta P_{12}(s) = \frac{2\pi T_p}{s}(\Delta F_1(s) - \Delta F_2(s)) \tag{3.45}$$

The incremental power ($P_G - P_D$) is the rate of increased conserved kinetic energy due to a rise in the load followed by a rise in the frequency in an isolated control area.

3.7 Three Area Power System Modeling

The complexities and non-linearities of the power system network are increased by the various interconnected control region. These control regions are linked by tie lines, which necessitate power flow and frequency deviation control. The goal of the frequency control scheme is for each control region to be able to feed its demand while also being capable of frequency control. To eliminate frequency steady-state error, tie-line power exchange, also known as bias, can be used. It means that each of the regulating areas must contribute to frequency control while also looking after their net exchange. In this control, the inaccuracy of each region is retained as a linear function of frequency error and tie-line power error [4].

$$\left.\begin{aligned} ACE_1 &= \Delta P_{21} + B_1 \Delta f_1 \\ ACE_2 &= \Delta P_{32} + B_2 \Delta f_2 \\ ACE_3 &= \Delta P_{31} + B_3 \Delta f_3 \end{aligned}\right\} \tag{3.46}$$

where $B_i = D_i + \frac{1}{Ri}$, R_i stands for droop characteristics of area *i*, and ACE stands for the area control error, *B1, B2 & B3* are fixed gains defined as frequency bias for their respective areas.

For each power generation area, this ACE signal is used as the plant output. When ACE is set to zero across the full range, the system frequency error is zero, and tie-line power faults are zero. To achieve the best frequency and tie-line power, areas with power-producing units can be interconnected. Figure 3.11 shows how to build a complete three-area power generating unit.

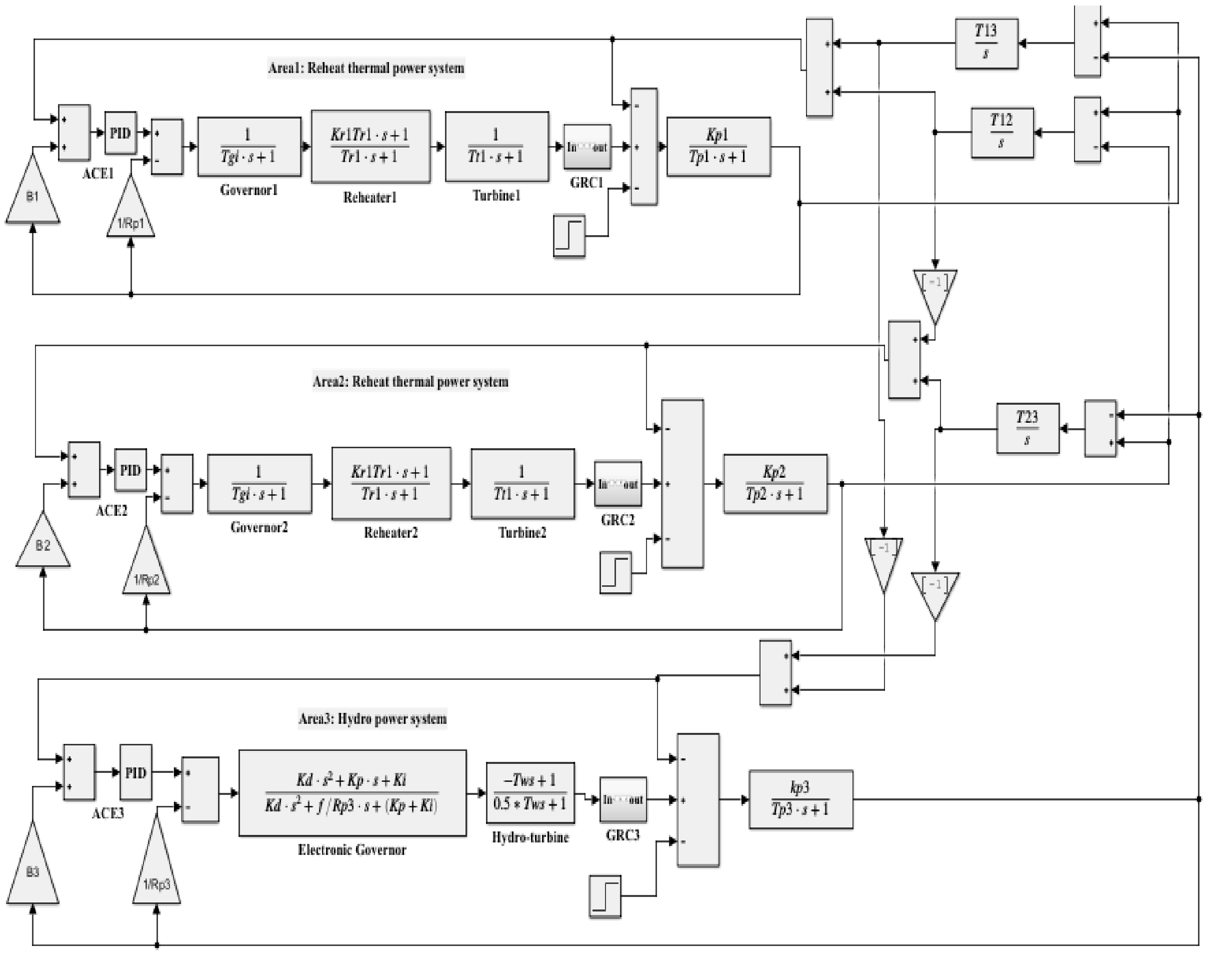

Figure 3. 11 Block diagram of three-areas interconnected power system.

Figure 3.11, shows an interconnected three-area thermal-hydropower system for load frequency control. In this block diagram, there are three inputs (the controller input *U(s)*, load disturbance $\Delta P_L(s)$, and tie-line power error $\Delta P_{tie}(s)$, one *ACE* output *Y(s)*, and one generator output Δf.

The model of three area hydro-thermal reheat power system is shown in Figure 3.11. Transfer function (T/F) [62] each components are shown in Equation (3.47-3.52).

Transfer function (T/F) of hydraulic Turbine is: $\frac{-Tw.s+1}{0.5Tw.s+1}$ (3.47)

T/F of hydraulic Governor is: $\frac{Kd.s^2+Kp.s+Ki}{Kd.s^2+(Kp+f/R_3).s+Ki}$ (3.48)

T/F of governor (thermal plant) is: $\frac{1}{Tg.s+1}$ (3.49)

T/F of steam turbine is: $\frac{Kr.Tr.s+1}{Tr.s+1}$ (3.50)

T/F of Re-heater is: $\frac{1}{Tt.s+1}$ (3 .51)

Transfer function of Generator is: $\frac{Kp}{Tp.s+1}$ (3.52)

where B1, B2, B3 represents the frequency bias factor; R1, R2, R3 represents the self regulation parameter for the governor; Tg1, Tg2 represents speed governor time constant of thermal power plant; Tr1, Tr2 is the reheat time constant; Kr1, Kr2 is the reheat gain; Tt1, Tt2 is the steam chest time constant; Tw represents water starting time for hydro turbine; Tp1,Tp2, Tp3, Kp1, Kp2, Kp3 is the load frequency constant (Tp = 2H/f*D, Kp=1/D); T12, T13, T23 Synchronization coefficient , Kp represents Proportional controller gain ; Ki represents Integral controller gain; Kd represents Derivative controller gain; delF incremental frequency deviation; delPtie Tie line power flow; SLP stands for Step Load Perturbation; GRC represents Generation Rate Constraint; ACE stands for area control error.

3.8 Mathematical Problem Formulation

3.8.1 Adopted Control Methodology

A feedback control system is commonly employed to control the operation of a plant and maintain its desired output. The major goals of the feedback control systems are to minimize the effect of disturbances at the output. A commonly used compensator employed in feedback control systems is a PID compensator which provides for varying degrees of gain and phase shift of the signal according to the frequency of the signal. The important features of the PID controller are most commonly used in all industries these days for simple construction and execution. The addition of a PID raises the system's type, assuring that the steady-state error for a given load demand will be zero. It must not be excessively high; else, instability may develop. Equation (3.53) can be used to express the transfer function model for the PID.

$$G_{PID}(s) = Kp + \frac{Ki}{T_i s} + K_d T_d s \qquad (3.53)$$

where K_P is the proportional gain, K_i is the integral gain, K_D is the derivative gain, T_i is the integral action time, and T_d is the derivative action time. The proportional, integral, and derivative modes are the three modes of the PID controller. Figure 3.12 shows an internal configuration of the PID controller.

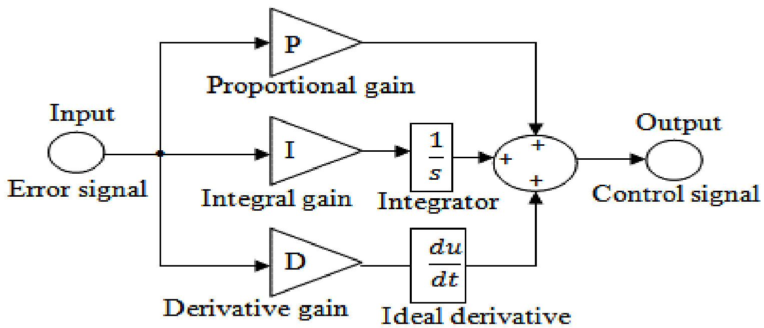

Figure 3. 12 Block diagram of PID controller.

The PID controller creates an appropriate control output signal based on the input to keep the power system response within the set range. The equation gives the expression for the generated control signal (3.44).

$$\left.\begin{aligned} U_1 &= K_{p1}ACE_1 + K_{i1}\int ACE_1 dt + K_{d1}\frac{dACE_1}{dt} \\ U_2 &= K_{p2}ACE_2 + K_{i2}\int ACE_2 dt + K_{d2}\frac{dACE_2}{dt} \\ U_3 &= K_{p3}ACE_3 + K_{i3}\int ACE_3 dt + K_{d3}\frac{dACE_3}{dt} \end{aligned}\right\} \tag{3.54}$$

where *ACE* is for area control error, and *Ui* stands for plant input.

The ChOA, MFO, MVO, and QOHS optimization methods are used to optimize the parameters of the PID controller's gain values in the current study.

3.8.2 Design of Objective Function

An objective function can be used as a performance criterion for verifying the designed model's performance. The proper design of the controller is based on the appropriate selection of its objective function. The objective function is created using the required specifications, restrictions, and the closed-loop response of the complete system output with the time-domain specification. The peak overshoot, undershoot, settling time, and steady-state error is the outputs of the time domain specification analysis. The Integral Square Error (ISE), Integral Time Square Error (ITSE), Integral Square Error (ISE), and Integral Time Absolute Error (ITAE) are some of the cost functions that can be used. According to the literature [62], the ITAE-based objective function surpasses all other objective functions. As a result, the suggested system employs the ITAE object function, which is expressed as shown in (3.49).

$$\text{ITAE}=\int_{0}^{t_s} t\left|ACE\right|dt \tag{3.55}$$

where ACE stands for the area control error and ts stands for stoping time.The governing equation for ACE is described in (3.46).

3.8.3 Constraints of the Problem

The PID controller gains, which should be kept within certain limits in the current ALFC system, are the constraints. As a result, the intended problem is transformed into an optimization problem, which may be expressed in the form of an equation (3.55):

$$\left.\begin{array}{l} K_{Pi}^{\min} \le K_{Pi} \le K_{Pi}^{\max} \\ K_{Ii}^{\min} \le K_{Ii} \le K_{Ii}^{\max} \\ K_{Di}^{\min} \le K_{Di} \le K_{Di}^{\max} \end{array}\right\} \tag{3.55}$$

where the superscripts min and max denote the variable's minimal and maximum values, respectively. In the optimization process, the minimum values for K_P, K_i, and K_D are set to *0.001*, while the maximum values are set to *1*. Since, in optimization process as soon as the iteration process going for 60 cycles, the value of each PID gain is in between 1 and 0.001 evenif the value of upper and lower value varies.

3.8.4 Measure of Performance

The purpose of this research is to select the best PID controller gains for dynamic responses that are neither too fast nor too slow. To analyze the dynamic behavior of the test system, the settling time (*Ts*), peak overshoot, and peak undershoots are determined at the end of the created program. To design LFC, an optimization problem is solved using the ChOA, QOHS, MFO, and MVO algorithms to minimize the ITAE index and produce the ideal PID controller values.

3.9 Adopted Optimization Technique

Considering the effort and time required by the above approaches to obtain the controller's optimum values, we choose a more advanced strategy that includes an optimization algorithm based on natural processes. To date, several optimization techniques have been suggested or developed. The majority of the research and comparison is done using approaches that have recently been published.

3.9.1 Chimp Optimization Algorithm

Khishe and Mosavi presented the Chimp optimization method in 2020 [65]. Chimpanzees (sometimes known as chimps) are one of only two African great ape species. They are as near as people can get to living relatives. Because they are descended from a single progenitor species (Hominoid) that lived seven or eight million years ago, chimp and human DNA are so similar [62]. There are four categories of chimps in a chimp colony: driver, barrier, chaser, and attackers [63]. They each have their own set of abilities, and these differences are crucial for a successful hunt. The drivers pursue the prey without making any attempt to catch up with it [63]. Barriers establish a dam across the progression of the prey by embedding themselves in a tree [62]. To catch up with the prey, chasers move quickly after it. Finally, attackers predict the prey's escape route to drive it back towards the chasers or down into the lower canopy. Attackers are remunerated with a greater piece of meat following a successful hunt because they are thought to require significantly more cognitive effort in predicting the prey's forthcoming moves. This crucial role (attacking) is linked to age, intelligence, and physical ability [63]. Furthermore, chimps can switch jobs during the same hunt or stay with the same one throughout. Chimps have been shown to hunt for meat in exchange for social favors such as coalitional support, sex, or grooming [62].

Figure 3. 13 The first phase of the hunting process (“exploration”) [65].

As a result, smartness may have an ancillary outcome on hunting by opening up a new arena of privileges. To the best of our knowledge, this social incentive has only been proposed for chimps [62] in addition to humans. As a result, there would constitute a significant distinction between chimps and other social predators that rely on cognitive abilities. This social incentive (sexual desire) causes chimps to act erratically in the last stages of the hunting process, with all chimps abandoning their unique roles and frantically attempting to obtain meat. In the following part, all of these ChOA notions are mathematically formulated.

$$\left.\begin{aligned} X_1(t+1) &= \mathrm{X}_{\mathrm{Attacker}}(\mathrm{t}) - \mathrm{a}_1.\mathrm{d}_{\mathrm{Attacker}} \\ X_2(t+1) &= \mathrm{X}_{\mathrm{Barrier}}(\mathrm{t}) - \mathrm{a}_2.\mathrm{d}_{\mathrm{Barrier}} \\ X_3(t+1) &= \mathrm{X}_{\mathrm{Chaser}}(\mathrm{t}) - \mathrm{a}_3.\mathrm{d}_{\mathrm{Chaser}} \\ X_4(t+1) &= \mathrm{X}_{\mathrm{Driver}}(\mathrm{t}) - \mathrm{a}_4.\mathrm{d}_{\mathrm{Driver}} \end{aligned}\right\} \tag{3.56}$$

$$X_{chimp}(t+1) = \frac{X_1 + X_2 + X_3 + X_4}{4} \tag{3.57}$$

The chimp's position is updated according to the four categories of position saved, where t is the current iteration's number (XAttacker, XBarrier, XChaser, and XDriver). Equation (3.55) expresses the dynamic coefficient a and the vector d.

$$
\left.\begin{aligned}
a_1 &= 2.f_1 - f_1, \quad \mathrm{d}_{\text{Attacker}} = \left|c.X_{Attacher}(t) - m.X(t)\right| \\
a_2 &= 2.f_2 - f_2, \quad \mathrm{d}_{\text{Barrier}} = \left|c.X_{\text{Barrier}}(t) - m.X(t)\right| \\
a_3 &= 2.f_3 - f_3, \quad \mathrm{d}_{\text{Chaser}} = \left|c.X_{\text{Chaser}}(t) - m.X(t)\right| \\
a_4 &= 2.f_4 - f_3, \quad \mathrm{d}_{\text{Driver}} = \left|c.X_{\text{Driver}}(t) - m.X(t)\right|
\end{aligned}\right\} \tag{3.58}
$$

where the coefficient f decreases nonlinearly from 2.5 to 0 with the lapse of iteration. $c = 2r_2$. $r1$ and $r2$ are random numbers in [0, 1]. m is a chaotic map vector.

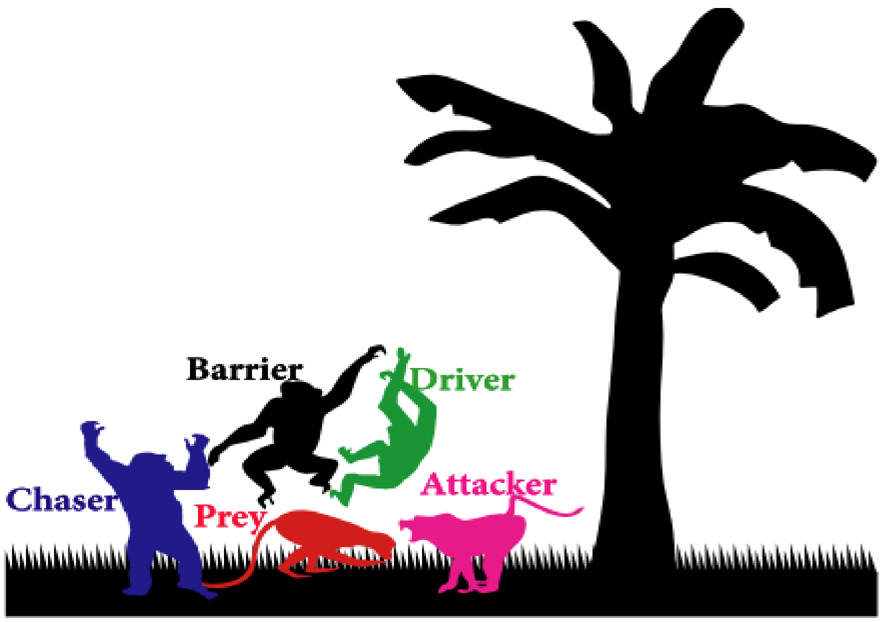

Figure 3. 14 The second phase of the hunting process (“exploitation”) [63].

Assuming the probability μ is a random number in [0, 1], the chaotic model is used for position updating when $\mu \geq 0.5$, as shown in equation (3.53).

$$
X_{chimp}(t+1) = Chaotic\_Value \tag{3.59}
$$

The pseudo-code of the ChOA algorithm is shown in Table 3.

Table 3 Algorithm: Pseudo-code of ChOA

Algorithm: Pseudo-code of ChOA

(i) Initialize the chimp population size and maximum number of iteration
(ii) Initialize positions of chimp
(iii) Calculate the fitness of each chimp
(iv) Select attacker, barrier, chaser, and driver
(v) While t<the maximum number of iterations
(vi) For each chimp
(vii) If μ <0.5
(viii) Update the position of the current chimp using eq. (3.4)
(ix) Else if
(x) Update the position of the current chimp using eq. (3.6)
(xi) End if
(xii) End for
(xiii) Update f, c, m, a and d
(xiv) Calculate the fitness of all chimp
(xv) Update XAttacker, XBarrier, XChaser, and XDriver
(xvi) t=t+1
(xvii) End while
(xviii) Return $X_{Attacker}$

3.9.1.1 Chimp Optimization-Based Controller Design

Fig. 3.12 below illustrates a system considered disturbance between systems. In this case, when we tune the PID controller of system-1, we must consider the coupling factor of others as a disturbance. Therefore, ChOA should compute the disconnected factor (disturbance reduce) of others, P, I, D, together.

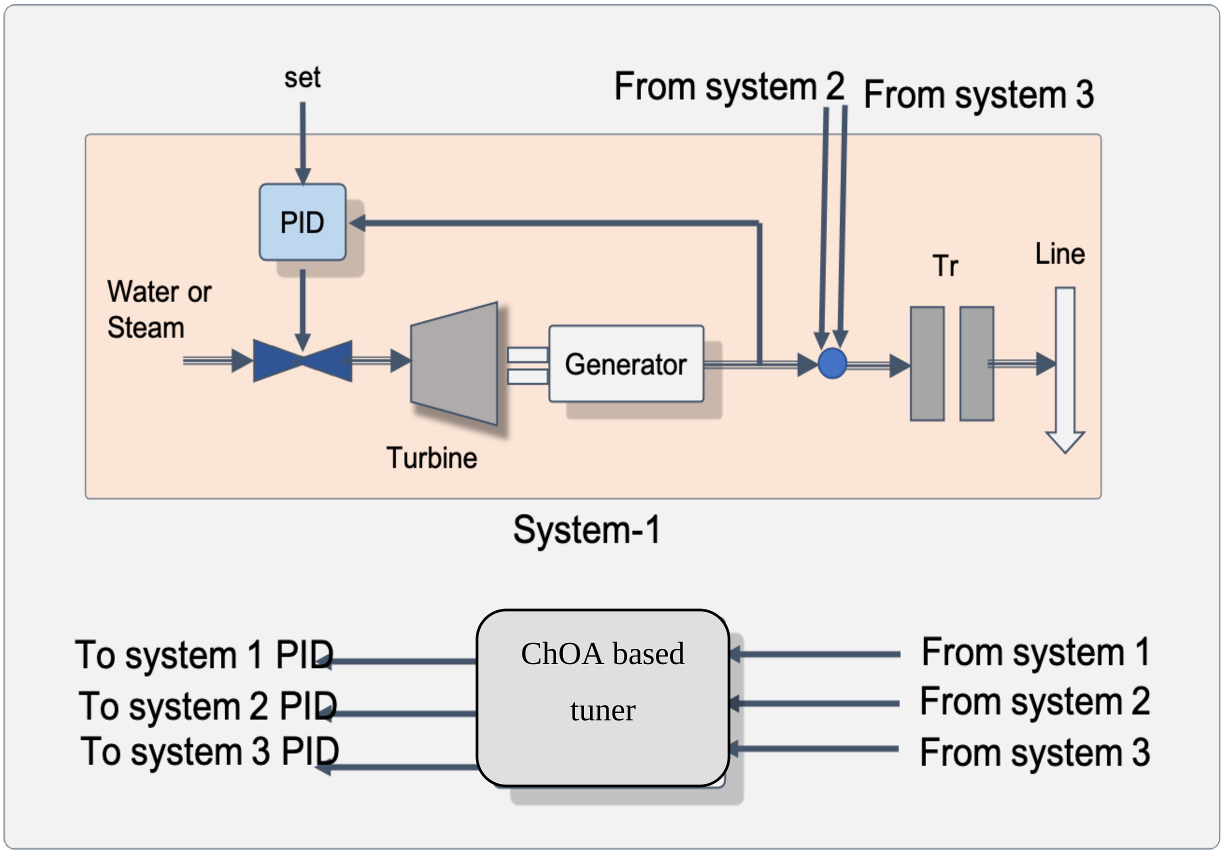

Figure 3. 15 ChOA based PID tuning considering disturbance.

3.9.2 Mothe Flame Optimization Algorithm

S. Mirjalili created the Moth Flame Optimization method, a new population-based algorithm, in November 2015. Moths are beautiful insects that are closely related to butterflies. In nature, there are about 160,000 different species of this insect [64]. They go through two stages in their lives: larvae and adults. Cocoons transform the larvae into moths. The most fascinating thing about moths is their unique night navigation methods. They navigated using a technique known as transverse orientation [59]. Depending on the moths' flying characteristics, the MFO algorithm is designed. Mathematically, the moth possesses a unique navigational trait that allows them to keep a constant angle with the moon at night. For moths to fly millions of miles, this trait is a very successful approach. Furthermore, the presence of artificial lights along a spiral pattern may trap the moths. For the design of the MFO approach, [58] used the moth navigation notion in a mathematical form. Assume that the potential solutions are moths and that the variables in the problem are moth positions in space. By adjusting their position vectors, the moths can fly in 1-D, 2-D, 3-D, or hyperdimensional space. We describe the set of moths in a matrix as follows because the MFO algorithm is a population-based algorithm:

$$M = \begin{bmatrix} m_{1,1} & m_{1,2} & \cdots & m_{1,d} \\ m_{2,1} & m_{2,2} & \cdots & m_{2,d} \\ \vdots & \vdots & \vdots & \vdots \\ m_{n,1} & m_{n,2} & \cdots & m_{n,d} \end{bmatrix} \tag{3.60}$$

where d is the number of variables (dimension) and n is the number of moths We also suppose that there is an array for each Moth that stores the appropriate fitness. The steps to solve the algorithm are outlined below in general [58].

Step one :(Initializing the population) The first condition mentions the above and lower bands, as well as their dimensions.

Step two: (Updating the location) The positions of moths are constantly modified to achieve the greatest results.

Step three: (Calculation of the objective function) The MFO technique is used to calculate the values of objective functions.

Step-4. (Updating the locations)

Locations of each Moth are updated using fitness value to get the best position

3.9.2.1 Mothe-Flame Optimization-Based Controller Design

Figure 3.13 below illustrates a system considered disturbance between systems. In this case, when we tune the PID controller of system-1, we must consider the coupling factor of others as a disturbance. Therefore, MFO should compute the disconnected factor (disturbance reduce) of others, P, I, D, together.

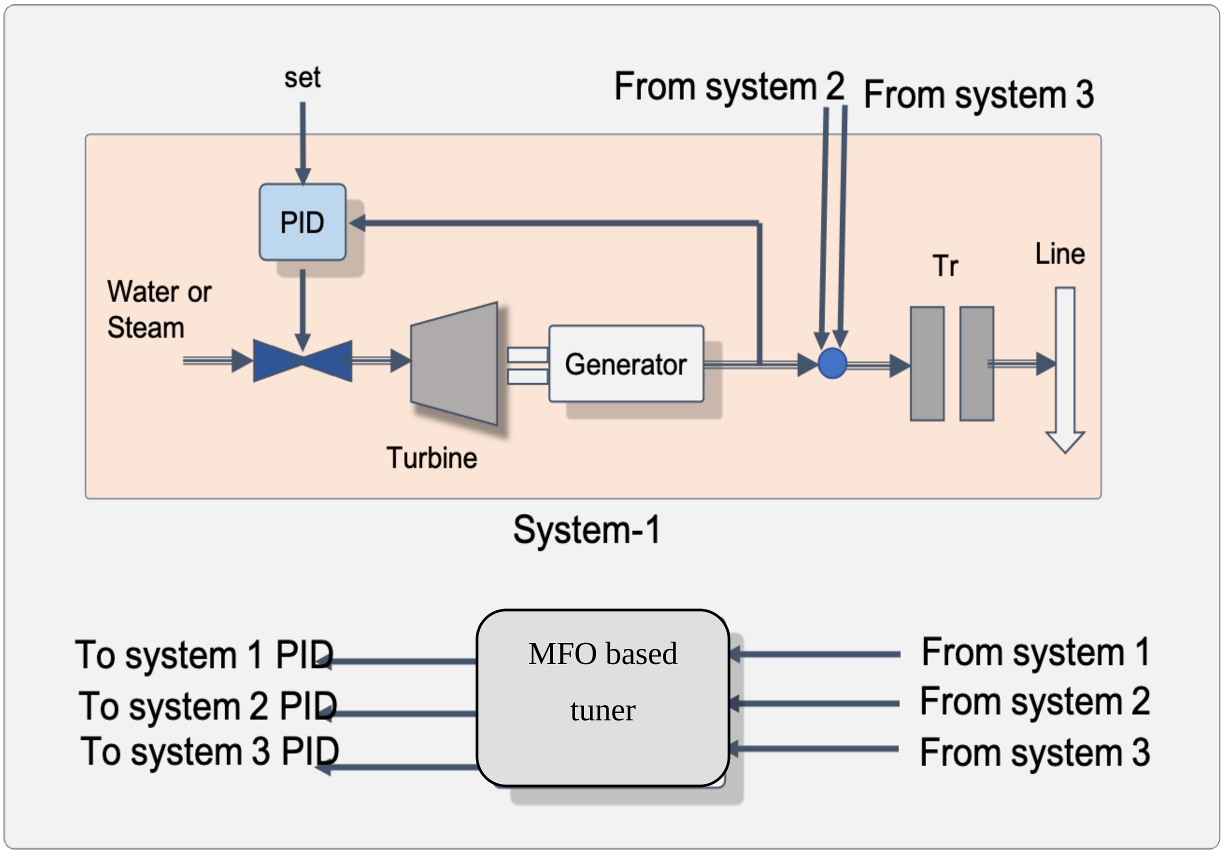

Figure 3. 16 MFO based PID tuning considering disturbance.

3.9.3 Multi-Verse Optimization Algorithm

S. Mirjalili invented the Multi-verse Optimizer (MVO) in March 2015 [65], which is another new but successful nature-inspired technique of optimization. Three cosmological notions inspired the Multi-Verse Optimizer (MVO): white hole, black hole, and wormhole. The MVO is based on the multiverse theory of physics, in which the multiverse represents the universe's polar opposite. Other universes, apart from the one in which we all live, are thought to exist according to this hypothesis. The theory proposes that multiple universes not only interact with each other but also collide sometimes [66]. Apart from that, each universe has its inflation rate or the rate at which it expands over space. Exploration, exploitation, and local search are all performed using mathematical models of these three notions. The black hole and white hole are cosmological concepts that probe the search space, whereas the wormhole aids in its application. During MVO optimization, the universes are exposed to the following rules [65]:

(i) The higher the inflation rate, the more likely there is to be a white hole.

(ii) The smaller the probability of black holes, the higher the inflation rate.

(iv) Objects are more likely to be sent into white holes in universes with a higher inflation rate.

(v) Black holes in universes with lower inflation rates are likely to receive more items.

(vi) Regardless of the inflation rate, items in all worlds may experience random travel towards the best universe via wormholes.

When two universes are connected by a white/black tunnel, the universe with the higher inflation rate is considered to have a white hole, while the universe with the lower inflation rate is assumed to have black holes. The objects are subsequently transferred from the source universe's white holes to the destination universe's black holes [60]. This mechanism facilitates the exchange of items between universes. We postulate that universes with high inflation rates are more likely to have white holes to improve the overall inflation rate of the universes. On the other hand, universes with low inflation rates are more likely to have black holes. As a result, moving objects from a universe with a high inflation rate to a universe with a low inflation rate is always a possibility. This can ensure that the average inflation rates of all universes improve over the iterations. The pseudo-codes for this part is as follows [61]:

SU=Sorted universes

NI=Normalize inflation rate (fitness) of the universes

for each universe indexed by i

Black_hole_index,j=i;

for each object indexed by j

r1=random ([0, 1]);

if r1<NI (Ui) White_hole_index= RouletteWheelSelection (-NI); U (Black_hole_index,j)= SU(White_hole_index);

end if

end for

end for

3.9.3.1 Mothe-Flame Optimization-Based Controller Design

Fig. 3.14 below illustrates a system considered disturbance between systems. In this case, when we tune the PID controller of system-1, we must consider the coupling factor of others as a disturbance. Therefore, MVO should compute the disconnected factor (disturbance reduce) of others, P, I, D, together.

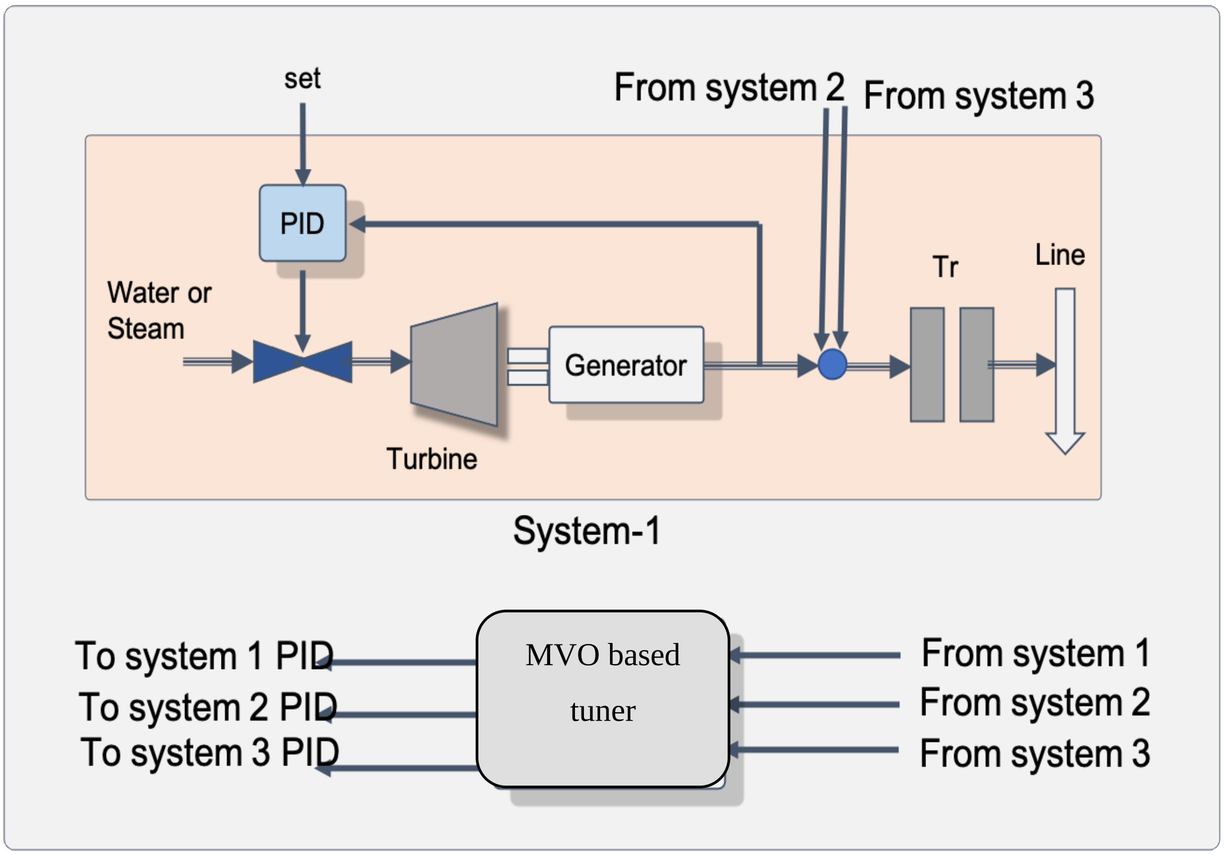

Figure 3. 17 MVO based PID tuning considering disturbance.

3.9.4 Novel Quasi-Oppositional Harmony Search Algorithm

The HSA was chosen as the core algorithm because it was inspired by the musical process of looking for a perfect state of harmony, which was invented in 2001. The solution vector in the HSA is comparable to musical harmony, and the local and global search strategies are comparable to musicians' improvisations [61]. The following three primary steps can be used to characterize the HSA's optimization process:

(a) Initialization: Program parameters are defined, and then the harmony memory (HM) is filled with random solutions to initialize it.

(b) Harmony improvisation (development of a new solution): The HSA determines each decision variable in the solution.

(c) Selection: The best harmony (solution) in the HM is updated when a terminating condition is reached. Otherwise, Steps (a) and (b) are repeated in that order. Fine-tuning the optimum solution vectors is also crucial and can help improve the algorithm's convergence rate [13]. The HM takes into account pitch adjustment or random selection for each variable in the new solution [61]. The core HSA's computing mechanism can be summarized as follows in the Algorithm:

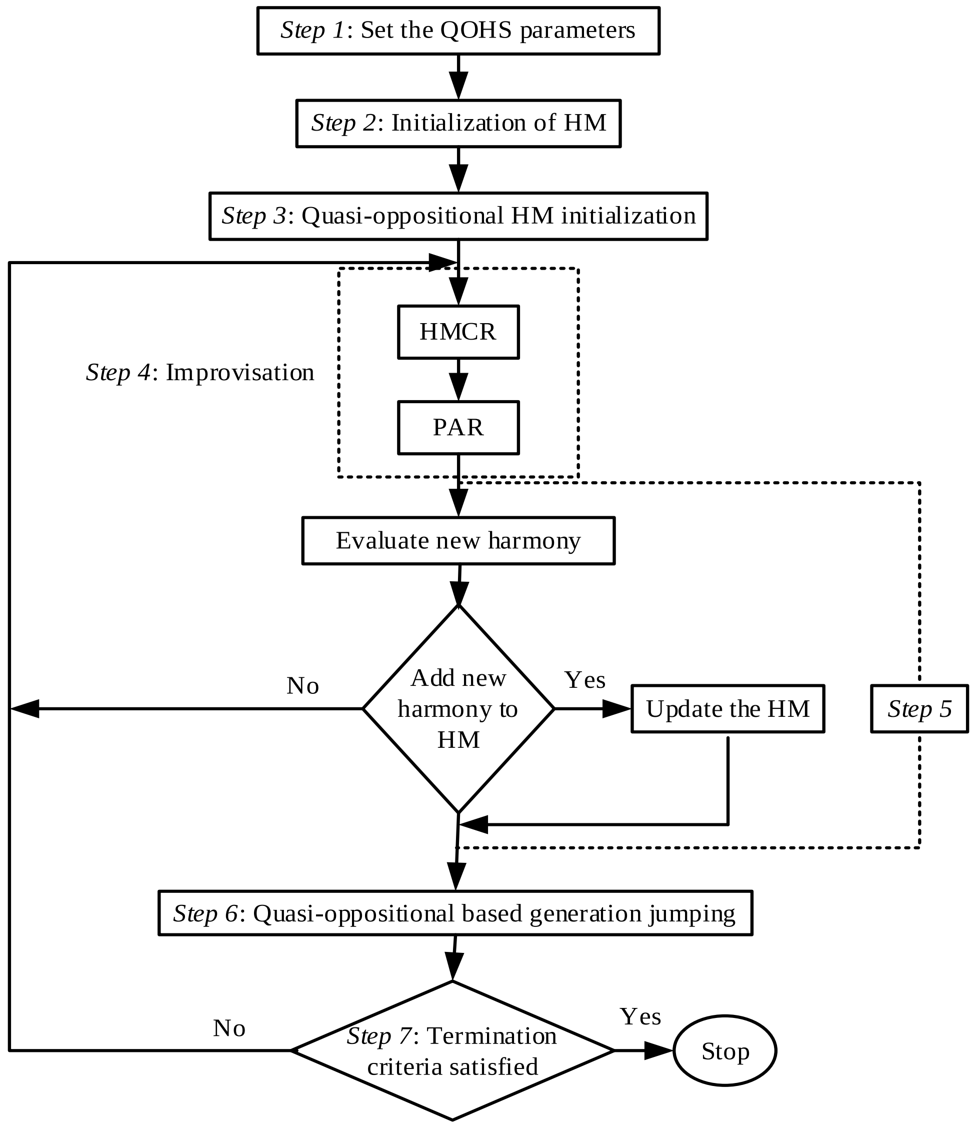

Figure 3. 18 Flow chart of QOHS algorithm implementation [61].

3.9.4.1 Novel-Quasi Opposition Harmony Search Algorithm-Based Controller Design

Fig. 3.13 below illustrates a system considered disturbance between systems. In this case, when we tune the PID controller of system-1, we must consider the coupling factor of others as a disturbance. Therefore, QOHS should compute the disconnected factor (disturbance reduce) of others, P, I, D, together.

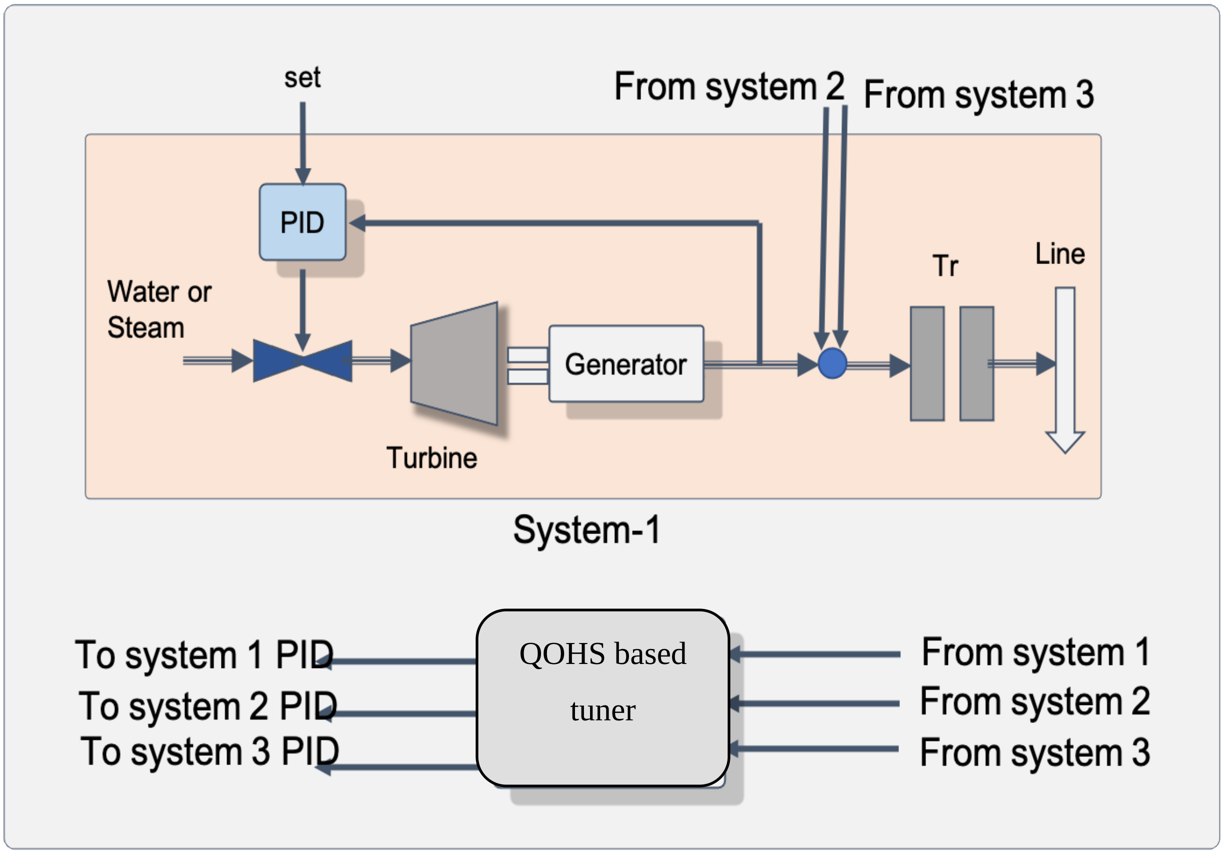

Figure 3. 19 QOHS based PID tuning considering disturbance.

CHAPTER FOUR

RESULTS AND DISCUSSION

4.1 Introduction

For the LFC study, a three-area interconnected power system is used. The thermal power plant is in area one, the second area is also a thermal power plant, and the third area of the three-area power system is the hydropower plant. In this scenario, each control region has a PID controller with three gains to tune, resulting in nine controller gains as variables in the LFC optimization problem. Using PID controllers improves the AGC scheme's performance even while increasing the number of optimization variables. Classic optimization methods may not be able to solve an optimization problem in this order (nine variables), but by using metaheuristic optimization algorithms (i.e. ChOA, QOHS, MFO, and MVO) as a valuable device applicable to many problems, solutions for many conditions can be quickly found. Thus, comparative performance analysis of ChOA-PID, QOHS-PID, MFO-PID, and MVO-PID controllers are made as shown in the below Figures 4.2. For the three-region power system model, the responses are shown as dynamic responses of each area frequency and the power of tie-line. Figure 4.1 depicts the MATLAB/Simulink model of the three-area interconnected power systems.

The results in this chapter are organized according to the order in which the system's control techniques were implemented. First, results of the comparative study of each controller in disturbance rejection are presented with 1% step load perturbation in area one. The second part of the result presents a comparative study of each controller in disturbance rejection is presented with 10% step load perturbation in area one, 5% SLP in area two, and 1% SLP in area three at once. Sensitivity analysis was done to check, the robustness of the designed controller by varying important parameters to $\pm$50% of their nominal values. Results of the comparative study are presented with 1% step load perturbation in area one.

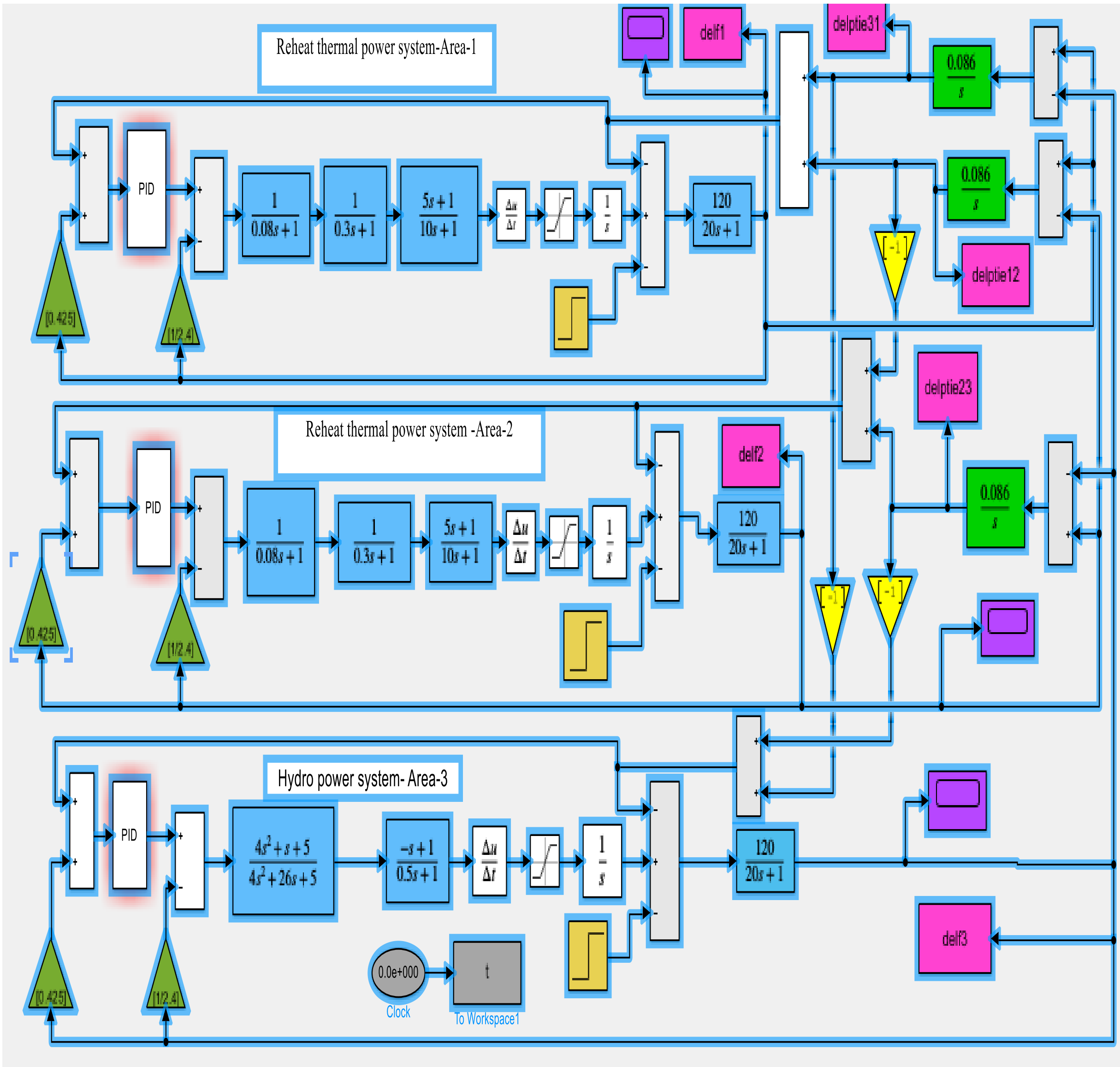

Figure 4. 1 Simulink Model of three areas thermal-thermal-hydro interconnected power system.

A Proportional-Integral-Derivative(PID) controller controlled interconnected three area unequal hydrothermal power system shown in Figure 4.1. The optimal values of thermal power plant and hydro plants are taken from [47],[62]. It consists of two equal thermal power systems (area 1 and area 2) and one hydro power system (area 3).Thermal areas are equipped with appropriate governor, reheater unit, turbine, generator and speed regulator. Similarly hydro power system is equipped with electric governor, turbine, generator and speed regulator. Arrangement of all the components and interconnection between the power generating units are shown in Figure 4.1. B1, B2, B3 represents the frequency bias factor in p.u MW/Hz with the magnitude of 0.425, R1, R2, R3 represents the self regulation parameter for the governor in p.u. Hz with the magnitude of 2.4 ; Tg1, Tg2 represents speed governor time constant in sec with the magnitude of 80msec; Tr1, Tr2 is the reheat time constant in sec with the magnitude of 10 sec; Kr1, Kr2 is the reheat gain with the magnitude of 0.5; Tt1, Tt2 is the steam chest time constant in sec with the magnitude of 300msec; Tw represents water starting time for hydro turbine in ses with the magnitude 1sec; Tp1,Tp2, Tp3, Kp1, Kp2, Kp3 is the load frequency constant (Tp = 2H/f*D, Kp=1/D); T12, T13, T23 Synchronization coefficient in MW/rad with the magnitude of 0.086; Kp represents Proportional controller gain with the magnitude of 1, Ki represents Integral controller gain with the magnitude of 5, Kd represents Derivative controller gain with the magnitude of 4; delPg incremental generation change; delF incremental frequency deviation; delPtie Tie line power flow; SLP stands for Step Load Perturbation; GRC represents Generation Rate Constraint; ACE stands for area control error. All three power systems are interconnecter through til-line as ring type connection. The appropriate Generation Rate Constraint (GRC) non linearity is considered [47], for the limitation of governor valve opening and closing. In practice, there exists a maximum and minimum limit on the rate of changes in the generating power. A Generation Rate Constraint (GRC) of the order of 3%/min for thermal power system and 4.5% sec-1 for rising generation and 6% sec-1 for lowering generation is considered for hydropower system in this present work. When non linearity added into the any power system, it produces more damping oscillations with higher steady state error in system response, when compared to system without considering GRC non linearity into the system.

4.2 Simulation Results and Discussion

In this study here, ChOA, QOHS, MFO, and MVO are applied to the PID controller to get an optimal value of K_p, Ki, K_d, and corresponding error value for enhancing power system stability, disturbance rejection, and robustness analysis. Results in this chapter are arranged in the sequence of control strategies applied to the considered system.

- case1- Results of the comparative study of each controller with disturbance rejection are presented with 1% SLP in area one.

- Case2- Presents the results of a comparative study of each controller with disturbance rejection are presented with 10%,5%, and 1% SLP in area one, area two, and area three, respectively at once.
- Case 3- The robustness of the controller is also checked by varying key parameters to ± 50% of their nominal values.

Finally, considered optimized controller's robustness effects in AGC are presented with 1% SLP in area one.

<u>Case1</u>: Step Load Perturbation in Area-1

The simulation results for each optimization technique by the application of 1%(0.01pu) step load perturbation when time reaches 2 seconds in area-1 while area-two and area three are unchanged. The comparative dynamic response of deviations in frequency and tie-line power to each area have been presented in Figure 4.2, and Figure 4.3 respectively using a different metaheuristics optimization algorithm.

Figure 4.2, reveals the responses of frequency deviation in area-1, area-2, and area-3 respectively while there is a 1% step load perturbation(SLP) in area-1. In this mentioned figure, the solid-blue lines show the response of the QOHS based PID controller equipped power system; the solid black line shows the response of the MFO based PID controller equipped power system, the solid green line shows the response of the MVO based PID controller equipped power system, and the solid-violet line illustrates the response of the ChOA based PID controller power system.

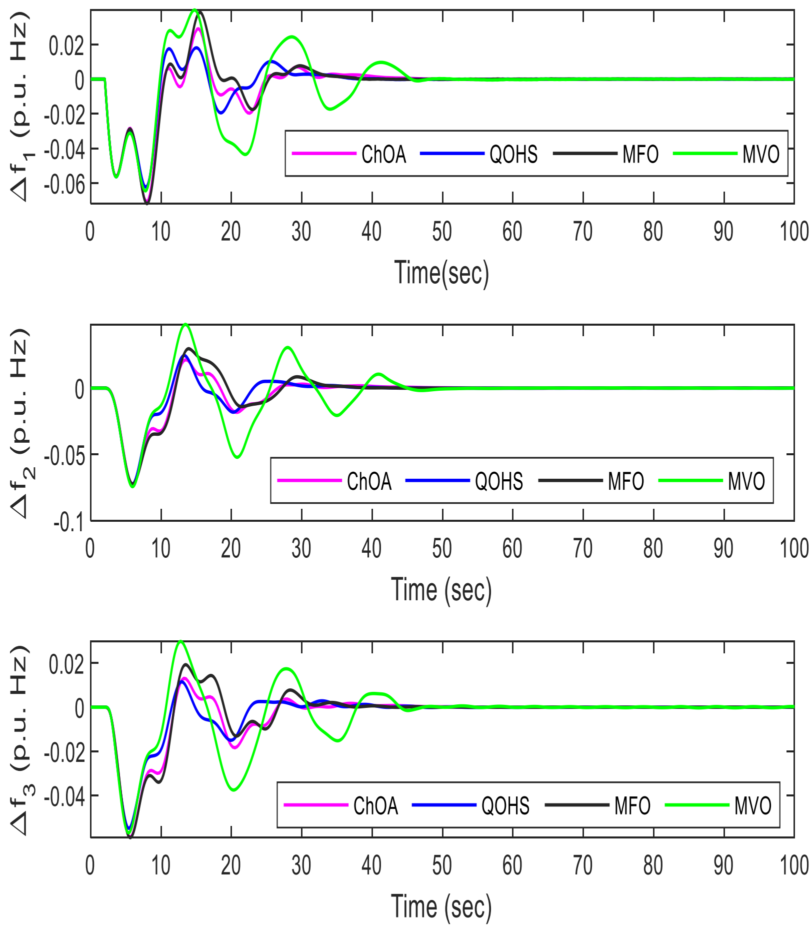

Figure 4. 2 Comparative frequency profiles of three-area power system due to step-change in area-1.

The frequency response of area 1 under the load disturbance of 0.01 p.u obtained by QOHS, ChOA, MFO, and MVO based PID controller is shown in Figure 4.2. The settling time of the three-areas developed model after frequency deviation in area 1 is 36 seconds with -0.062 p.u Hz, 39 seconds with -0.072 p.u Hz, 36 seconds with -0.07 p.u Hz, and 46 seconds with -0.074 p.u Hz for QOHS, ChOA, MFO, and MVO respectively. The settling time of the three-areas developed model after frequency deviation in area 2 is 35 seconds with -0.061 p.u Hz, 38 seconds with -0.071 p.u Hz, 36 seconds with -0.07 p.u Hz, and 43 seconds with -0.072 p.u Hz for QOHS, ChOA, MFO, and MVO respectively. While the settling time of the three-areas developed model after frequency deviation in area 3 is 39 seconds with -0.071 p.u Hz, 38 seconds with -0.064 p.u Hz, 35 seconds with -0.062 p.u Hz, and 61 seconds with -0.08 p.u Hz frequency deviation for QOHS, ChOA, MFO, and MVO respectively.

Table 4 Performance of metaheuristics optimization algorithms in settling time and for frequency variation

Parameters	**Transient response**	**Methods**			
		ChoA	QOHS	MFO	MVO
Delf1	Settling Time (sec)	39.53	36.31	36.39	46.20
	Frequency deviation (*p.u.Hz*)	-0.072	-0.062	-0.07	-0.074
Delf2	Settling Time (sec)	38.43	35.56	36.062	43.15
	Frequency deviation(*p.u.Hz*)	-0.071	-0.061	-0.07	-0.072
Delf3	Settling Time(sec)	38.04	39.65	35.32	61.51
	Frequency deviation(*p.u.Hz*)	-0.064	-0.071	-0.062	-0.08

where *Delf1*, *Delf2*, and *Delf3* are the frequency deviation in area1,2 and 3 respectively.

In terms of frequency deviation QOHS based tuned controller shows *0.06* p.u Hz, and *0.062* p.u Hz in areas 1 and area 2 respectively. While MFO based controller shows *0.064* p.u Hz of frequency variation in area 3.

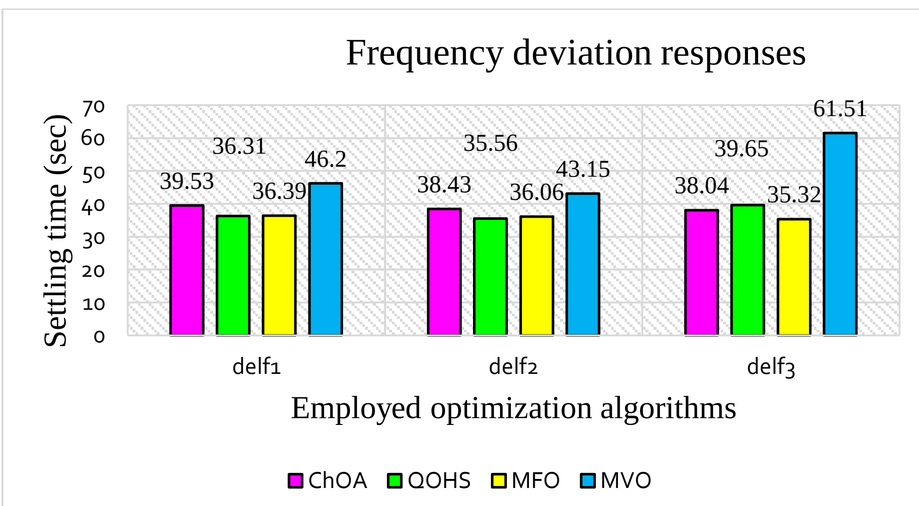

Figure 4. 3 Comparative performance ChOA, QOHS, MFO, and MVO with settling time.

Figure 4.4 depicts the tie-line (Tie-12, Tie-23, and Tie-31) power response in area-1, area-2, and area-3 respectively, under the load disturbance of 0.01 p.u obtained by QOHS, ChOA, MFO, and MVO based PID controllers. In this mentioned figure, the solid-blue lines indicate the response of the MVO based PID controller equipped power system; the solid black line shows the response MFO of the based PID controller equipped power system, the solid green line shows the response of the QOHS based PID controller equipped power system, and the solid- violet line illustrates the response of the ChOA based PID controller power system.

The deviation in tie-line power under the load disturbance of 0.01 p.u on area 1 obtained by QOHS, ChOA, MFO, and MVO based PID controller is shown in Figure 4.4. The settling time of the three-areas developed model after deviation in tie-line power created by coupling effect of area 1, and area 2(delptie12) is 49 seconds with -0.0059 p.u Hz, 59 seconds with -0.0057 p.u Hz, 48 seconds with -0.0058 p.u Hz, and 60 seconds with -0.006 p.u Hz, for QOHS, ChOA, MFO, and MVO respectively. The deviation in tie-line power created by coupling effect of area 2, and area 3 (delptie23) is 38 seconds with -0.0034 p.u Hz, 56 seconds with -0.0035 p.u Hz, 35 seconds with -0.0036 p.u Hz, and 87 seconds with -0.004 p.u Hz, for QOHS, ChOA, MFO, and MVO respectively. While the deviation in tie-line power created by coupling effect of area 1, and area 3 (delptie31) is 46 seconds with -0.0076 p.u Hz, 53 seconds with -0.0078 p.u Hz, 46 seconds with -0.0071 p.u Hz, and 60 seconds with -0.008 p.u Hz for QOHS, ChOA, MFO, and MVO respectively.

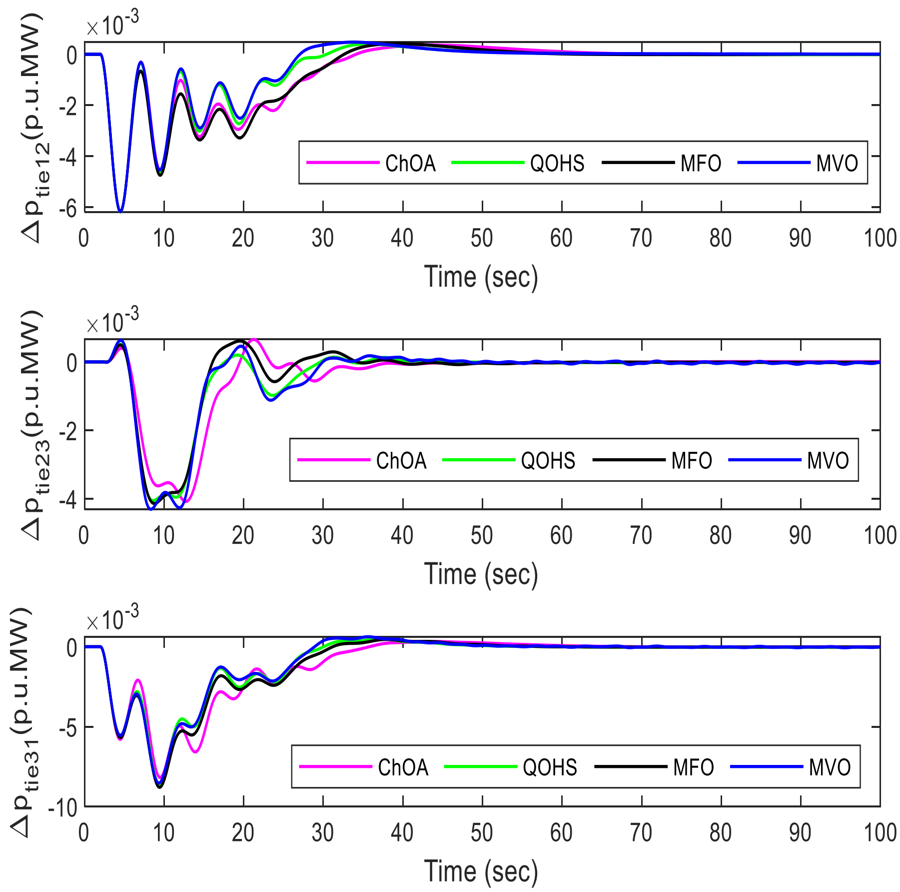

Figure 4. 4 Comparative study of variation in tie-line power of three-area power system due to step-change in area-1

Table 5 Comparison values of settling time of deviation in tie-line power flow for 60 iterations

Parameters	**Transient response**	**Methods**			
		ChoA	QOHS	MFO	MVO
Delptie12	Settling Time(sec)	59.80	49.14	48.75	60.379
	Deviation in tie-line power(p.u Hz)	-0.0057	-0.0059	-0.0058	-0.006
Delptie23	Settling Time(sec)	56.38	38.92	35.58	87.34
	Deviation in tie-line power(p.u Hz)	-0.0035	-0.0034	-0.0036	-0.004
Delptie31	Settling Time(sec)	53.71	46.36	46.12	60.34
	Deviation in tie-line power(p.u Hz)	-0.0071	-0.0076	-0.0078	-0.008

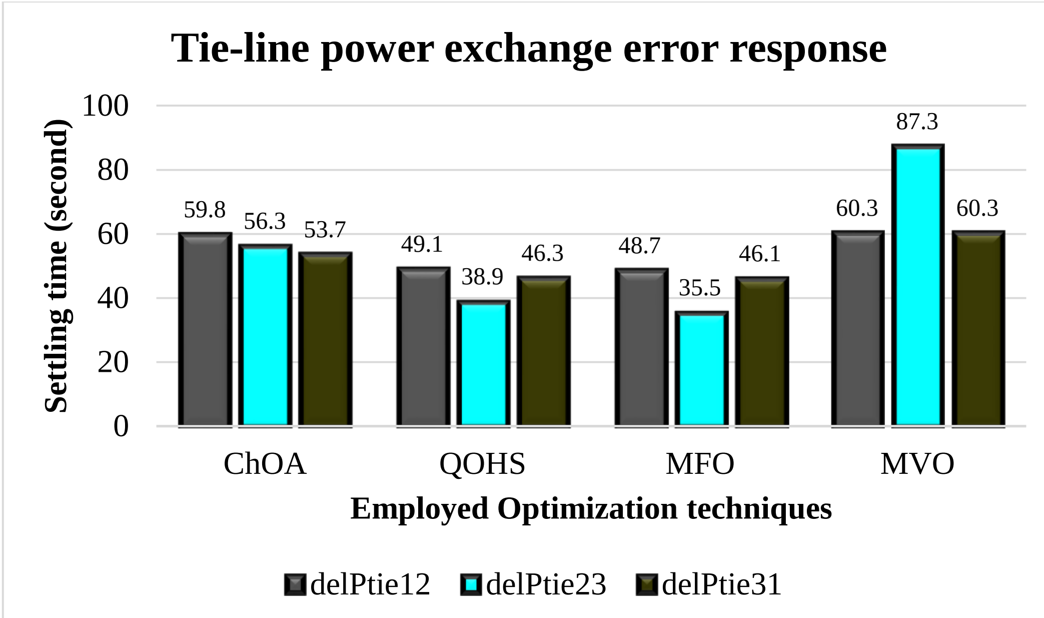

Figure 4. 5 Comparative performance ChOA, QOHS, MFO, and MVO with settling time.

So from the over two sets of Figures (Figure 4.4 and Figure 4.5), it is obtained to know that, for load change in area-1 the ChOA, QOHS, MFO, and MVO can bring the area frequencies and tie-line power flow to their pre-defined values or nominal values. But the capabilities in reducing errors are different. The optimized controller gains obtained when 1% step load perturbation in area-1 is shown in Table 5 below. The results of each PID gain are obtained to be negative.

Table 6 Optimized gain values and error for each method applied

Method	**Area1**			**Area2**			**Area3**			**ITAE**
	Kp	Ki	Kd	Kp	Ki	Kd	Kp	Ki	Kd	
ChoA	0.002	0.240	0.004	0.001	0.060	0.003	0.001	0.001	0.002	22.86
QOHS	**0.917**	**0.634**	**1**	**0.510**	**0.235**	**0.868**	**0.404**	**0.001**	**0.001**	**18.26**
MFO	0.828	0.582	1	0.618	0.155	0.874	0.368	0.001	0.001	18.45
MVO	0.983	0.453	0.705	0.722	0.188	0.890	0.2392	0.1594	0.0391	43.552

The simulation parameters taken for optimizations are Population size is 20, Maximum number of iterations 60, and simulation time 100 seconds of all optimization techniques.

The convergence profile of FOD(ITAE) with iteration cycle is also recorded in table 7. In this table, relative convergence mobility of the FOD value, obtained by the ChOA, QOHS, MFO, and MVO techniques has been shown. This shows the superiority of the QOHS technique over the other optimization techniques in terms of the tuning process while viewing the FOD value. Figure 4.6 below shows the comparison metaheuristics optimization techniques in terms of objective function (ITAE) values.

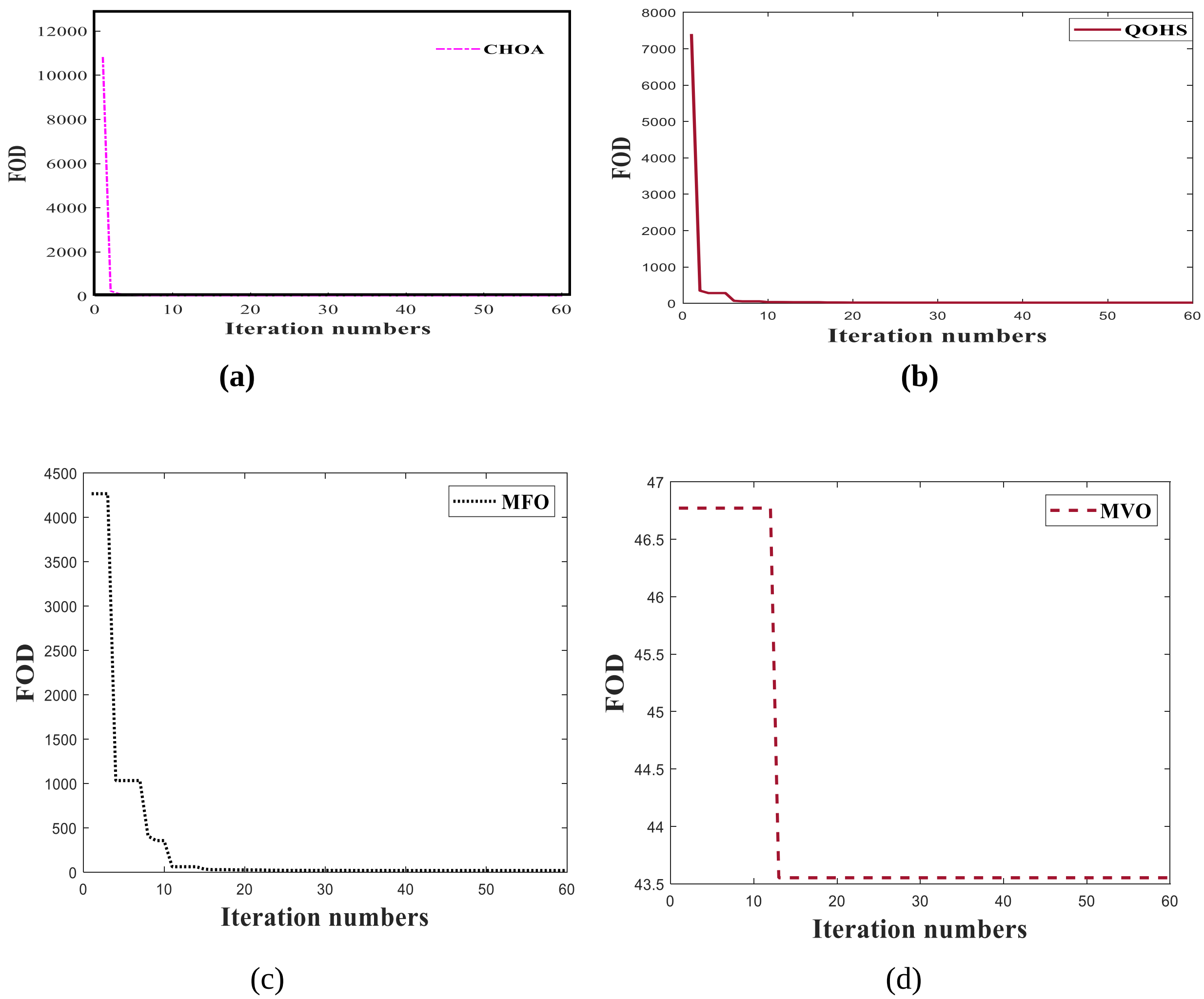

Figure 4. 6 Comparative analysis of object function, (a) ChOA, (b) QOHS (c) MFO, and (d) MVO.

Additionally, as Table7 and Appendix B show that the QOHS algorithm optimized PID controller equipped power system achieved the least damping oscillations for frequency in area-1, and area-2. For the tie-line power flow, the MFO algorithm optimized PID controller equipped power system achieved the least damping oscillations. As compared to overshoot peak MVO shows minimal overshoot peak for frequency in area-1, and area-2, ChOA shows minimal overshoot peak to the frequency in area-3, and the tie-line power flow. As compared to peak undershoot MVO shows minimal peak undershoot for frequency in area-1, area-2, and area-3. To the tie-line power flow, the MFO algorithm optimized PID controller equipped power system achieved minimal peak undershoot concerning tie-12, tie-23 and tie-31.

Furthermore, computational time comparison is also done between the proposed ChOA-PID, QOHS-PID, MFO-PID, and MVO-PID controller as shown in table 8 as shown below:

Table 7 Comparison values of the computational time of the four Algorithms

Iteration	**Execution time(Sec)**			
	ChOA	QOHS	MFO	MVO
60	39.6	166.8	139.7	588.0

Table 8 proves that a 39.6 second PID controller shows a lower execution time compared to the one obtained in QOHS, MFO, and MVO. So, ChoA-PID is superior to the ones obtained with the QOHS-PID, MFO-PID, and the MVO-PID in execution time.

Case 2: A step-change in area-1, area-2, and area-3 simultaneously

In this case, 10% step load perturbation in the first area, 5% step load perturbation in the second area, and 1% step load rise in demand of the third area respectively are applied. The response of the deviation in frequency of the power systems for each area is shown in figure 4.7.

As seen in Figure 4.7 multiple load perturbations, have an impact on the system's dynamic performance. Due to the inherent non-minimum phase characteristics of the hydropower plant, the severity is more for interconnected power systems which include hydropower systems. The ability to reestablish the steady-state operating point is a key debate topic in this case. As a result, at a time that reaches 2 seconds, step load perturbations are applied.

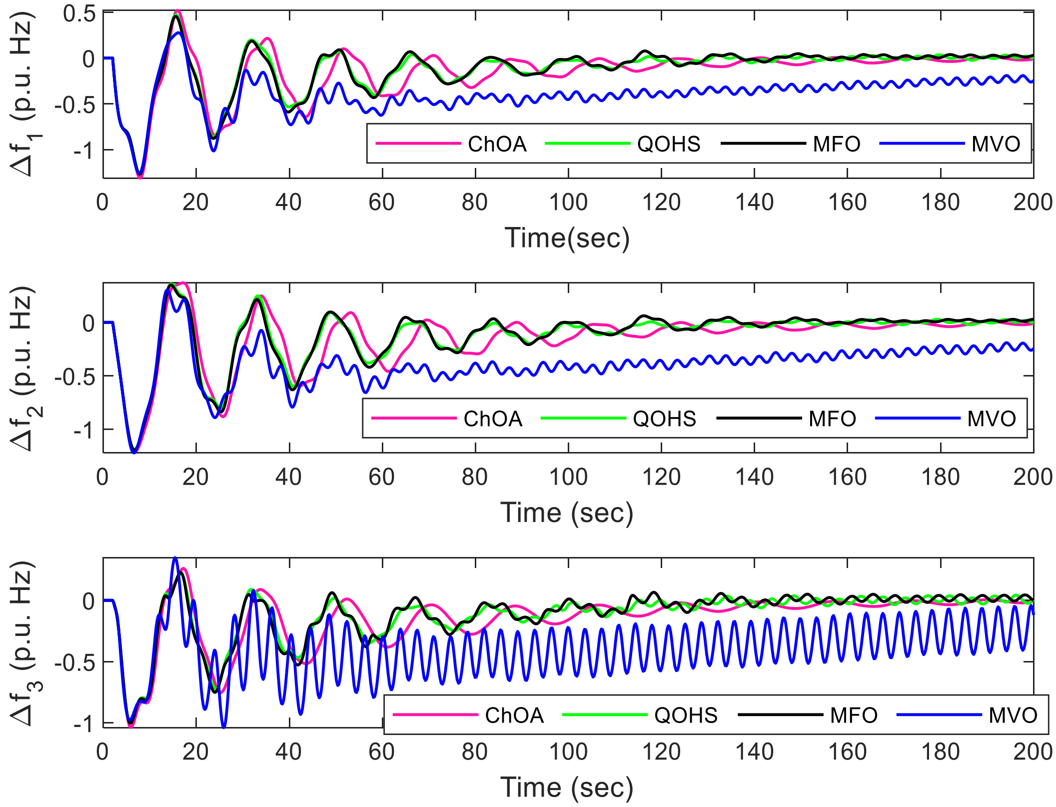

Figure 4. 7 Comparative performance analysis of ChOA, QOHS, MFO, and MVO, for 0.1 p.u step load change in area-1, 0.05 p.u step load change in area-2, and 0.01 p.u step load change in area-3 simultaneously

Table 8 Performance of metaheuristics optimization algorithms in settling time and for frequency variation

Parameters	**Transient response**	**Methods**			
		ChoA	QOHS	MFO	MVO
Delf1	Settling Time(sec)	183.1	194.2	189.3	198.5
	Frequency deviation(p.u Hz)	-1.43	-1.46	-1.44	-1.48
Delf2	Settling Time(sec)	183.3	198.6	175.3	198.4
	Frequency deviation(p.u Hz)	-1.45	-1.44	-1.42	-1.46
Delf3	Settling time(sec)	183.7	199.9	199.3	199.9
	Frequency deviation(p.u Hz)	-1.1	-1.1	-1.1	-1.1

The comparative dynamic responses of ChOA-PID, QOHS-PID, MFO-PID, and MVO-PID are shown in Figure 4.7 and Table 9. Critical analysis of the dynamic responses reveals that the system performance with the ChOA based PID controller shows better in settling time peak overshoot, and undershoot for frequency deviation in area 1 and area 3. But for frequency deviation in area 2, MFO shows superior performance in settling time and peak overshoot.

From a tie-line power error control point of view, the comparative performance of the employed optimization technique is shown in figure 4.8.

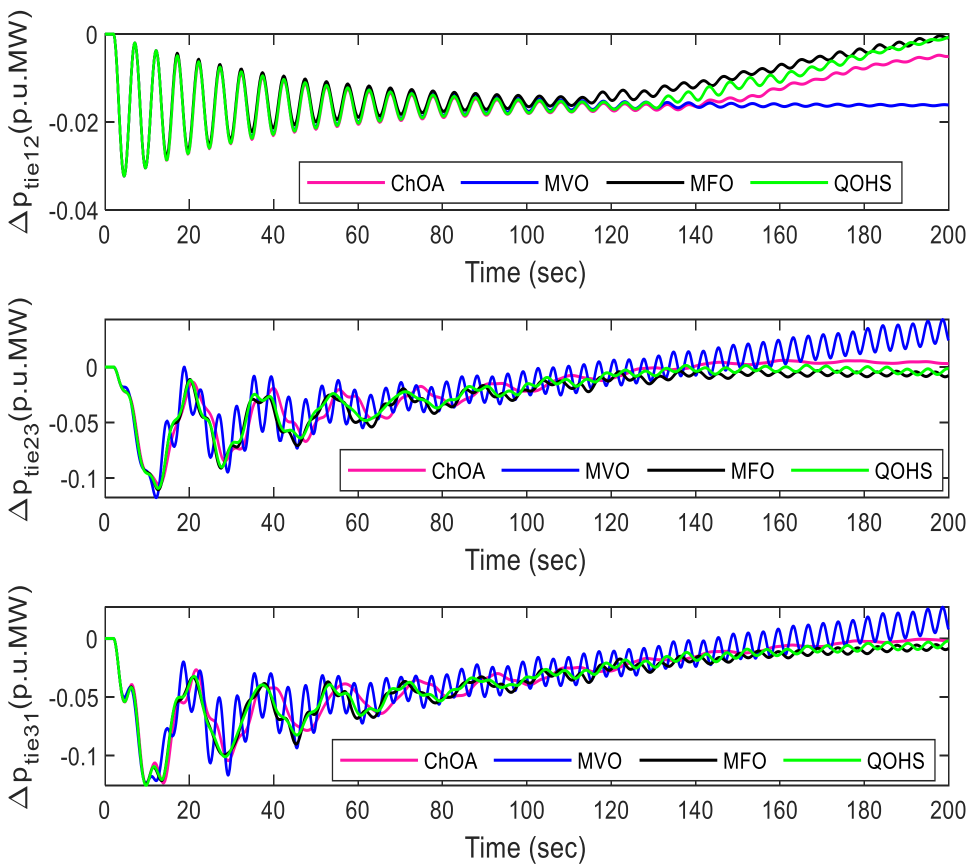

Figure 4. 8 Comparative performance analysis of ChOA, QOHS, MFO, and MVO for 0.1 p.u Step load change in area-1, 0.05 p.u area-2, and 0.01 p.u area-3 in a change of tie-line power simultaneously.

The response of tie-line power deviation for 0.1 p.u step load change in area-1, 0.05 p.u area-2, and 0.01 p.u area-3 simultaneously is shown in Figure 4.8, and Table 8. Comparative performance analysis of ChOA, QOHS, MFO, and MVO is done by applying the various amount of load for each area, and the ChOA based controller response has a substantially shorter peak overshoot and settling time in all areas. Simulations have been run with a variety of instantaneous load changes, and all have been successful.

Table 9 Comparison values of settling time of deviation in tie-line power flow for 60 iterations

Parameters	Transient response	Methods			
		ChOA	QOHS	MFO	MVO
Delptie12	Settling Time(sec)	195.2	198.6	195.9	161.4
	Peak overshoot	4.4	4.6	4.4	4.5
Delptie23	Settling Time(sec)	180.2	198.6	197.6	199.7
	Peak overshoot	12.9	12.6	12.6	12.2
Delptie31	Settling Time(sec)	173.4	198.6	197.7	199.8
	Peak overshoot	9.8	9.7	9.7	9.6

Case3: Robustness Analysis

The steady-state operating characteristics of interconnected power networks may fluctuate due to variations in load and other operating variables. These issues are more relevant to an integrated power supply that includes hydroelectric plants. This issue could develop as a result of changes in local characteristics and tie-line power flows. Due to the minimal phase lag of the water column in a hydro-power system, if the input signals of the speed governor change, it will not react instantly until the input reaches a predetermined value. Even for wide phase lag, the performance of ALFC may be significantly lower [13].

The governor is forced to respond too late due to the phase delay. In this situation, the frequency variation could last for a long time. This makes robustness analysis of interconnected power system which considers hydro-power plant becomes a worst-case scenario. To verify the robustness of the proposed controller scheme, a ± 50% uncertainty is introduced into some of a system parameters, i.e., Kp = [60, 180], Tp= [10,30], Tg= [0.15, 0.45], Tt= [0.04, 0.5], and R= [1.2, 3.6]. The efficiency of the employed technique is validated by the value of objective functions, as shown in Tables 11 and Table 12. For nominal system parameters, the values of the ITAE performance index achieved with QOHSA based PID controller are superior to those obtained with ChOA, MFO, and MVO based PID controller, as shown in Table 11.

For lower and upper bound system parameters, the results are similar to those produced by ChOA, MFO, and MVO using ITAE as the objective function. The controller's optimality is indicated by the objective functions. It can be concluded that the ChOA, QOHS, MFO, and MVO based PID control schemes are optimal in terms of the ITAE criterion, based on the values obtained for nominal, lower, and upper bound system parameters. Table 12 shows the sensitivity of PID controller-based employed optimization techniques.

Table 10. Comparative study of performance indices for three-area Power System

Algorithm	Nominal Parameters				50% parameter change							
					Lower Limit (-50%)				Upper Limit (+50%)			
	ISE	ITSE	IAE	ITAE	ISE	ITSE	IAE	ITAE	ISE	ITSE	IAE	ITAE
ChOA	0.0533	0.4309	1.7625	22.8625	0.0531	0.4684	1.9275	31.5303	0.0583	0.4990	1.9146	26.7892
QOHS	0.0458	0.3420	1.5627	18.2658	0.0430	0.2906	1.3918	15.2472	0.0487	0.3760	1.6587	20.6342
MFO	0.0467	0.3439	1.5623	18.4536	0.0526	0.4313	1.8278	25.0199	0.0501	0.3894	1.6930	22.4862
MVO	0.0758	0.9423	2.5619	43.5527	0.0450	0.4083	1.7325	23.6101	0.0599	0.5478	2.0412	29.8213

Table 11.Comparison of settling time (sec) for variation in model parameters

Algorithm	Settling time(sec)								
	Δf_1			Δf_2			Δf_3		
	Nominal	+50%	-50%	Nominal	+50%	-50%	Nominal	+50%	-50%
ChOA	39.53	41.91	34.14	38.43	40.67	35.41	38.04	39.35	40.96
QOHS	36.31	34.01	39.73	35.56	23.53	38.16	39.65	28.58	40.87
MFO	36.39	37.64	38.6	36.06	36.81	34.5	35.32	38.84	33.31
MVO	46.2	41.56	38.07	43.15	32.48	37.13	61.51	44.27	36.52

A 50% parameter variation considered for hydro, and thermal power are graphically shown below for each optimization technique. Tuning of PID controller for sensitivity analysis is done by varying some of the important parameters of each power system are discussed for each optimization technique.

Case 3.1. Responses of PID controller based on ChOA for frequency deviation

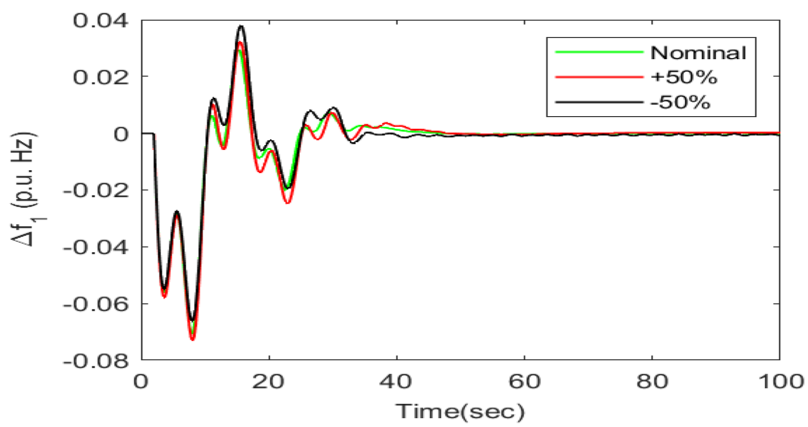

(a)

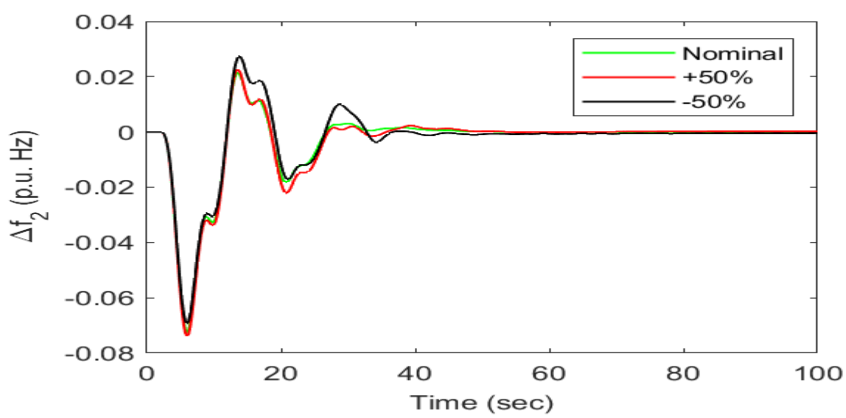

(b)

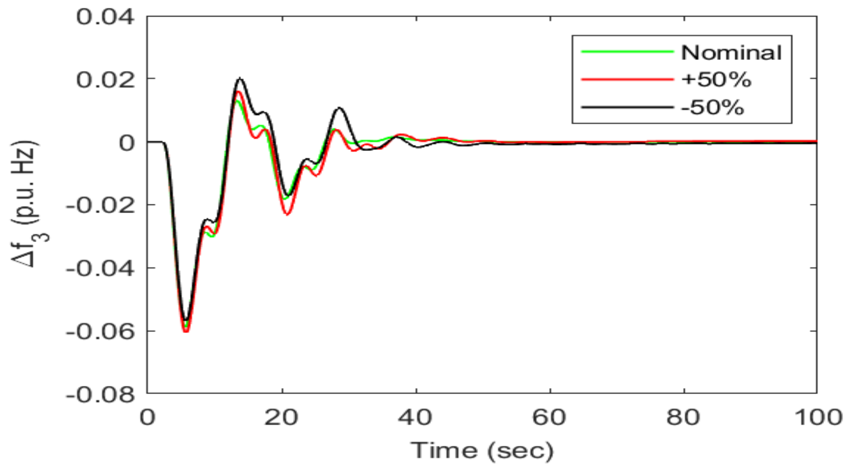

(c)

Figure 4. 9 Sensitivity analysis using chimp optimization of frequency deviation in (a) area-1, (b) area-2, and (c) area-3 for 1% step load perturbation in area-1.

<u>Case 3.2</u>. Responses of PID controller based on QOHS for frequency deviation

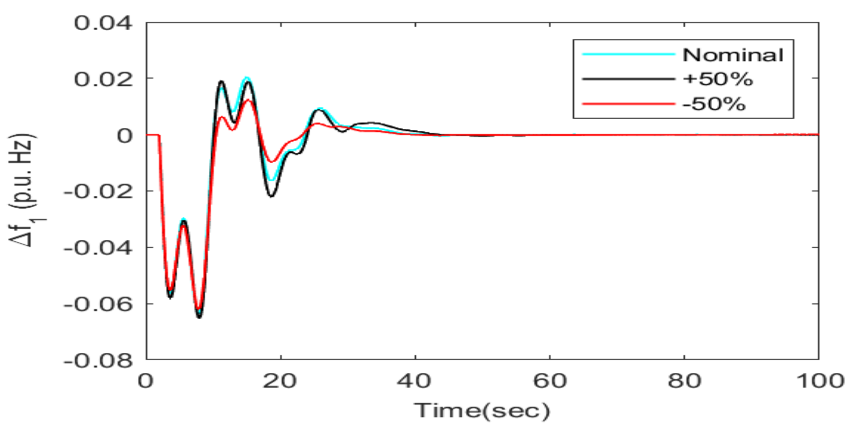

(a)

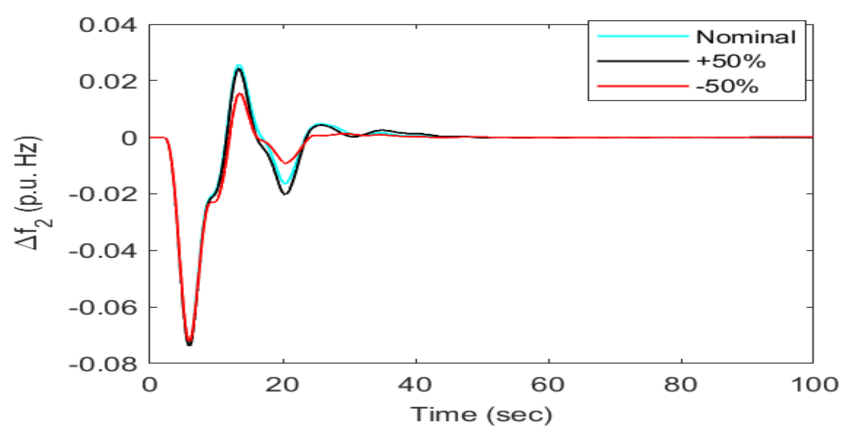

(b)

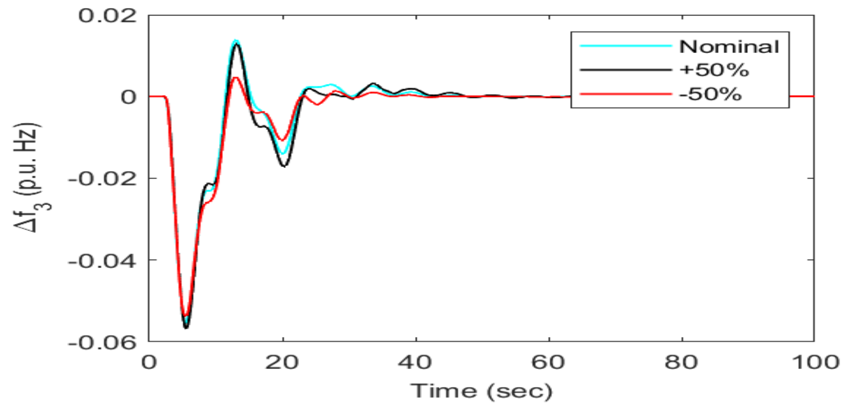

(c)

Figure 4. 10 Sensitivity analysis using Quasi-oppositional harmony Search algorithm for frequency deviation in area-1(a), area-2 (b), and area-3 (c) for 1% step load perturbation in area-1

Case 3.3. Responses of PID controller based on MFO for frequency deviation

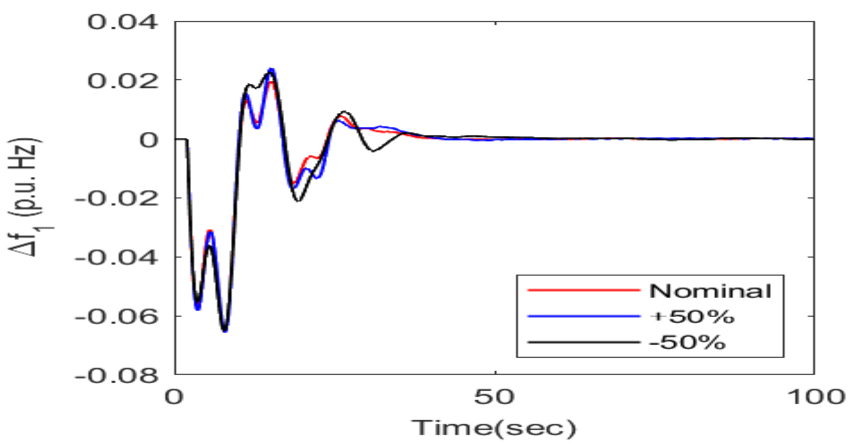

(a)

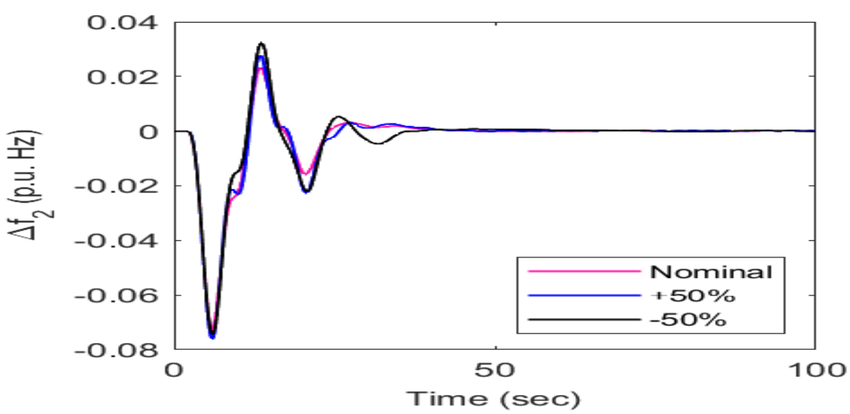

(b)

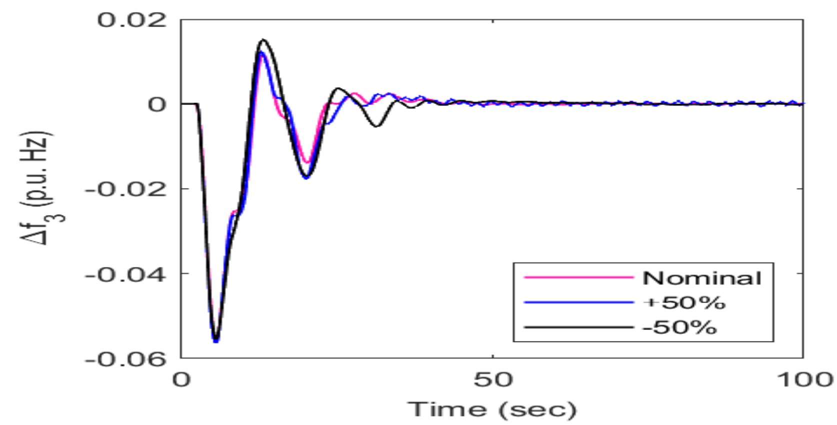

(c)

Figure 4. 11 Sensitivity analysis using Mothe-flame optimization algorithm for frequency deviation in area-1(a), area-2 (b), and area-3 (c) for 1% step load perturbation in area-1

Case 3.4. Responses of PID controller based on MFO for frequency deviation

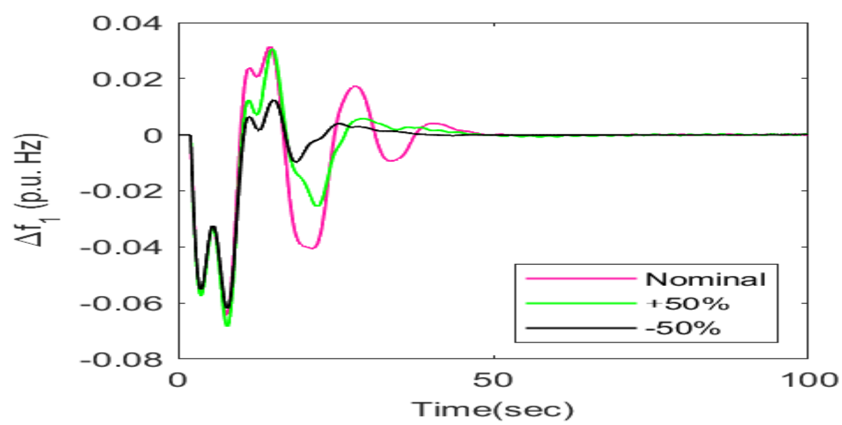

(a)

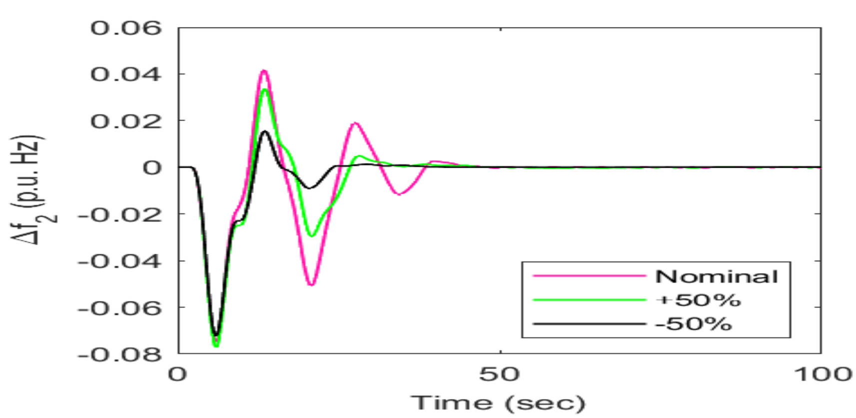

(b)

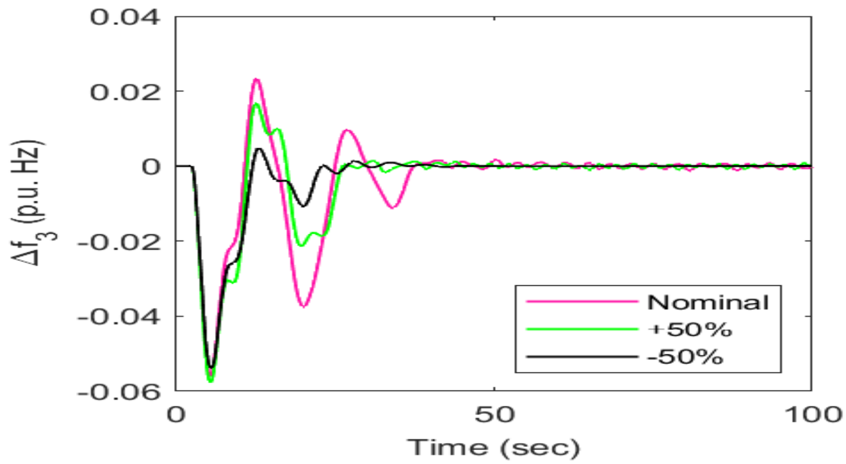

(c)

Figure 4. 12 Sensitivity analysis using Multi-verse optimization algorithm for frequency deviation in area-1(a), area-2 (b), and area-3 (c) for 1% step load perturbation in area-1

From the point of view of transient response specification, we have considered settling time as it indicates the speed of response of the system or how rapidly the system settles back to its nominal frequency after the system is subjected to disturbances. The observations illustrated in the tables and figures depict the efficiency of the system in terms of settling time. The variations obtained in the settling time introduced due to parameter uncertainty are found to be within appreciable limits. Thus, it can be asserted that the proposed control scheme is optimal considering the ability of the system to nullify frequency fluctuations within minimum settling time resulting from step load change.

We can see from the simulation results that, despite such huge parameter fluctuations, the system responses do not differ much from those shown in Figures 9, 10, 11, and 12. As a result, the simulation results show that a three-area interconnected power system can withstand changes in system parameters. Because the model for each area is similar, changing the system parameters for reheat and hydraulic units yields the same conclusion.

CONCLUSION AND RECOMMENDATION

5.1 Conclusion

The main objective of this thesis work is to tune a PID controller by applying different types of metaheuristics optimization techniques like Chimp optimization algorithm (ChOA) (Evolutionary metaheuristics optimization algorithm), Novel Quasi Oppositional Harmony Search algorithm (QOHS) (Physics-based metaheuristics optimization algorithm), Moth-flame Optimization algorithm(MFO) (Nature-inspired metaheuristics optimization algorithm), and Multi-verse optimization algorithm (MVO) (Physics-based metaheuristics optimization algorithm) to Automatic Load Frequency Control (ALFC) of interconnected three areas thermal-thermal-hydro-power system.

Results of a mixed system consisting of reheat and hydro turbine with GRC are presented. Robustness was also checked utilizing applying different load changes to different areas and found that the system is achieving a steady-state position within the permissible time frame. Frequency deviations and tie-line deviations are plotted. Each optimization technique's performance in providing optimal PID gains is compared for a comparative study. In evaluating the controller's performance in disturbance rejection two scenarios are considered.

The first scenario is when 1% SLP is applied to area 1 only; simulation result shows that the novel quasi harmony search algorithm based PID tuning gave a response with a settling time of 36 sec, and a frequency deviation of 0.062 per unit (p.u). This is a better result than that of a PID controller tuned with MVO, MFO, and ChOA in settling time of frequency deviation of in area -1, and area-2. But for frequency deviation in area-3; Mothe- flame optimization algorithm gave a response with a settling time of 35 sec, and a frequency deviation of 0.06 per unit (p.u). This reveals MFO shows better results than that of a PID controller tuned with QOHS, MVO, and ChOA. Again in reducing a tie-line power deviation MFO shows a better result than that of a PID controller tuned with QOHS, MVO, and ChOA.

The second scenario is when 10% SLP on the first area, 5% SLP in the second area, and 1% step load rise in demand of the third area are applied the simulation results are analyzed.

The simulation result reveals that the comparative dynamic responses of the system performance with the ChOA based PID controller gave a better result in area 1, and area 3, while MFO based PID controller tuning gave a better result in area-2. Again in reducing deviation in tie-line power error ChOA-PID tuning gives better results in all areas.

The sensitivity analysis of the system is also discussed to observe the robustness of the system against parameter variation. Thus, the simulation results reveal that, with such large parameter variations, the system responses do not show notable differences from nominal values. From an execution time efficiency point of view, ChOA shows superiority over that of a PID controller tuned with QOHS, MVO, and MFO.

It is to be concluded that a single control design method cannot do the best for all the requirements such as robustness to system uncertainties, simple/systematic design, handles nonlinearity, and systematic constraint handling.

5.2 Recommendation

Future works that can be pursued related to this research area can add the following points:

- Expanding the number of system areas to larger, and considering multiple generators in a given area.
- AGC system used can be investigated, and implemented for each type of Generator.
- In the present work, the load disturbances d1, d2, and d3 considered are deterministic. The work can be extended to dynamic (time-varying) load disturbances.
- Comparison of different optimization methods in terms of computation speed can be a valuable work through LFC studies
- Developing automatic generation control schemes for renewable energy integration is also an emerging research field.
- Moreover, a detailed discrete LFC model which utilizing optimal sampling rate in its control loops can be a good topic for the future works
- Consideration of Governor dead band, boiler model, and communication link delay can be a good topic for future research work.
- Using adaptive control along with metaheuristics optimization algorithm can be good future work.

REFERENCES

[1] M. Alemu Tikuneh and G. Biru Worku, "Analysis of the Power Blackout in the Ethiopian Electric Power Grid," *Sci. J. Circuits, Syst. Signal Process.*, vol. 8, no. 2, p. 53, 2019, doi: 10.11648/j.cssp.20190802.14.

[2] M. A. H. Mondal, E. Bryan, C. Ringler, D. Mekonnen, and M. Rosegrant, "Ethiopian energy status and demand scenarios: Prospects to improve energy efficiency and mitigate GHG emissions," *Energy*, vol. 149, 2018, doi: 10.1016/j.energy.2018.02.067.

[3] M. Raju, L. C. Saikia, N. Sinha, and A. Saha, "AGC of multi-area ST - Thermal - hydro system incorporating redox flow batteries," in *2017 Innovations in Power and Advanced Computing Technologies, i-PACT 2017*, 2017, vol. 2017-January, doi: 10.1109/IPACT.2017.8244981.

[4] "Power System Stability Controls," in *Power System Stability and Control*, 2020.

[5] S. Prakash and S. K. Sinha, "Four area load frequency control of interconnected hydro-thermal power system by intelligent PID control technique," 2012, doi: 10.1109/SCES.2012.6199090.

[6] J. Nanda and A. Mangla, "Automatic generation control of an interconnected hydro-thermal system using conventional integral and fuzzy logic controller," *Proc. 2004 IEEE Int. Conf. Electr. Util. Deregulation, Restruct. Power Technol.*, vol. 1, no. 8, pp. 372–377, 2004, doi: 10.1109/drpt.2004.1338524.

[7] V. Kushwaha, K. Pandey, S. Sehrawat, and D. Sharma, "Adaptive neuro-fuzzy based load frequency controller for three area inter-connected hydro-thermal power system," *2nd IEEE Int. Conf. Innov. Appl. Comput. Intell. Power, Energy Control. with their Impact Humanit. CIPECH 2016*, pp. 34–38, 2017, doi: 10.1109/CIPECH.2016.7918732.

[8] T. Masuta and A. Yokoyama, "Supplementary load frequency control by use of a number of both electric vehicles and heat pump water heaters," *IEEE Trans. Smart Grid*, vol. 3, no. 3, pp. 1253–1262, 2012, doi: 10.1109/TSG.2012.2194746.

[9] S. Sat and Z. Min, "Modeling and Simulation of Load Frequency Control for Three

Area Power System Using Proportional Integral Derivative (PID) Controller," pp. 301–315, 2016.

[10] S. W. Fardo and D. R. Patrick, *Modern Power Systems*. 2020.

[11] R. Rajbongshi, L. C. Saikia, W. Tasnin, A. Saha, and D. Saha, "Performance Analysis of Combined ALFC and AVR System Incorporating Power System Stabilizer," *2nd Int. Conf. Energy, Power Environ. Towar. Smart Technol. ICEPE 2018*, pp. 1–6, 2019, doi: 10.1109/EPETSG.2018.8658874.

[12] M. Mahdavian, G. Shahgholian, M. Janghorbani, B. Soltani, and N. Wattanapongsakorn, "Load frequency control in power system with hydro turbine under various conditions," *ECTI-CON 2015 - 2015 12th Int. Conf. Electr. Eng. Comput. Telecommun. Inf. Technol.*, no. 1, pp. 3–7, 2015, doi: 10.1109/ECTICon.2015.7206938.

[13] C. K. Shiva and V. Mukherjee, "Automatic Generation Control of Hydropower Systems Using a Novel Quasi-oppositional Harmony Search Algorithm," *Electr. Power Components Syst.*, vol. 44, no. 13, pp. 1478–1491, 2016, doi: 10.1080/15325008.2016.1147103.

[14] Ibraheem, N. Hasan, and A. A. Hussein, "Decentralized automatic generation control of interconnected power systems incorporating asynchronous tie-lines," *Springerplus*, vol. 3, no. 1, pp. 1–8, 2014, doi: 10.1186/2193-1801-3-744.

[15] C. Tan *et al.*, "Multi-area automatic generation control scheme considering frequency quality in southwest china grid: Challenges and solutions," *IEEE Access*, vol. 8, pp. 199813–199828, 2020, doi: 10.1109/ACCESS.2020.3035067.

[16] S. A. Azeer, R. Ramjug-Ballgobin, and S. Z. Sayed Hassen, "Intelligent Controllers for Load Frequency Control of Two-Area Power System," *IFAC-PapersOnLine*, vol. 50, no. 2, pp. 301–306, 2017, doi: 10.1016/j.ifacol.2017.12.062.

[17] I. A. Chidambaram and S. Velusami, "Decentralized biased controllers for load - Frequency control of interconnected power systems considering governor dead band non-linearity," *Proc. INDICON 2005 An Int. Conf. IEEE India Counc.*, vol. 2005, pp. 521–525, 2005, doi: 10.1109/INDCON.2005.1590225.

[18] X. Liu, X. Zhan, and D. Qian, “Load frequency control considering generation rate constraints,” *Proc. World Congr. Intell. Control Autom.*, pp. 1398–1401, 2010, doi: 10.1109/WCICA.2010.5554815.

[19] S. Bhowmik, K. Tomsovic, and A. Bose, “Communication Models for Third Party Load Frequency Control,” *IEEE Trans. Power Syst.*, vol. 19, no. 1, pp. 543–548, 2004, doi: 10.1109/TPWRS.2003.818700.

[20] V. Shanmugasundaram, “Artificial bee colony algorithm based automatic generation control in two-area non-reheat thermal power system using SMES,” *IEEE Int. Conf. Power, Control. Signals Instrum. Eng. ICPCSI 2017*, pp. 2126–2130, 2018, doi: 10.1109/ICPCSI.2017.8392092.

[21] M. R. I. Sheikh, R. Takahashi, and J. Tamura, “Multi-area frequency and tie-line power flow control by coordinated AGC with TCPS,” *ICECE 2010 - 6th Int. Conf. Electr. Comput. Eng.*, no. December, pp. 275–278, 2010, doi: 10.1109/ICELCE.2010.5700681.

[22] D. G. Ramey and J. W. Skooglund, “Detailed Hydrogovernor Representation for System Stability Studies,” *IEEE Trans. Power Appar. Syst.*, vol. PAS-89, no. 1, pp. 106–112, 1970, doi: 10.1109/TPAS.1970.292676.

[23] H. Bevrani, *Robust Power System Frequency Control (Power Electronics and Power Systems)*. 2009.

[24] I. Gupta and M. Hemanth, “A Case Study on Load Frequency Control with Automatic Generation Control on a Two Area Network using MiPower,” *2018 20th Natl. Power Syst. Conf. NPSC 2018*, pp. 1–6, 2018, doi: 10.1109/NPSC.2018.8771714.

[25] B. Tech and I. V. Y. I. Sem, “POWER SYSTEM OPERATION AND CONTROL DIGITAL NOTES Mr . P Raji Reddy , Assistant Professor,” vol. 2, 2020.

[26] X. Hao, H. Zheng, X. Liu, Q. Guo, and L. Bo, “Experimental research and parameter optimization for speed governing system of isolated network operation area,” in *2017 IEEE Conference on Energy Internet and Energy System Integration, EI2 2017 - Proceedings*, 2017, vol. 2018-Janua, no. 1, pp. 1–6, doi: 10.1109/EI2.2017.8245281.

[27] W. Gil-Gonzalez, A. Garces, A. Escobar-Mejia, and O. D. Montoya, “Passivity-Based

Control for Hydro-Turbine Governing Systems," *Proc. 2018 IEEE PES Transm. Distrib. Conf. Exhib. - Lat. Am. T D-LA 2018*, pp. 0–4, 2018, doi: 10.1109/TDC-LA.2018.8511641.

[28] Utrechtseweg 310; Postbus 100; 6800 AC Arnhem, "Synchronous Machine Turbine-Governing Systems Vision Dynamical Analysis Manual," vol. 31, no. 0, 2016, [Online]. Available: www.phasetophase.nl.

[29] J. Keerthana and K. Selvi, "Load frequency control of Multi-area Power System in Deregulated Environment," *2018 Natl. Power Eng. Conf. NPEC 2018*, pp. 1–7, 2018, doi: 10.1109/NPEC.2018.8476702.

[30] J. Morsali, K. Zare, and M. T. Hagh, "Appropriate Generation Rate Constraint (GRC) Modeling Method for Reheat Thermal Units to Obtain," *5th Conf. Therm. Power Plants (IPGC2014), June 10-11, 2014, Shahid Beheshti Univ. Tehran, Iran*, pp. 29–34, 2014.

[31] S. W. Blume, "Electric Power System Basics for the Nonelectrical Professional: Second Edition," *Electr. Power Syst. Basics Nonelectrical Prof. Second Ed.*, pp. 1–235, 2016, doi: 10.1002/9781119180227.

[32] F. Potentials, *Power Interconnection*, no. March. 2000.

[33] M. Yang, C. Wang, Y. Hu, Z. Liu, C. Yan, and S. He, "Load frequency control of photovoltaic generation-integrated multi-area interconnected power systems based on double equivalent-input-disturbance controllers," *Energies*, vol. 13, no. 22, pp. 1–19, 2020, doi: 10.3390/en13226103.

[34] N. Ngoc-khoat, "Designing Intelligent Load-Frequency Controllers for Large-Scale Multi-Control-Area Interconnected Power Systems," vol. 1, no. 1, pp. 38–51, 2014, doi: 10.6007/IJARCSEE/v1-i1/1382.

[35] B. Smith, "Classical vs Intelligent Control," *EN9940 Spec. Top. Robot.*, p. 20, 2002.

[36] B. F. Wollenberg, "Power system operation and control," *Power Syst. Stab. Control. Third Ed.*, pp. III-1-III–2, 2017, doi: 10.4324/b12113.

[37] Y. Mi, Y. Yang, H. Zhang, A. Yu, L. Wang, and L. Ren, "Sliding mode based load frequency control for multi-area interconnected power system containing renewable

energy," *IEEE Transp. Electrif. Conf. Expo, ITEC Asia-Pacific 2014 - Conf. Proc.*, pp. 1–6, 2014, doi: 10.1109/ITEC-AP.2014.6941131.

[38] J. Nömm, S. K. Rönnberg, and M. H. J. Bollen, "An analysis of frequency variations and its implications on connected equipment for a nanogrid during Islanded operation," *Energies*, vol. 11, no. 9, pp. 1–13, 2018, doi: 10.3390/en11092456.

[39] R. Umrao, S. Kumar, M. Mohan, and D. K. Chaturvedi, "Load Frequency Control methodologies for power system," *ICPCES 2012 - 2012 2nd Int. Conf. Power, Control Embed. Syst.*, 2012, doi: 10.1109/ICPCES.2012.6508133.

[40] M. K. Debnath, T. Jena, and R. K. Mallick, "Novel PD-PID cascaded controller for automatic generation control of a multi-area interconnected power system optimized by grey wolf optimization (GWO)," *1st IEEE Int. Conf. Power Electron. Intell. Control Energy Syst. ICPEICES 2016*, pp. 1–6, 2017, doi: 10.1109/ICPEICES.2016.7853271.

[41] K. Janprom, W. Permpoonsinsup, and S. Wangnipparnto, "Intelligent Tuning of PID Using Metaheuristic Optimization for Temperature and Relative Humidity Control of Comfortable Rooms," *J. Control Sci. Eng.*, vol. 2020, 2020, doi: 10.1155/2020/2596549.

[42] G. Chicco and A. Mazza, "Metaheuristic optimization of power and energy systems: Underlying principles and main issues of the 'rush to heuristics,'" *Energies*, vol. 13, no. 19, 2020, doi: 10.3390/en13195097.

[43] T. P. Kumar and R. Kiranmayi, "Load frequency control of multi area power system using particle swarm optimization algorithm," *J. Adv. Res. Dyn. Control Syst.*, vol. 11, no. 2 Special Issue, pp. 2341–2350, 2019.

[44] N. Kumar, B. Tyagi, and V. Kumar, "Multiarea automatic generation control using model predictive based control in deregulated environment," *Int. Conf. Energy Econ. Environ. - 1st IEEE Uttar Pradesh Sect. Conf. UPCON-ICEEE 2015*, pp. 1–6, 2015, doi: 10.1109/EnergyEconomics.2015.7235074.

[45] A. Dhamanda, A. D. Dehradun, and A. K. B. Allahabad, "Automatic generation control of thermal generating unit using evolutionary controller," *Int. J. Adv. Intell. Paradig.*, vol. 9, no. 5–6, pp. 490–504, 2017, doi: 10.1504/IJAIP.2017.088144.

[46] S. Prakash and S. K. Sinha, “Simulation based neuro-fuzzy hybrid intelligent PI control approach in four-area load frequency control of interconnected power system,” *Appl. Soft Comput. J.*, vol. 23, pp. 152–164, 2014, doi: 10.1016/j.asoc.2014.05.020.

[47] J. Morsali, K. Zare, and M. T. Hagh, “AGC of interconnected multi-source power system with considering GDB and GRC nonlinearity effects,” *6th Conf. Therm. Power Plants, CTPP 2016*, pp. 12–17, 2016, doi: 10.1109/CTPP.2016.7482927.

[48] M. Zribi, M. Al-Rashed, and M. Alrifai, “Adaptive decentralized load frequency control of multi-area power systems,” *Int. J. Electr. Power Energy Syst.*, vol. 27, no. 8, pp. 575–583, 2005, doi: 10.1016/j.ijepes.2005.08.013.

[49] R. R. Shoults and J. A. Jativa Ibarra, “Multi-area adaptive lfc developed for a comprehensive agc simulator,” *IEEE Trans. Power Syst.*, vol. 8, no. 2, pp. 541–547, 1993, doi: 10.1109/59.260829.

[50] K. P. S. Parmar, S. Majhi, and D. P. Kothari, “Load frequency control of a realistic power system with multi-source power generation,” *Int. J. Electr. Power Energy Syst.*, vol. 42, no. 1, pp. 426–433, 2012, doi: 10.1016/j.ijepes.2012.04.040.

[51] F. Tabassum and M. S. Rana, “Robust Control of Frequency for Multi-Area Power System,” *2020 IEEE Reg. 10 Symp. TENSYMP 2020*, no. June, pp. 86–89, 2020, doi: 10.1109/TENSYMP50017.2020.9230682.

[52] B. K. Sahu, S. Pati, P. K. Mohanty, and S. Panda, “Teaching-learning based optimization algorithm based fuzzy-PID controller for automatic generation control of multi-area power system,” *Appl. Soft Comput. J.*, vol. 27, pp. 240–249, 2015, doi: 10.1016/j.asoc.2014.11.027.

[53] S. K. Gautam and N. Goyal, “Improved particle swarm optimization based load frequency control in a single area power system,” *Proc. 2010 Annu. IEEE India Conf. Green Energy, Comput. Commun. INDICON 2010*, pp. 106–110, 2010, doi: 10.1109/INDCON.2010.5712725.

[54] J. Seekuka, R. Rattanawaorahirunkul, S. Sansri, S. Sangsuriyan, and A. Prakonsant, “AGC using particle swarm optimization based PID controller design for two area power system,” *20th Int. Comput. Sci. Eng. Conf. Smart Ubiquitos Comput.*

Knowledge, ICSEC 2016, no. 1, pp. 7–10, 2017, doi: 10.1109/ICSEC.2016.7859951.

[55] J. Mudi, C. K. Shiva, and V. Mukherjee, “Multi-verse Optimization Algorithm for LFC of Power System with Imposed Nonlinearities Using Three-Degree-of-Freedom PID Controller,” *Iran. J. Sci. Technol. - Trans. Electr. Eng.*, vol. 43, no. 4, pp. 837–856, 2019, doi: 10.1007/s40998-018-0166-1.

[56] N. Patel, P. Bharat, and B. Jain, “Automatic Generation Control of Three Area Power Systems Using Ann Controllers,” pp. 1–7, 2013.

[57] J. A. Jaleel and T. P. I. Ahammed, “Simulation of artificial neural network controller for automatic generation control of hydro electric power system,” *IEEE Reg. 10 Annu. Int. Conf. Proceedings/TENCON*, pp. 13–16, 2008, doi: 10.1109/TENCON.2008.4766636.

[58] S. Chatterjee, C. K. Shiva, and V. Mukherjee, “Automatic Generation Control of Multi-Area Hydro Power System using Moth Flame Optimization Technique,” 2019, doi: 10.1109/RDCAPE47089.2019.8979090.

[59] P. M. Dash, S. K. Mohapatra, and A. K. Baliarsingh, “Tuning of LFC in Multi-source Electrical Power Systems Implementing Novel Nature Inspired MFO Algorithm Based Controller Parameter,” *Int. Conf. Comput. Intell. Smart Power Syst. Sustain. Energy, CISPSSE 2020*, pp. 1–5, 2020, doi: 10.1109/CISPSSE49931.2020.9212199.

[60] A. Chawpattnaik, R. K. Sahu, and P. C. Pradhan, “Design and analysis of hybrid fuzzy fractional order PD-PI controller for frequency regulation problem,” *Int. Conf. Comput. Intell. Smart Power Syst. Sustain. Energy, CISPSSE 2020*, pp. 29–34, 2020, doi: 10.1109/CISPSSE49931.2020.9212194.

[61] C. K. Shiva and V. Mukherjee, “A novel quasi-oppositional harmony search algorithm for AGC optimization of three-area multi-unit power system after deregulation,” *Eng. Sci. Technol. an Int. J.*, vol. 19, no. 1, pp. 395–420, 2016, doi: 10.1016/j.jestch.2015.07.013.

[62] K. Jagatheesan, “Automatic Generation Control of Three Area Hydro- Thermal Power Systems with Electric and Mechanical Governor,” 2014.

[63] H. Jia, K. Sun, W. Zhang, and X. Leng, "An enhanced chimp optimization algorithm for continuous optimization domains," *Complex Intell. Syst.*, no. 0123456789, 2021, doi: 10.1007/s40747-021-00346-5.

[64] S. Mirjalili, "Moth-flame optimization algorithm: A novel nature-inspired heuristic paradigm," *Knowledge-Based Syst.*, vol. 89, no. July, pp. 228–249, 2015, doi: 10.1016/j.knosys.2015.07.006.

[65] S. Mirjalili, S. M. Mirjalili, and A. Hatamlou, "Multi-Verse Optimizer: a nature-inspired algorithm for global optimization," *Neural Comput. Appl.*, vol. 27, no. 2, pp. 495–513, 2016, doi: 10.1007/s00521-015-1870-7.

[66] K. Vivek, M. Deepak, Chetna, J. Mohit, R. Asha, and S. Vijander, "Development of multi-verse optimizer (mvo) for labview," *Adv. Intell. Syst. Comput.*, vol. 624, pp. 731–739, 2018, doi: 10.1007/978-981-10-5903-2_75.

APPENDIXES

APPENDIX A: Nominal values of three areas power system parameters

Parameters	Nominal Values
Steam Turbine- Area one and two	
Speed Governor time constant(Tg1,Tg2)	0.08second
Reheat turbine time constant(Tt1,Tt2)	0.3second
Speed governor regulation (R1,R2,R3)	2.4Hz/pu MW
Low Pressure reheat time (Kr1,Kr2)	0.5second
High-pressure reheat time(Tr1,Tr2)	10second
Hydro turbine-Area three	
Kp, Ki, and Kd	1, 5,and 4 respectively
Water time constant	1second
Speed governor regulation	2.4Hz/pu MW
Power systems	
Frequency bias constant(B1,B2,B3)	0.425pu MW/Hz
Torque synchronizing coefficient(a=2*pi*T12=2*pi*T23=2*pi*T31)	0.086
Load Model gain(Kpi=1/Di)	120Hz/pu MW
Load time Constant(Tpi=2H/B*f)	20second
Inertia constant(H1,H2,H3)	5 second
Max tie-line power(P tie, max)	200MW
Load damping(Di=Δfi/ΔPdi)	$8.33x10^{-3}$ pu.MW/Hz
Generation rate limit	
For Reheat thermal power plant	
Upper limit and lower limit	3%p.u. MW/min

For Hydropower plant	
Upper limit	6% p.u.MW/sec
Lower limit	4.5% p.u.MW/sec
Frequency(f)	50Hz

APPENDIX B: List of Symbols

ΔP_{ref}	Incremental speed reference setting
ΔP_m	Turbine output
P_{12}	Power due to tie line between area 1 and area 2
P_{23}	Power due to tie line between area 2 and area 3
P_{13}	Power due to tie line between area 1 and area 3
Δf_1	Deviation of frequency in area 1
Δf_2	Deviation of frequency in area 2
Δf_3	Deviation of frequency in area 3
ΔPm_1	Turbine output of area 1
ΔP_{m2}	Turbine output of area 2
ΔP_{m3}	Turbine output of area 3
ΔP_{d1}	Increase of load in area 1
ΔP_{d2}	Increase of load in area 2
ΔP_{d3}	Increase of load in area 3
ΔP_G	Active power generation
ΔP_D	Active power demand
$\Delta Pv(s)$	The input to the turbine
$\Delta P_T(s)$	The output from the turbine
$\Delta Pg(s)$	The input to the governor
$\Delta Pv(s)$	The output from the governor
Tg	Speed governor time constant
Tt	Turbine time constant
Tp	Power System time constant
Ri	Regulation constant

Bi	Frequency bias constant
Kp	Gain of the power system
K_T	Gain of the turbine
Kr	Reheat coefficient
H	Inertia constant
$\Delta\omega$	Drift in frequency for step change in load or steady state frequency deviation
q	Per unit deviation inflow,
h	Per unit change in the head,
w	Per unit change in speed,
t	Per unit variation in torque
P_{GV}	Gate position
P_M	Mechanical time constant
TW	Water time constant
V	Velocity of water
H_T	Water head
g	Gravitational acceleration
Ta	Net accelerating torque (N.m)
T_{me}	Machine mechanical torque (N.m)
T_{el}	Electrical torque (N.m)
J	The generator combined moment of inertia in the turbine (Kg.m2)
Wm	The rotor angular velocity (mech. rad/sec)
T	Time (sec)
ω_r	Rotor angular velocity [elec. Rad/s]
ω	Rated speed
ω_o	Rated angular velocity [elec. Rad/s]
w	The weight of steam in the vessel (kg)
V	The volume of a vessel (m3)
ρ	Density of a steam (kg/m3)
Q	Steam mass flow rate (Kg/s)

APPENDIX C: A PID controller tuning result for each metaheuristic's optimization techniques

Table C1: Optimal values of PID controller parameters subjected to step-change in area 1

Algorithm	**Best No. Iteration**	**Area**	**Controllers parameters**		
			Kp	Ki	Kd
ChOA	4	1	0.00230455070834663	0.240372471287808	0.00478719102598926
		2	0.00120131196743431	0.0602684524612006	0.00323676675202651
		3	0.00189221627524783	0.00186867499139970	0.00271867858925900
QOHSA	6	1	0.917883530535552	0.634514192359346	1
		2	0.510923218879333	0.235126071986890	0.868528281353619
		3	0.404221340111333	0.00100000000000000	0.00106649917707423
MFO	2	1	0.828068912565189	0.582263845259606	1
		2	0.618593354202268	0.155324814583825	0.874804035706096
		3	0.368019943071471	0.00100000000000000	0.00100000000000000
	13	1	0.983532328680935	0.453665901422427	0.705032461141103
		2	0.722659753552877	0.188771535185562	0.890766199139665
		3	0.239234002031240	0.159431414310823	0.0391927331331974

Table C2: Performance Index subjected to step-change in area 1

Algorithm	**Areas**	**Index**				**Algo. Exec. time**
		ISE	ITSE	IAE	ITAE	
ChOA	1	0.0533	0.4309	1.7625	22.8625	39.664085
	2	0.0618	0.5859	2.0280	28.4012	43.662381
	3	0.0533	0.4308	1.7687	23.2683	40.410874
QOHSA	1	0.0458	0.3420	1.5627	18.2658	166.8160
	2	0.0448	0.3378	1.5492	18.2993	181.3756
	3	0.0447	0.3422	1.5523	18.2681	170.9235
MFO	1	0.04720	0.34930	1.58716	18.60687	143.155404
	2	0.04678	0.34392	1.5623688	18.4536	139.73709
	3	0.047125	0.34432	1.571310	18.78540	131.263616
MVO	1	0.133311	4.49274	5.270465	232.28438	613.432
	2	0.241976	8.33624	7.7591824	334.79285	689.721
	3	0.0758155	0.94238	2.5619157	43.552779	588.005

Table C3: Transient response specifications subjected to step-change in area 1 using Chimp algorithm

Algorithm	Iteration	Para.	Rise Time	Settling Time	Settling Min	Settling Max	Overshoot	Undershoot	Peak	Peak Time
ChOA	4	Delf1	0.0019	39.5304	-0.0199	0.0295	5.5213e+04	1.3264e+05	0.0707	7.8592
		Delf2	0.0015	38.7366	-0.0182	0.0214	4.7720e+04	1.6204e+05	0.0724	5.8870
		Delf3	0.0021	38.0488	-0.0183	0.0130	2.7484e+04	1.2443e+05	0.0588	5.6809
		delptie12	1.4196	59.8079	6.0835e-05	5.8079e-04	813.9214	9.8991e+03	0.0063	4.4454
		delptie23	0.2364	56.3872	-0.0037	5.5411e-04	9.4762e+03	6.4352e+04	0.0037	12.0414
		delptie31	0.5340	53.7128	6.2080e-05	4.1010e-04	491.4695	1.1675e+04	0.0081	9.4215

Table C4: Transient response specifications subjected to step change in area 1 using QOHSA

Algorithm	Iteration		Rise Time	Settling Time	Settling Min	Settling Max	Overshoot	Undershoot	Peak	Peak Time
QOHSA	6	Delf1	1.0921e-04	36.3180	-0.0637	0.0204	7.7784e+05	2.4909e+05	0.0637	7.8018
		Delf2	0.0545	35.5674	-0.0724	0.0258	7.7746e+05	2.7683e+05	0.0724	5.8509

		Delf3	0.0810	39.6524	-0.0554	0.0139	2.7781e+05	6.9741e+04	0.0554	5.3958
		delptie12	0.0454	49.1428	-0.0062	4.0157e-04	3.9233e+04	2.5621e+03	0.0062	4.4651
		delptie23	3.0672	38.9226	-0.0040	6.2318e-04	3.3324e+04	5.2311e+03	0.0040	8.6715
		delptie31	0.0668	46.3674	-0.0086	5.0138e-04	3.0943e+04	1.8175e+03	0.0086	9.3742

Table C5: Transient response specifications subjected to step-change in area 1 using MFO

Algorithm	**Iteration**		**RiseTime**	**Settling Time**	**SettlingMin**	**Settling Max**	**Overshoot**	**Undershoot**	**Peak**	**Peak Time**
MFO	2	Delf1	0.00006	36.3923	-0.0653	0.0194	1.2691e+06	3.7695e+05	0.0653	7.8399
		Delf2	0.0022	36.0626	-0.0159	0.0233	4.4473e+04	1.3897e+05	0.0727	5.9489
		Delf3	0.0014	35.3284	-0.0139	0.0116	4.5385e+04	2.1821e+05	0.0558	5.5038
		delptie12	0.0555	48.7569	-2.809e-05	4.8405e-04	5.5631e+03	7.2131e+04	0.0062	4.4912
		delptie23	3.0587	35.5833	-0.0040	3.2683e-04	3.0153e+04	3.6038e+03	0.0040	11.6414

		delptie31	0.0255	46.1232	-0.0086	4.9497e-04	1.8173e+05	1.0439e+04	0.0086	9.4102
		Delf2	0.0015	36.5397	-0.0165	0.0201	5.5588e+04	2.0177e+05	0.073	5.9104
		Delf3	0.0021	40.0750	-0.0145	0.0084	2.5002e+04	1.6522e+05	0.0556	5.4580
		delptie12	0.0106	54.4552	-0.0062	5.7862e-04	7.1829e+05	6.7515e+04	0.0062	4.4928
		delptie23	3.0399	46.4573	-0.0042	1.8286e-06	3.0223e+04	3.4509e+03	0.0042	11.5323
		delptie31	0.0449	50.1338	-0.0088	5.0475e-04	5.9286e+04	3.4105e+03	0.0088	9.5182

Table C6: Transient response specifications subjected to step-change in area 1 using MVO

Algorithm	**Iteration**		**RiseTime**	**Settling Time**	**SettlingMin**	**Settling Max**	**Overshoot**	**Undershoot**	**Peak**	**Peak Time**
	13	Delf1	0.0023	46.2045	-0.0642	0.0315	3.6456e+04	1.7929e+04	0.0642	7.6691
		Delf2	0.1431	43.1540	-0.0748	0.0416	4.5506e+04	2.5342e+04	0.0748	5.8926
		Delf3	0.0879	61.5111	-0.0560	0.0234	4.0053e+04	1.6746e+04	0.0560	5.2838

delptie31	delptie23	delptie12
0.1737	0.1687	0.0140
60.3624	87.3478	60.3793
-6.561e-05	-0.0053	1.2623e-06
8.0066e-04	0.0014	2.6880e-04
1.7491e+03	3.2027e+03	1.5819e+04
2.1534e+04	1.2678e+04	3.6521e+05
0.0093	0.0053	0.0062
9.4009	11.9284	4.5147